THE GEOCHEMISTRY AND GEOCHRONOLOGY OF THE BARBY FORMATION IN THE SINCLAIR AREA, SOUTHERN NAMIBIA

THESIS SUBMITTED IN FULFILMENT

OF THE REQUIREMENTS FOR THE DEGREE OF

MASTER OF SCIENCE IN GEOLOGY

OF

THE UNIVERSITY OF NAMIBIA

BY

THERESIA R. MALOBELA

201152568

APRIL 2018

MAIN SUPERVISOR: Prof BS Mapani, (University of Namibia)

……

CO-SUPERVISOR(S): Prof D Cornell (University of Gottenburg)

ABSTRACT

Volcanic and sedimentary rocks of the Sinclair Supergroup occur in the Konkiep Terrane of Southern Namibia. Three volcanic and sedimentary cycles are recognised. The Barby Formation belongs to the second cycle which consists of the Kunjas Formation, Barby Formation and the Guperas Formation. In this work, the volcanic rocks of the Barby Formation, a key unit in the Sinclair area are described and dated. The coeval Spes Bona Syenite and the Tiras Granite are also described and dated. The rock types in the Barby Formation are rhyolites, basaltic trachyandesites, trachybasalts and trachydacites as well as volcanoclastic rocks. The rocks are largely undeformed and partly altered by deuteric processes and also mildly metamorphosed. Based on geochemistry of the rock samples and previous work, the bulk of rock types are calc-alkaline although some alkaline rocks are present. U-Pb dating and Lu-Hf isotopic microbeam analyses were made on zircon and baddeleyite grains from four samples using cathodoluminescent images. A Barby rhomb porphyry sample gives an U-Pb baddeleyite age of 1217 ±2 Ma and a Barby felsic tuff has an $^{207}Pb/^{206}Pb$ zircon age of 1214 ±5 Ma. The Spes Bona Syenite which intrudes the Barby formation has a U-Pb baddeleyite age of 1217 ±3 Ma and an indistinguishable Rb-Sr biotite isochron age of 1238 ±20 Ma, showing that there was no regional metamorphic event. Subduction zone assemblages are generally made of high potassium basalts or calc-alkaline association. The Barby Formation records such assemblages. The Barby Formation reflects a subduction event which took place during the assembly of the Rodinia supercontinent. It is slightly younger at 1204 ±9 Ma and reflects the end of subduction-related volcanism due to the collision of Namaqua terranes with the Konkiep Terrane. The Spes Bona syenite and the Barby units have Lu-Hf crustal residence ages between

1682 and 1873 Ma suggesting the two units probably formed from a mixture of juvenile and older crustal material.

Table of Contents

LIST OF TABLES

LIST OF FIGURES

LIST OF ABBREVIATIONS

act	**-**	actinolite
bio	–	biotite
cal`	-	calcite
cpx	-	clinopyroxene
ep	-	epidote
gnt	-	garnet
gte	-	granite
hnb	-	hornblende
OIB	**-**	Ocean Island Basalts
MORB	-	Mid-Oceanic Rigde Basalts
oli	-	olivine
plag	-	plagioclase
REE	-	Rare Earth Element
zeo	-	zeolite

ACKNOWLEDGEMENTS

This work was supported by a Swedish Research Links grant to Benjamin S. Mapani and Dave H. Cornell. Special thanks go to the two supervisors, Professor Benjamin Mapani and Dave Cornell. I am thankful for all the help from the staff at UNAM, Ministry of Mines and Energy, Gothenburg University and the NordSIM facility in Sweden. The NordSIM facility was supported by the research councils in Denmark Norway and Sweden and the Geological Survey of Finland, together with the Swedish Museum of Natural History. I am also thankful to Tom Andersen and Magnus Kristoffersen at the University of Oslo, Norway for helping me with Hf isotope analyses. Many thanks goes to my colleagues Martin Harris and Axel Sjöqvist for all the help in the field and laboratories. Last but not least, a special appreciation goes to my family and friends who encouraged me and motivated me through the hard times.

To my supportive parents, Raphael and Magreth Malobela and my mentor Professor Benjamin Mapani.

DECLARATIONS

- I, **Theresia Raphael Malobela,** declare hereby that this study is a true reflection of my own research, and that this work, or part thereof has not been submitted for a degree in any other institution of higher education.
- No part of this thesis may be reproduced, stored in any retrieval system, or transmitted in any form, or by means (e.g. electronic, mechanical, photocopying, recording or otherwise) without the prior permission of the author, or The University of Namibia in that behalf.
- I, **Theresia Raphael Malobela**, grant The University of Namibia the right to reproduce this thesis in whole or in part, in any manner or format, which The University of Namibia may deem fit, for any person or institution requiring it for study and research; providing that The University of Namibia shall waive this right if the whole thesis has been or is being published in a manner satisfactory to the University.

…… Date……..

Theresia Raphael Malobela

1. INTRODUCTION

1.1 Background of the study

The Sinclair Supergroup forms part of the Rehoboth Province and the Namaqua-Natal Province in South Africa. The Rehoboth Province extends from the Excelsior Lord Hill Shear Zone SW of Helmeringhausen and continues northwards to the Gamsberg area in a north-easterly direction through the Rehoboth inlier to the north of Gobabis and continues into Botswana (Miller, 2008) (Fig. 1-1) where it is covered by the Kalahari Group. According to Becker et al. (2006), the Sinclair Supergroup includes the Kgwebe Formation in Botswana and the Koras Group in South Africa. The Konkiep Group of the Konkiep Terrane in Namibia is part of the Sinclair Supergroup that occupies the north-western part of the Rehoboth Province, bounded further to the southwest by the Namaqua Province (Fig. 1-1). Some of the geological units in the Konkiep Terrane have been described as reflecting subduction that took place from 1.3 Ga to 1.1 Ga (Becker et al., 2006; Cornell et al., 2015).

According to Becker et al. (2006) and Miller (2008), the plate tectonic setting of the regional arc is constrained in the Barby Formation which has high calc-alkaline rocks that suggest that the emplacement was in an active continental margin setting.

The study of igneous rocks in certain tectonic environments is helpful in the understanding of the crustal activities that took place in the past and enhances mineral exploration. Igneous rocks are a major source of heat that drives hydrothermal systems over periods of years and yields mineral deposits such as porphyry copper systems, volcanic massive sulphides and sedimentary exhalative sulphides deposits. These

rocks also act as a source of chemical components that enrich hydrothermal systems (Seyfried et al., 1999; Yang & Scott, 2006).

The last detailed work on the Sinclair Supergroup was done by the Watters (1974), followed by Hoal (1993); and most of the work done only focused on the geochemistry and lithostratigraphy of the Sinclair Supergroup. The geochronological work done by Hoal (as sited by Miller, 2008) shows that there is a mismatch in the established stratigraphy in the Sinclair Supergroup, therefore a better understanding of the geological history of the area is required and more work has to be done using modern techniques for dating rocks.

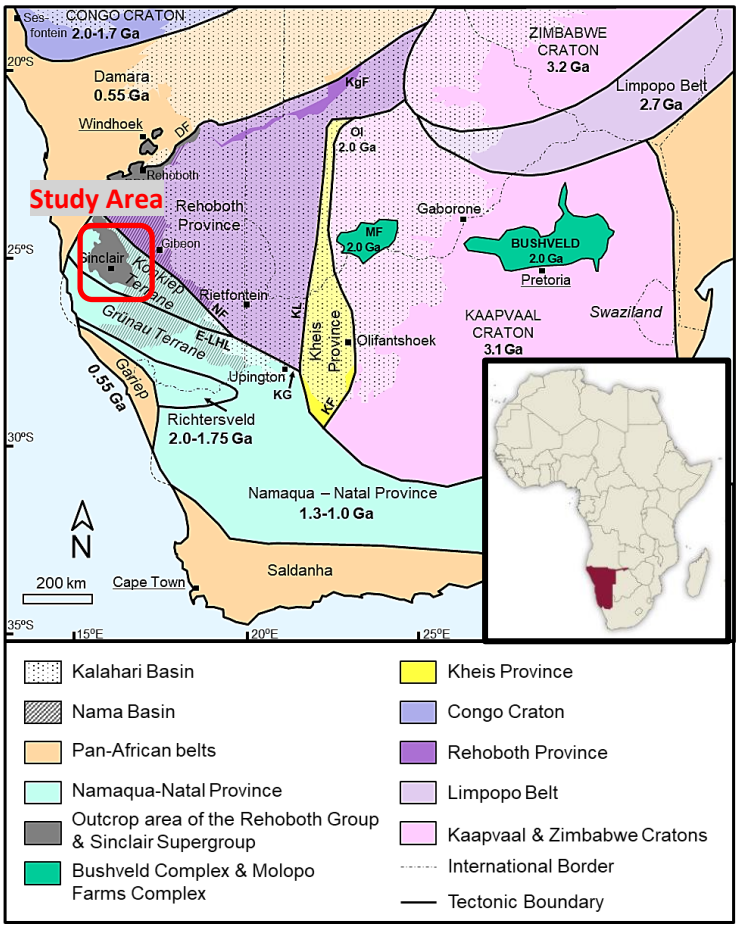

Figure 1-1: Tectonic framework of Southern Africa showing the location of the Palaeoproterozoic Rehoboth Group, the Mesoproterozoic Konkiep Group of the Sinclair Supergroup and cover sediments. Modified after van Schindel et al. (2011).

1.2 Statement of the problem

The Barby Formation in the Sinclair Supergroup is not dated and its geochemistry is not well understood. This research will investigate geochemistry and geochronology of the Barby Formation and therefore ascertain whether or not it indicates subduction in the Sinclair Supergroup.

1.3 Objectives of the study

The objectives of the study are the following:

a) To constrain the geochronological ages of the Barby Formation.
b) To investigate whether the Barby Formation represents a subduction event or collision rift related event using the geochemistry of the lithologies.

1.4 Hypothesis of the study

Subduction zone areas produce distinct rock types and have specific geochemical trends. It is envisaged that the ancient subduction zone in the Sinclair Supergroup represented in part by the Barby Formation also produced rock types similar to those observed elsewhere in the world.

1.5 Significance of the study

This study will provide precise geochronological data for the Barby Formation and improve our understanding of the tectonic setting and regional geology of the Konkiep Terrane.

1.6 Limitations of the study

a) There are limited or no specialized laboratories in Namibia that can be used for geochronology and because of this short coming, geochronological analyses were done in Sweden by the author.

b) Due to financial constraints, only few but representative and sufficient samples can be collected for analysis.

1.7 Delimitation of the study

This study is limited to the Barby Formation in the Konkiep Terrane, Sinclair Supergroup. The previous work done was mainly inconclusive Rb-Sr dates. This study will mainly focus on precise U-Pb geochronology and geochemistry.

2. THEORETICAL FRAMEWORK

2.1 Regional Geology

The Sinclair Supergroup

The regional setting of the Sinclair Supergroup is part of a curvilinear association of the Rehoboth magmatic arc (Becker et al., 2006; Hoal, 1989; Watters, 1974). The Rehoboth magmatic arc, now known as the Rehoboth Province, has ca. 700 km long margins, roughly defining an equilateral triangle (Fig. 1-1) and was a subprovince of the Namaqua-Natal Province (van Schijndel et al., 2014). The Sinclair Supergroup forms part of the Rehoboth Province and the Namaqua-Natal Province in South Africa. The Sinclair Supergroup evolved during the late Precambrian and comprises of a wide variety of high level comagmatic intrusive and volcanic rocks with intercalated clastic sediments (Watters, 1974; Becker et al, 2006; Miller, 2008). The metamorphic basement of the Sinclair Supergroup has been grouped both with the Kheis Group (Von Brunn, 1969) and the Namaqua Metamorphic Complex (Becker, 2006; Miller, 2008). This grouping is partly due to the robust radiometric dates that has better defined the terrane involved.

Watters (1977) viewed the Sinclair Supergroup as having evolved in three cycles, each cycle being initiated by the emplacement of basic magma and terminated by sedimentation (Fig. 2-1). However, Hoal (1989) argues that each cycle is rather initiated by sedimentation, followed by volcano-sedimentary activity, and completed by plutonism which led to the final development of the Sinclair Supergroup. Both these outcomes were based on field and geochemical data with little geochronological data.

The Sinclair Supergroup is subdivided into the Konkiep Group and the Nauzerus and Tsumis Group, which covers the Helmeringhausen-Awasib Mountains-Gamsberg region and extends from Gamsberg to the Botswana border (Miller, 2008). This supergroup ranges from approximately 1400 to 1000 Ma in age (Hoal & Heaman, 1995; Becker et al., 2006). The Mesoproterozoic was a time of major crust generation within a global accretionary event commonly linked to the assembly of the Rodinia Supercontinent (Pattersson et al., 2007).

Rodinia formed at approximately 1.23 Ga by accretion and collision of fragments produced by breakup of an older supercontinent, Columbia, assembled by global-scale 2.1–1.82 Ga collisional events (Dalziel et al., 2000). This accretion of fragments produces what we call mobile belts such Kibaran, Irumide and Namaqua.

2.2 Local geology

The Konkiep Group

"The name Konkiep follows the initial usage by Beetz (1922) since many of the Sinclair rocks in the Helmeringhausen area occur in the upper catchment of the Konkiep River" (Miller, 2008, p. 8-2).

The Konkiep Group is a supracrustal sequence underlain by rocks of the Namaqua Metamorphic Complex (NMC) in the marginal Konkiep Subprovince of the Namaqua Belt (Miller, 2008). The Konkiep Subprovince has a distinctive rough magnetic fabric as seen in the map which is in contrast to the smooth fabric seen in the Rehoboth Province (Corner, 2008). The Konkiep Terrane also has a distinctive magnetic

boundary with the Grünau Terrane of the Namaqua Province, which has lower frequency magnetic variations (Corner, 2008).

The Rehoboth Province is a large domain with approximately 700 km long margins defining an equilateral triangle and was first defined by Hartnady, Joubert and Stowe (1985).

Research conducted by Cornell et al. (2015) have suggested that the crust of the Konkiep Terrane may have originated from the Palaeoproterozoic Rehoboth Province which split during (a) 1360-1330 Ma rift phase of the Namaqua Wilson cycle, followed by (b) ocean basin development to about 1300 Ma. Then (c) subduction began, with arc volcanism creating the Areachap and Kakamas (=Grü-nau) Terrane and the Wilgenhoutsdrif back arc basin from 1300 to 1200 Ma. (d) Several terranes with distinct lithostratigraphy and crustal development histories collided between 1210 and 1200 Ma, assembling the Namaqua-Natal Province which was accreted to the Kalahari.

During the 1210 Ma collision, parts of the accreted Grünau Terrane were thrust over the Rehoboth Province (van Schijndel et al., 2011; van Schijndel et al., 2014). This gave rise to the Konkiep Terrane which is on the western margin of the Rehoboth Province, consisting of pre-tectonic basement overlain by the rocks of the Konkiep Group of the Sinclair Supergroup.

The oldest lithostratigraphic unit in the Konkiep Terrane is the Kairab Formation, this is also the beginning of the first cycle, consisting of bimodal, tholeiitic volcanic rocks and interbedded sedimentary rocks (Becker, 2008; Miller, 2008). The oldest post-

Kairab rocks are the ignimbrites and felsites of the Nagatis Formation which rest unconformably on the Houmoed Granodiorite and older rocks (Von Brunn, 1969; Miller, 2008). Sedimentary rocks of the Kunjas Formation is the end of the first cycle which follow in the Helmeringhausen-Awasib Mountains region (Fig. 2-2). This formation unconformably overlies rocks of the Kairab Formation in the Awsaib Mountains and lies above the Nagatis Formation and Haremub granite in the Helmeringhausen area (Watters, 1974; Von Brunn, 1969; Miller, 2008). The Kunjas Formation consists of conglomerate or grit, feldspathic quartzites, shales and sandstones (Watters, 1974; Von Brunn, 1969; Miller, 2008). The Barby Formation which is the beginning of the second cycle (Sinclair Formation in von Brunn, 1969) overlies the Kunjas Formation conformably to unconformably (Watters, 1974; Miller, 2008) (Fig. 2-1). Lateral equivalent of the Barby Formation is the Haiber Flats Formation in the Awasib Mountains (Hoal, 1989; Hoal & Heaman, 1995). The Guperas Formation rests unconformably on the Barby Formation (Watters, 1974; Miller, 2008) though Becker et al (2006) states that the Guperas Formation disconformably overlies the Barby Formation and the Nubib granite but the location was not stated. The Guperas Formation is the beginning of the third cycle. Redbed succession forms the top of the Sinclair Supergroup (Miller, 2008). The Aubures Formation in the Helmeringhausen area is part of the red bed succession and consists of hematite beds that are red in colour and are included in the Konkiep Group (Watters, 1974 and 1977; Miller, 2008).

The Barby Formation

The Barby Formation is a major volcanic episode of the Sinclair Supergroup within the Konkiep Terrane (Watters, 1974; Becker, 2006). The bulk of the Barby Formation is made up of intermediate, porphyritic lavas and minor intercalated clastic sediments which have been intruded by gabbroic, dioritic and monzonitic bodies which may be similar to the rocks found in the Haiber Flats Formation (Watters, 1974; Brown & Wilson, 1986; Hoal, 1989; Hoal & Heaman, 1995). Most of the units mapped by Watters (1974) are marked as lava flows, with limited intrusive units directly associated with the volcanic activity. Hoal (1993) has suggested that these rocks accumulated in extensional basins that formed as a result of oblique subduction along the convergent margin.

In terms of present day outcrop, volcanic units of the Barby Formation cover a total of about 40 km2 (Watters, 1974). The regional correlation and accurate determination of the Barby Formation has been very difficult due to various contributing factors, such as block-faulting, intense intrusion of the Nubib granite and erosion (Watters, 1974). Lava types tend to form such distinct units that the formation has been subdivided into various units which are termed ‘members’ until such a time that the distribution and stratigraphic limits of each unit making up the Barby Formation can be defined in detail for the Sinclair Supergroup and adjacent area (Watters, 1974, Miller, 2008).

Both the Barby and the Haiber Flats Formation contain calc-alkaline and shoshonitic lavas (Brown & Wilson, 1986; Miller, 2008). The geotectonic setting of this association has been variously interpreted as an ancient active continental margin (Watters, 1974; Hoal, 1987; Miller, 2008), or a collision-related rift (Hoal, 1987).

Miller (2008) reviewed the geochronology of the Konkiep Group in the Sinclair area. Most of the early Rb-Sr ages reviewed by Hoal (as cited in Miller, 2008) seem to be inconclusive due to the Rb-Sr analysis used back in those days. Hoal and Heaman (1995) established a precise conventional U-Pb zircon dates for three granites west of the study area namely; the Aunis Tonalite, Awasib Granite and Chowachasib Granite. The Awasib Granite and Chowachasib Granite which intruded the Haiber Flats Formation, northwest of the Barby Formation is thought to be correlated to the Haiber Flats Formation, giving ages of 1216 ±1 Ma and 1216 ±2 Ma respectively.

In the Konkiep Terrane north of the Sinclair area, Cornell et al. (2015) dated an unmetamorphosed lava or welded tuff of the Welverdiend Formation, thought to be Barby Formation correlated and was dated at 1327 ±10 Ma. Thereon, a geochronological age gap of Barby Formation and mismatching stratigraphic correlation exists between the analysis carried by latter and former authors.

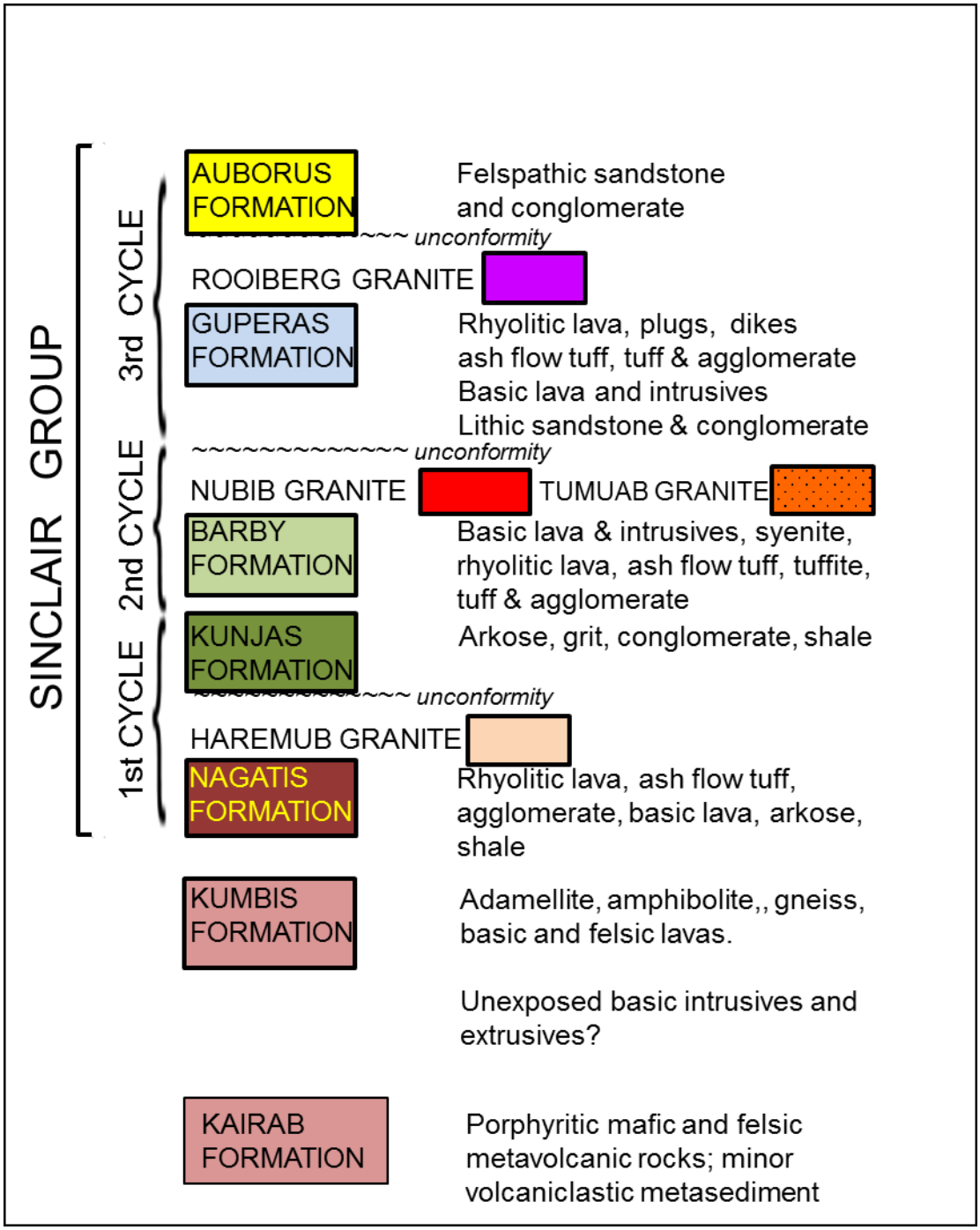

Figure 2-1: The stratigraphic column showing the three evolutionary cycles of the Sinclair Supergroup by Watters, 1974

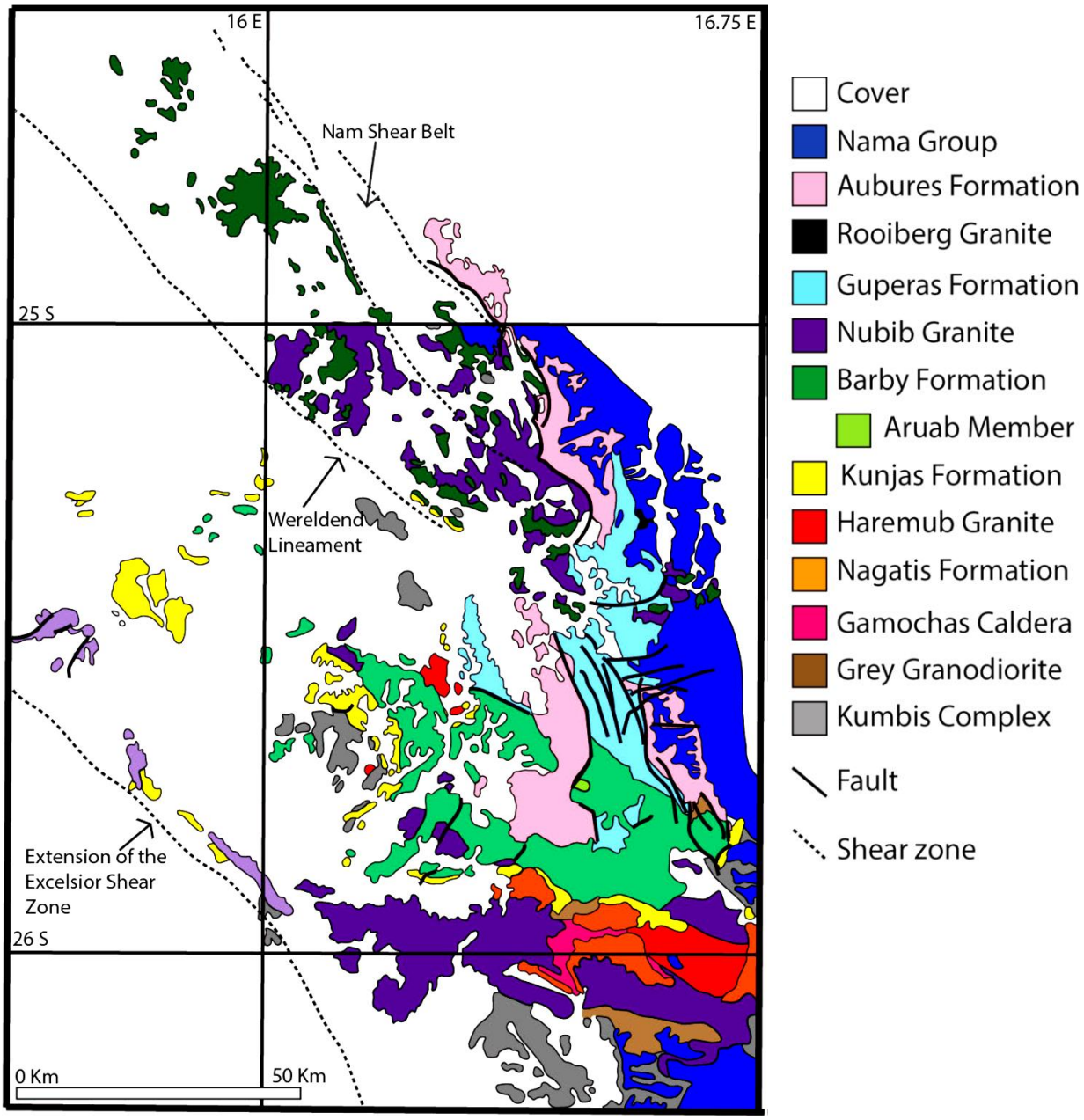

Figure 2-2: Map of the Konkiep Terane midfield from Waters (1974), Von Brunn (1969), Miller (2008)

3. METHODOLOGY

3.1 Research design

The research utilized qualitative and the quantitative generic design. Field work was undertaken. Rocks were collected and each rock was split into two, one for petrographic studies under the microscope for qualitative mineralogical chemical data and one other part was used for quantitative geochemistry data. Another extra sample was picked from the same outcrop for geochronology, if the material was fresh. Field work was planned in such a way that areas that had the best exposures of the Barby Formation units and contacts between the Barby Formation and other Formations and suites were visited. In the first field season, samples were collected from the southern area only. The southern area contains farms; Klein Haremub 1, Aubures 22, Vergenoeg 56, Naus 27 and Barby 26. The second field session, samples were taken from the northern areas only. The volcanics in the northern areas crop out on the farms Nubib West 109, north of Betta 87 and Welverdiend 140

3.2 Research Instruments

The following instruments were used: FRANTZ, Hitachi Scanning Electron Microscope (SEM), laser ablation ICP-MS, secondary ion mass spectrometry (SIMS), XRD, XRF, ICP-MS and ICP-ES.

- FRANTZ- This device used to separate minerals based on their magnetic properties. Minerals fall into one of three magnetic properties: ferromagnetic, paramagnetic and diamagnetic. Ferromagnetic minerals are themselves magnetic (i.e., magnetite and pyrrhotite) and can be easily separated from other minerals with a magnet since they will stick to the poles of the magnet. Paramagnetic and diamagnetic minerals are not magnetic, but they differ in

how they interact with a magnetic field. Paramagnetic minerals are weakly attracted into a magnetic field and diamagnetic minerals are weakly repelled by a magnetic field. Thus, if a mixture of paramagnetic and diamagnetic minerals is passed through a magnetic field, they will be pulled into the field (paramagnetic) or repelled from the field (diamagnetic) and may be separated. Furthermore, paramagnetic minerals with different degrees of paramagnetism can be separated from one another in the same way. The magnetic separator consists of a large electromagnet through which mineral mixtures can be passed on a metal trough which is divided near its exit end. Varying the strength of the magnetic field and/or slope of the separation trough is used to separate minerals.

- SEM- The scanning electron microscope uses a focused beam of high-energy electrons to generate a variety of signals at the surface of solid specimens. The electron beam is scanned in a raster scan pattern, and the position of the beam is combined with the detected signal to produce an image. The signals that derive from electron-sample interactions reveal information about the sample including external morphology (texture), chemical composition, and crystalline structure and orientation of materials making up the sample. In most applications, data are collected over a selected area of the surface of the sample, and a 2-dimensional image is generated that displays spatial variations in these properties. Areas ranging from approximately 1 cm to 5 microns in width can be imaged in a scanning mode using conventional SEM techniques (magnification ranging from 20X to approximately 30,000X, spatial resolution of 50 to 100 nm). The design and function of the SEM is very similar to the

Electron Probe Micro-Analyser (EPMA) and considerable overlap in capabilities exists between the two instruments.

- Laser Ablation ICP-MS- Laser Ablation Inductively Coupled Plasma Mass Spectrometry is a powerful analytical technology that enables highly sensitive elemental and isotopic analysis to be performed directly on solid samples. In LA-ICP-MS, a pulsed laser focuses on and vaporizes a very small amount of a solid sample. The ablated particles are then transported to the secondary excitation source of the ICP-MS instrument for digestion and ionization of the sampled mass. The excited ions in the plasma torch are subsequently introduced to a mass spectrometer detector for both elemental and isotopic analysis.
- SIMS- Secondary-ion mass spectrometry is a technique used to analyse the composition of solid surfaces and thin films by sputtering the surface of the specimen with a focused primary ion beam and collecting and analysing ejected secondary ions. The mass/charge ratios of these secondary ions are measured with a mass spectrometer to determine the elemental, isotopic, or molecular composition of the surface to a depth of 1 to 2 nm. SIMS is the most sensitive surface analysis technique, with elemental detection limits ranging from parts per million to parts per billion.
- XRD- X-Ray Diffraction is a fast analytical technique primarily used for phase identification of a crystalline material. It provides information on crystal structure, phase, preferred crystal orientation (texture), and other structural parameters, such as average grain size, crystallinity, strain, and crystal defects.

- XRF- X-ray fluorescence is a non-destructive analytical technique used to determine the elemental composition of a sample. XRF analysers determine the chemistry of a sample by measuring the secondary X-ray emitted from a sample when it is excited by a primary X-ray source. Each of the elements present in a sample produces a set of characteristic fluorescent X-rays that is unique for that specific element.
- ICP-MS- Inductively Coupled Plasma Mass Spectrometry is an analytical technique used for elemental determinations. ICP-MS can determine low-concentrations (range: ppb) and ultra-low-concentrations of elements (range: ptt).

3.3 Procedures

3.3.1 Sampling

Field work was planned in such a way that areas that had the best exposures of the Barby Formation units and contacts between the Barby Formation and other Formations and suites were visited. In the first field season, samples were collected from the southern area only. The southern area contains farms; Klein Haremub 1, Aubures 22, Vergenoeg 56, Naus 27 and Barby 26. The second field session, samples were taken from the northern areas only. The volcanics in the northern areas crop out on the farms Nubib West 109, north of Betta 87 and Welverdiend 140. A total of 38 samples were collected, 38 samples were for geochemical analysis, 14 samples for

geochronological analysis of which only 4 samples had zircons or baddeleyite and a total of 27 samples were used for petrology.

Figure 3-1: Field images while collecting samples from the Barby Formation, South-west of Helmeringhausen. The images show the various tools used while sampling such as hummer, newspaper, cello tape, notebook and GPS

3.3.2 Laboratory work

Geochronology

The collected sample were crushed and sorted, only the unweathered surface chips were taken for pulverizing. There were two stages for pulverizing the samples: in the first stage, samples were pulverized for 2 minutes and 30 seconds at 1300 rpm and sieved through a 400-micron sieve. The sieved material was for geochronology. The sieved samples were then washed until all the dust was gone. The washed sampled was

then panned to separate the heavy from the light minerals. The panned sample was taken to the FRANTZ machine to separate the magnetic material from the non-magnetic material (Fig. 3-2a). Only the non-magnetic material was used. Zircons were then handpicked under the binocular microscope and placed on a glass plate (Fig. 3-2b). The handpicked zircons were mounted on a puck using epoxy glue. When the epoxy dried up, it was then polished and ready for use in the spectrometer for U-Pb and Lu-Hf analysis.

Figure 3-2: The panned samples were taken to the FRANTZ machine to separate the magnetic material from the non-magnetic material. b) Sample after going through the FRANTZ are then hand-picked under the binocular microscope from the glass plates and placed on a separate glass plate.

The theory of U-Pb zircon dating

There are only a few minerals that are suitable for dating; zircon is one since it is a common, durable mineral that can retain uranium and radiogenic lead. When zircon, ZrSiO4, crystallizes from a melt, small amounts of uranium are generally incorporated into the crystal lattice. After crystallization, this trace uranium starts to decay to stable isotopes of lead. U-Pb zircon ages are calculated using the ratio of the radioactive U parent to daughter Pb. ^{204}Pb is a non-radiogenic isotope incorporated into zircon during the mineral formation, recrystallization or due to contamination during analysis. The 204-isotope is used for common lead corrections, since even small amounts of

common lead will affect the U-Pb ages. Many zircon grains have more than one age domain, i.e. core and rim, as seen in CL-images made by SEM. With the CL detector, zones that contain more uranium appear dark and zones with less uranium bright, with the core (magmatic or xenocryst) often being bright and the rim (metamorphic or magmatic resetting) dark. The zoning is not as evident using a BS detector, although the backscattered images show cracks that should be avoided to obtain data with as low common lead as possible. If a zircon, or age domain in zircon, appears dark in both BS and CL images it is interpreted as being metamict. Metamict zircon has a damaged crystal lattice caused by uranium decay, and is not suitable for dating. To interpret the data from the ICPMS analyses, a program producing concordia and discordia plots is used. In a concordia diagram, the $^{207}Pb/^{235}U$ ratio is plotted along the abscissa and $^{206}Pb/^{238}U$ along the ordinate axis, the concordia curve representing spots with equal ages in both systems. The curvature is due to the different half-lives of the two uranium isotopes (Rollinson, 1993). Zircon data that do not plot on the concordia curve are discordant, usually indicating lead loss. If discordant points define a discordia line which intersects the Concordia curve at two places, you can see when the lead loss occurred. The upper intercept of the discordia line represents the formation age of the zircons and the lower intercept shows the age of the lead loss event. Discordia calculations may be difficult for sedimentary rocks or samples containing xenocrysts with different ages, and in this case concordia or Pb-Pb age calculations for individual grains are made. For both discordia and concordia calculations, the Mean Sum of Weighted Deviates (MSWD) should be lower than 2.0 and probability greater than 0.16.

Lu/Hf dating and source magma determination

Lu/Hf is a geochronometer based on the parent-daughter ratio between lutetium and hafnium. In the isochron approach $^{176}Hf/^{177}Hf$ and $^{176}Lu/^{177}Hf$ are plotted on the y- and x-axis respectively in a diagram and the spots form a straight line called an isochron. The isochron slope shows the age of the system since it became closed e.g. crystallization of magma. Another method is to plot εHf units against U/Pb ages for individual zircon grains to try to define a $^{176}Lu/^{177}Hf$-dependant slope for material after mantle extraction, and the time of mantle extraction. An alternative method is to plot $^{176}Hf/^{177}Hf$ instead of εHf against U/Pb ages. In the two latter methods, model evolution lines for CHUR (Chondrite Uniform Reservoir) and DM (Depleted Mantle) along with probable slopes for granitic or mafic crust are plotted, following Schersten (personal communication with David Cornell 2016). These two methods are used to determine source magma composition as well. The model slopes are compared with the slopes that measured data produces, to see the composition directly after mantle extraction. The intersection between the measured model slope and the CHUR or DM models defines the age of mantle extraction, depending on which type of mantle was involved. The Lu/Hf isotopic evolution of the mantle through time can be calculated (Appendix C). During partial melting of the mantle to produce basalt, hafnium is the more incompatible element, so in the melt you will get more Hf and thus a lower Lu/Hf ratio. The remaining mantle becomes depleted and will have a higher Lu/Hf ratio than the chondritic value, calculated for the once uniform bulk silicate earth (Kinny and Maas, 2003). The use of Lu/Hf data has a great advantage compared to its counterpart in e.g. Sm/Nd, because the $^{176}Hf/^{177}Hf$ ratio of a zircon shows the ratio of the source when the zircon formed and can be related to a source which had the same ratio at a

specific time, giving a model age (Scherer et al. 1997). Thus you can see when the sample could have been derived from CHUR or depleted mantle.

Rb-Sr dating by LA-ICPMS/MS

Large igneous biotites were found in the Spes Bona syenite sample which enabled us to apply the microbeam Rb-Sr method recently developed for laser ablation collision cell ICPMS by Zack and Hogmalm (2016). The method allows simultaneous measurements of Rb and Sr isotopes in an ICP-MS fitted with two quadrupoles and a collision/reaction cell sandwiched in between Agilent 8800 and Agilent 8900 ICP-MS. It has been demonstrated that Sr ions react efficiently with reactive gases such as O_2, N_2O and SF_6 forming molecules of SrO^+ and SrF^+ respectively while rubidium does not react at all (Zack & Hogmalm, 2016; Hogmalm et al., 2017). In this study the N_2O was used as the ICP-MS reaction gas with a 50 µm laser spot size and analyzed Sr isotopes as SrO^+ and therefore avoided the isobaric overlap between ^{87}Rb and ^{87}Sr. Note that the recently modified ^{87}Rb decay constant of $1.3972 \pm 0.0045 \times 10^{-11}$ was used following Villa et al. (2015), rather than the $1.42 \pm 0.01 \times 10^{-11}$ a value which has been used for the past 40 years. The data was reduced by examining the time resolved spectra manually. In order to avoid calibration problems for pulse/analog factors for mass-shifted masses in the ICP, concentrated matched standards for each mineral analysed was used. Minerals with a high concentration of Rb and low concentration of Sr (biotite) were quantified using Mica-Mg (Hogmalm et al., 2017) minerals high in both Rb and Sr (K-feldspar) were quantified using the standard NIST SRM610 (Woodhead & Hergt, 2001; Wise & Watters, 2012) and minerals low in both Rb and

high in Sr (apatite and plagioclase) were quantified using the standard BCR-2g (Elburg et al., 2005).

Geochemistry

Thirty-eight samples were prepared for geochemical analysis. Samples were prepared at the Geological survey of Namibia and analysed at ALS Sweden and at the University of Stellenboch. The sample localities are shown in figure. The sample was pulverized at the speed of 1300 rpm for 4 min. This pulverized material was used for whole rock geochemistry where the XRF was used for Major elements and the ICP-MS for trace elements (Appendix B). There are more samples for geochemistry than those for geochronology.

The elements Ba, Ce, Cr, Cs, Dy, Er, Eu, Gd, Hf, Ho, La, Lu, Nb, Nd, Pr, Rb, Sm Sr, Ta, Tb, Th, Tm, U, V, Y, Yb, Zr were determined by Inductively Coupled Plasma (ICP) Mass Spectrometry, whereas Al_2O_3, Fe_2O_3, K_2O, MgO, CaO, MnO, P_2O_5, SiO_2, TiO_2, Na_2O have been determined by X-Ray Fluorescence.

4. RESULTS

4.1 Introduction

This chapter outlines the researcher's findings based on the field and analytical observations that were done in the study area. Petrographic, geochemical and geochronological studies were done to give more support on the hypothesis that was made. A total of thirty samples were collected, thirty samples were for geochemical analysis and fourteen samples were for geochronological analysis of which only four samples had zircons or baddeleyite. A total of twenty-seven samples were used for petrology.

4.2 Field Work

. Field work was planned in such a way that areas that had the best exposures of the Barby units and contacts between the Barby units and other units were visited (Fig 4-1). The Barby stratigraphic units observed on the Barby Farm show three flow cycles (Fig 4-2). These three flows cycles can be observed starting from the southernmost part of the Barby farm going in a north-west direction. The flow cycles start with a basal unit of a porphyritic coarse to medium grained rhyolite or sometimes tuff. The flow overlying the basal flow cycle is a medium grained basalt with disseminated plagioclase phenocrysts, this middle flow is where we find the shoshonite rocks and the unit at the top is a fine-grained basalt which is found at the Vergenoeg Farm.

In the first field session, samples were collected from the southern area only. The southern area contains farms; Klein Haremub 1, Aubures 22, Vergenoeg 56, Naus 27

and Barby 26 (Fig 4-1). The second field session, samples were taken from the northern areas only. The volcanics in the northern areas crop out on the farms Nubib West 109, northern Betta 87 and Welverdiend 140, Saffier 148 and Aandster 147(Fig 4-1).

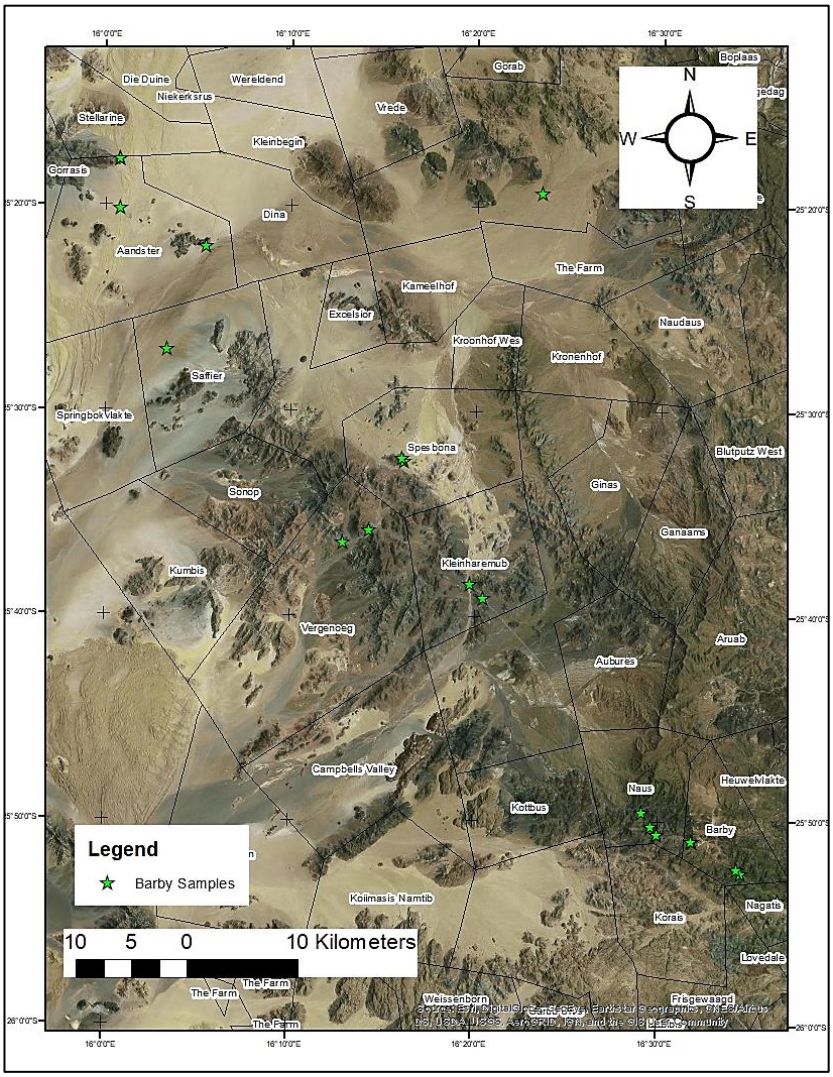

Figure 4-1: Google Earth image showing the localities of the samples collected in different farms. There are Thirty samples collected for geochemistry (duplicated in some area), which include fourteen samples for geochronology and twenty-seven hand specimens for petrography.

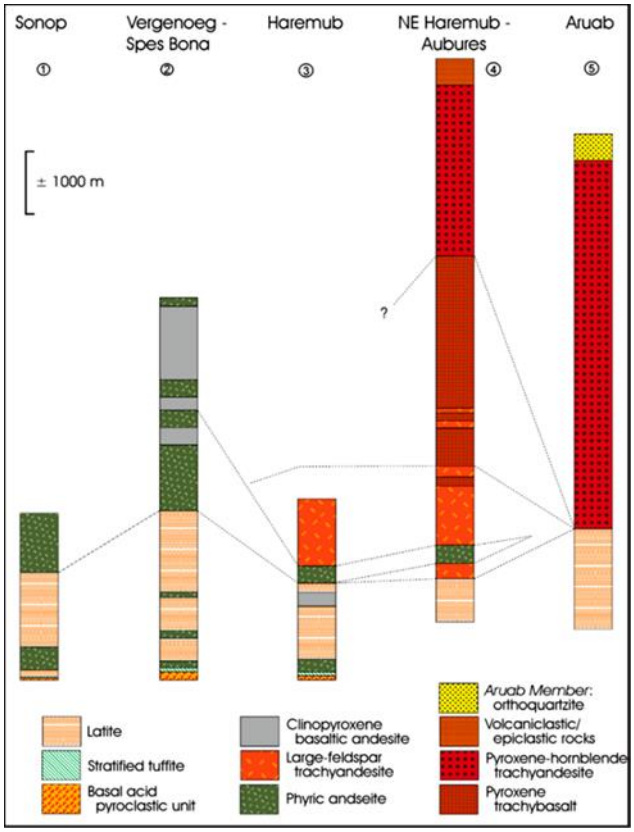

Figure 4-2: The stratigraphic profile of the Barby Formation. This profile is found in the Barby area showing the rock units found in each evolution flow cycle of the Barby Formation. Modified after Miller, 2008.

4.2.1 Southern Region

Basal pyroclastic volcanics

Field description:

This unit is seen on Klein Haremub Farm and Aruab Farm. The base of this unit is the first pyroclastic flow which is directly overlying the Kunjas sedimentary rock. The felsic tuffs are the main rock types with minor lava flows. This felsic tuff is pyroclastic with lithic fragments (Fig. 4-3). The lithic fragments composed of cryptocrystalline felsite not more than 5cm in size. The colour of the rock is pale red-brown on the weathered surface and dark red-brown on fresh surfaces. The groundmass is very fine for mineral identification. The felsic lava flows are fine-grained with a porphyritic

texture. Both the felsic tuff and felsic lava flow contain plagioclase laths and quartz amygdales (Fig. 4-3). A rather inconspicuous planar flow banding is generally present in these units. There are stockworks of quartz veins indicative of multiple hydrothermal events. Epidote is present on joint planes and in amygdales.

Figure 4-3: Photograph of the Basal pyroclastic unit. a) The felsic tuff with small lithic fragments, this unit is in contact with the Kunjas sandstone on Klein Haremub Farm. b) Felsic lava flow with plagioclase laths and quartz amygdales on Aruab Farm.

Petrography:

In thin section, the rock groundmass is devitrified and cryptocrystalline. Phenocrysts of quartz (8 %), orthoclase (3%) and plagioclase (<1%) are observed. Quartz and orthoclase phenocrysts have embayment textures. Subhedral plagioclase laths (An33-35) up to 4 mm long, generally in glomeroporphyritic clusters, and accessory amounts of anhedral to euhedral opaque ore grains up to 1 mm across are the only phyric phases present. Almost 10 % of the rock has suffered varying degrees of saussuritisation. Chlorite is a minor to accessory component that replaces plagioclase.

Phyric andesite lava

Field description:

This lava is found east of Klein Haremub Farm and in the Naus-Barby area. This unit is the transition point from the first flow cycle to the second flow cycle. The lava forms flows up to 250m thick. Small plagioclase phenocrysts and fewer clinopyroxene (cpx) phenocrysts ranging from 1 mm to 2mm are distinctive in this unit. The phenocrysts make up about 55% of the rock volume. The porphyritic character is very well displayed on the weathered surface where the plagioclase is washed out white and the ferromagnesian minerals are a rusty red colour (Fig. 4-4). There are minor mafic clasts. All clasts have a size from 2 mm to 6 mm in a fine-grained matrix. Amygdaloidal texture is sometimes seen, and the amygdales are composed of quartz. This unit has flow banding and the phenocrysts are elongated along the flow banding.

Figure 4-4: Photograph of the phyric andesite lava. The porphyritic character is very well displayed on the weathered surface where the plagioclase is washed out white.

Petrography:

In thin section, the fine-grained groundmass is made up of albite (40%), clinopyroxene (25%), quartz (20%), K-feldspar (10%), actinolite (3%), chlorite (2%) and Fe-Ti oxides (<1%). Dominant textural features are phenocrysts of plagioclase, clinopyroxene (clinopyroxene) and olivine (Fig. 4-5A). The plagioclase phenocrysts (37%) are tabular shaped and the crystals range from 0.5 mm to 10 mm long. Glomeroporphyritic aggregates are fairly common (Fig. 4-5B). Seen in thin section, polysynthetic twinning in the albite is universal. Phenocrysts of clinopyroxene measuring up to 0.5 mm. The clinopyroxene phenocrysts show zoning and twining (Fig 4-5C). Embayment of the clinopyroxene is visible with slight flow texture. Replacement texture of the clinopyroxene by the amphibole. The shape of clinopyroxene and the cleavage is that of an amphibole (Fig 4-5D). The olivine is altered only residue of Fe-oxide is present. Fe-Ti oxides are mostly seen with these olivine phenocrysts and also seen within the olivine veins cross cutting the rock unit. Amygdales are composed of quartz, actinolite and sometimes epidote. The actinolite grains are in the shape of clinopyroxene. This unit is metamorphosed to lower greenschist facies

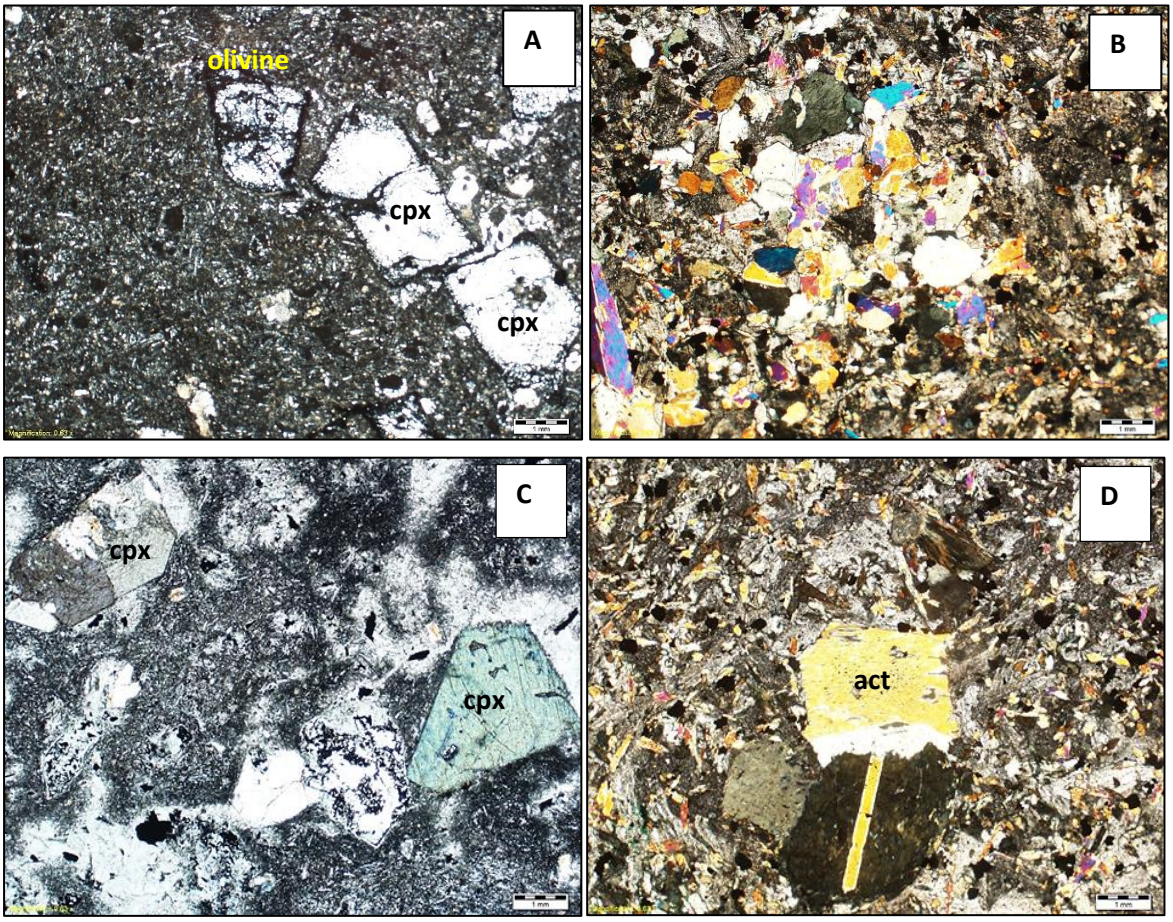

Figure 4-4: Mineral assemblage and textural relationships in the phhyric andesite lava. A) Phenocrysts of cpx and olivine in an aphanitic groundmass. B) Glomeroporphyritic aggregates are fairly common in this unit. C) The clinopyroxene phenocrysts show zoning and twining. D) Replacement texture of the clinopyroxene by the amphibole. The shape of cpx and the cleavage is that of an amphibole.

Felsic agglomerate

Field description:

This sample was taken from the farm Vergenoeg. It is from the lower rhyolite and agglomerate member. This unit belongs to the middle flow cycle. The outcrop of this unit is dark red in colour with felsic clasts that are elongated and visible at outcrop scale. There are no structures seen at this outcrop location. The rock type is very poorly sorted and contains both basic and felsic clasts in a fine mafic groundmass. The basic

clasts are tabular in shape whereas the felsic clasts are elongated, showing the initial stage of melt flowing (Fig. 4-6A).

Petrography:

The groundmass consists of quartz (30%), k-feldspar (10%) and plagioclase (8%). The clasts are angular to sub rounded. The clasts of basaltic lava are altered and contain phenocrysts of plagioclase and ferromagnesian minerals. This rock contains minerals such as quartz, altered plagioclase to sericite, K-feldspar, chlorite, calcite and opaque minerals. Embayment texture is seen mainly in feldspars (Fig. 4-6B). This sample was panned for geochronology but no zircons were found.

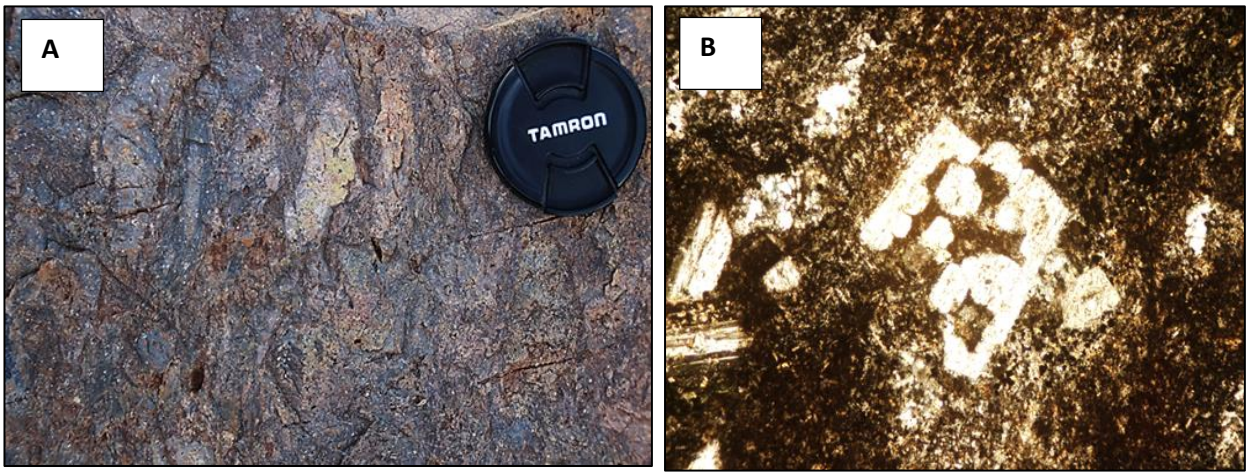

Figure 4-5: Photograph of the felsic agglomerate. A) Felsic elongated clasts in a fine mafic groundmass. The felsic clasts are elongated, showing the initial stage of melt flowing. B) Embayment texture is seen mainly in feldspars.

Large-feldspar trachyandesite

Field description:

This unit is found on Spes Bona Farm and Naus-Barby Farm. This unit has a characteristic appearance of subeuhedral to euhedral rhombohedral phenocrysts of plagioclase up to 55% of the total rock volume (Fig. 4-7A). The plagioclase

phenocrysts are pale green measuring up to 2cm in length and set in a grey aphanitic groundmass (Fig. 4-7B). On weathered surface the phenocrysts are white and the groundmass pale red-brown in colour. The rock texture is porphyritic with phenocrysts of plagioclase, feldspar, clinopyroxene, olivine, magnetite and ilmenite. The phenocrysts are sparsely distributed with irregular vesicles of different size. The vesicles are sometimes filled with epidote and quartz. This unit is about 100m thick and dips at 37° to the east.

Petrography:

In thin section, the rock unit is porphyritic with phenocrysts of plagioclase (85%) and clinopyroxene (10%). This rock unit contains minerals such as: plagioclase (45%), clinopyroxene (10%), olivine (2%), feldspar(2%), zeolite(<1%), epidote (1%) and pyrite (<1%) The plagioclase crystal form is subhedral to euhedral. The plagioclase phenocrysts are unzoned but occasionally contain a thin rim of k-feldspar which grades into the groundmass. There is embayment in the plagioclase crystals and also twinning (Fig. 4-7C & D). The plagioclase found in this unit is mainly alibite, oligoclase and andesine (An_7 to An_{28} SEM-EDS analysis. The clinopyroxene phenocrysts are altered to pale green fibrous chlorite and epidote. The crystal form varies from anhedral to euhedral and display embayment. The embayment in crystals indicate partial resorption. All olivine phenocrysts are completely altered to serpentine and opaque minerals. The association of calcite, quartz, chlorite, albite and epidote in parts of the rock whereas other parts retain their calcic plagioclase, olivine and clinopyroxene suggest deuteric alteration and not metamorphism.

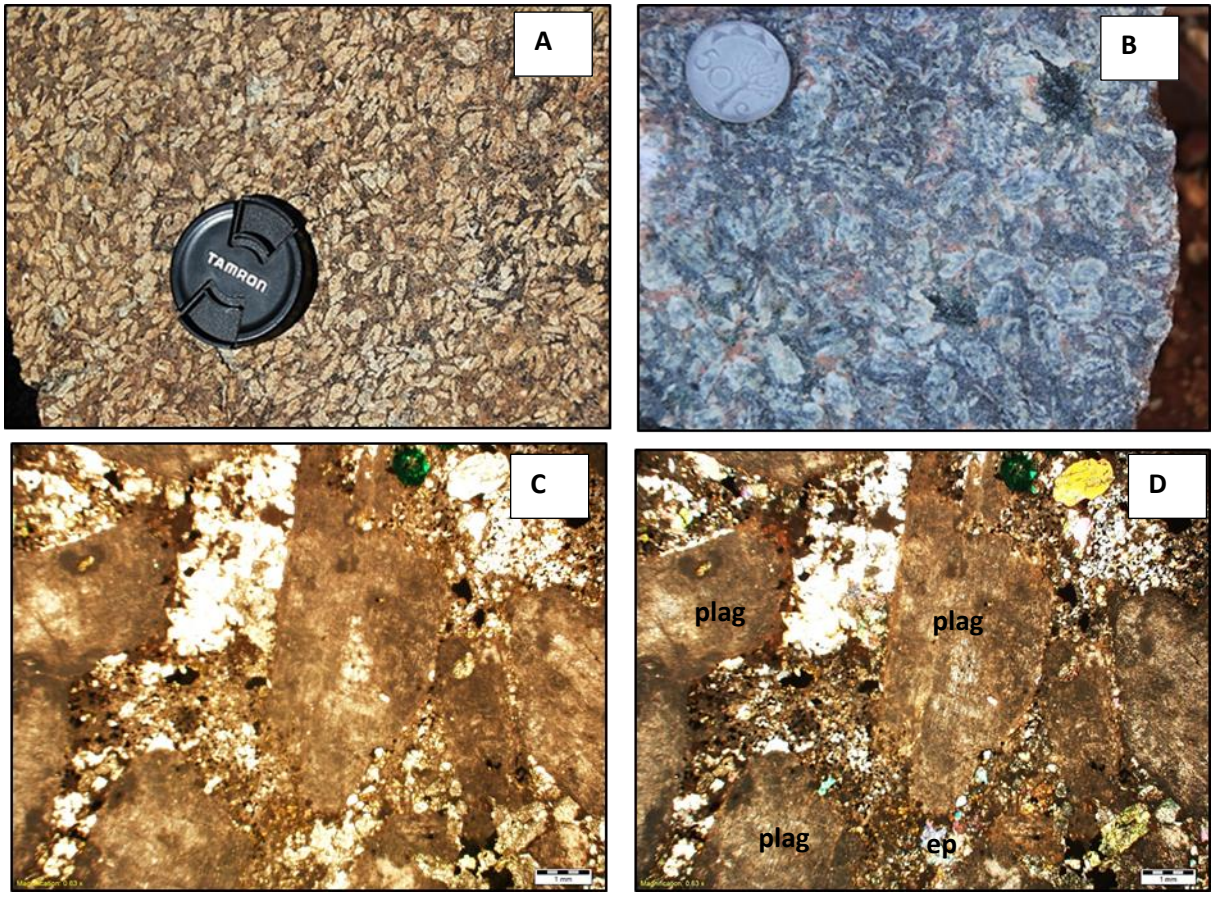

Figure 4-6: Photograph of the Large-feldspar trachyandesite. A) On weathered surface the phenocrysts are white and the groundmass pale red-brown in colour. B) The plagioclase phenocrysts are pale green measuring up to 2cm in length and set in a grey aphanitic groundmass. C and D) There is embayment in the plagioclase crystals. Images showing PPL (C) and XPL (D).

Clinopyroxene basaltic andesite

Field description:

The clinopyroxene basaltic andesite is greenish in colour and has a spotted appearance due to the presence of dark green phenocrysts of altered pyroxene. This unit found on Naus Farm. The outcrop unit is brownish in colour with clinopyroxene phenocrysts of about 1 to 2 mm long. The groundmass is fine grained. This unit belongs to the middle low cycle. Phenocrysts are distinctly rounded and show a faint flow lineation within the groundmass. Amygdales are present, but very small in size.

Petrography:

In thin section, the clinopyroxene minerals are embayed and simple twining is observed. The clinopyroxene crystal form is anhedral to subhedral, indicative of possible resorption. The clinopyroxene is strongly altered to amphiboles, opaque minerals and minor epidote. There are secondary chlorite veins visible and opaque minerals. Remnants of olivine are seen of what is now Fe-oxide which is found at the edge of the olivine mineral that has been altered to Fe-oxides. Zeolite is observed close or within plagioclase grains (Fig. 4-8). Amygdales maybe present are composed of quartz, calcite and minor epidote. The groundmass is cryptocrystalline and has a poorly defines politaxitic texture of plagioclase laths (Fig. 4-8).

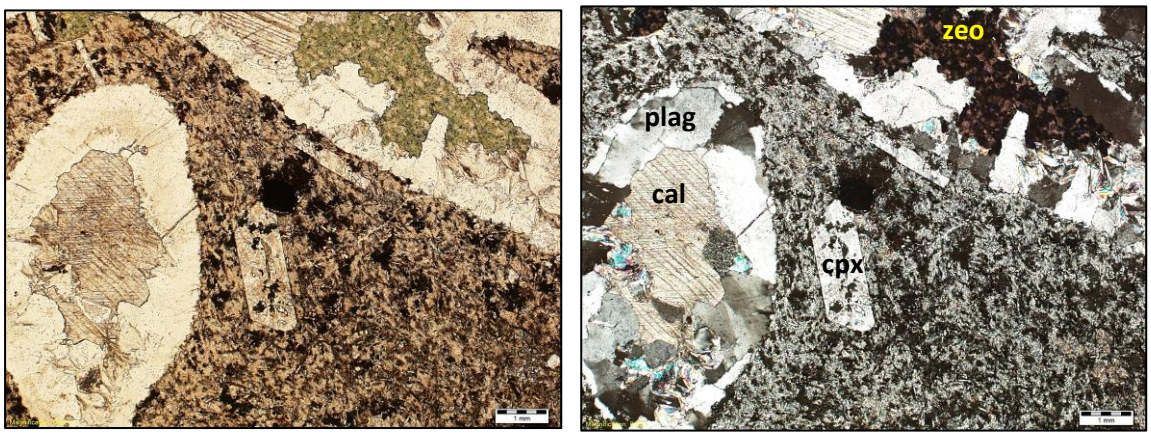

Figure 4-7: Mineral assemblage of the clinopyroxene basaltic andesite. The image shows the politaxitic texture and the amygdale that is composed of quartz, calcite and epidote. The image on the left is in PPL and on the right it is in XPL.

Barby Basalts
Field description:

This unit is found on the NamibRand Nature Reserve. The rock unit is found in contact with the Saffier syenite. The basalt is found as a xenolith in the Saffier syenite outcrop. The colour of the fresh surface is greenish and a brownish weathered surface. This basalt has olivine phenocrysts in fine-grained groundmass. The garnet bearing basalt is found at the base of the mountain. The outcrop on surface has a brown colour and has a dark grey-green colour on the fresh surface. The basaltic rock unit contains garnet phenocrysts in fine grained mafic groundmass. This unit is closed to a basalt unit which contains no garnet. This unit belongs to the top flow cycle.

Petrography:

The groundmass mostly contains albite and altered plagioclase to sericite and clustered olivine and clinopyroxene grains (Fig. 4-9). The olivine and the garnet grains are both altered leaving behind only Fe-oxides. Opaque minerals are found in the groundmass as phenocrysts. The clinopyroxene is zoned. The plagioclase is albite with polysynthetic twinning. The garnets are subeuhedral to euhedral with fractures and embayment (Fig. 4-9); there is a sericite rim around the garnet grains which are associated with plagioclase altered to sericite and biotite grains. The birefringe colour is up to 2nd order on the Mc Levy chart. The garnet mineral is almadine. The rock has a glomeroprophyrytic texture.

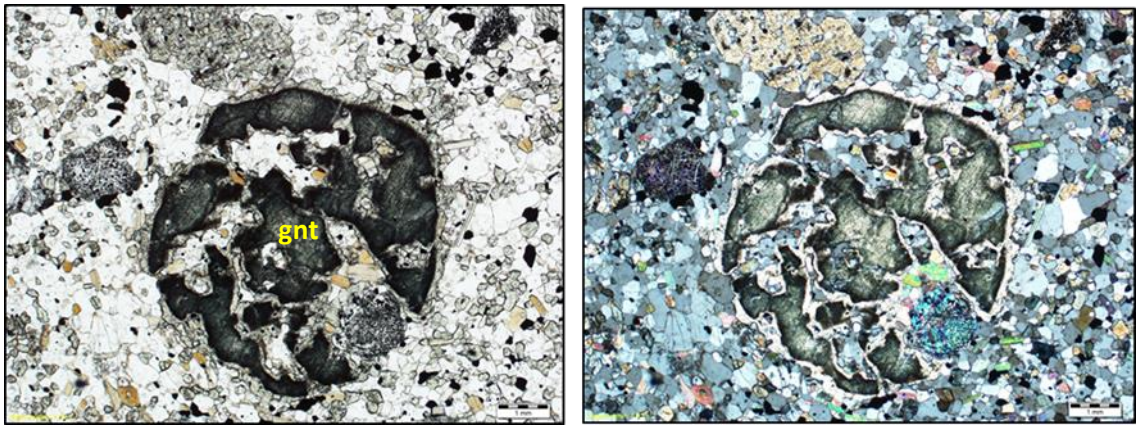

Figure 4-8: Mineral assemblage of the basalt unit found in the northern part. The garnet bearing basalt contains garnet phenocrysts. The garnets are subeuhedral to euhedral with fractures and embayment.

Saffier Intrusive Suite

Field description:

The Spes Bona syenite forms a large intrusion north of the main Barby Formation exposures which it intrudes. This unit is found between the Spes Bona Farm and Gorrasis Farm. The syenite body forms several large but scattered outcrops which suggest that it was emplaced by a single intrusion. The syenite is a very distinctive, coarse-grained grey rock displaying hypidiomorphic granular texture (Fig. 4-10A). The rock contains alkali feldspar (70%), plagioclase (16%), olivine (7%), clinopyroxene (1%) and accessory minerals: apatite and baddeleyite. The rock has been altered, evidenced by the olivine being partially replaced by talc and the clinopyroxene by chlorite. Mafic xenoliths are seen which are generally dioritic or gabbroic in composition.

Petrography:

The Spes Bona syenite in thin section has large anhedral to subhedral crystals of Carlsbad twined bead perthite. The k-feldspar makes up 85 % of the rock. Plagioclase

is also present making 9% of the rock, the crystals are subhedral to euhedral. The composition of the plagioclase is in the andesine range. Frequently the crystals have twin lamellae and wavy extinction (Fig. 4-10B). The clinopyroxene is unzoned subhedral and sometimes twinned. Biotite occurs anhedral to subhedral, prismatic or basal sections and is clearly associated with the opaque minerals, usually enveloping them.

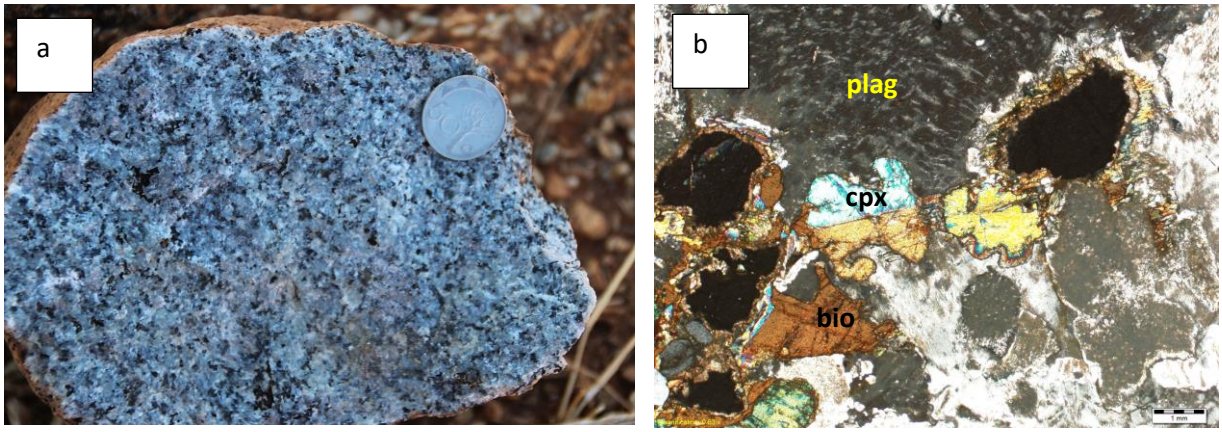

Figure 4-9: Photograph of the syenite. A) The syenite is a very distinctive, coarse-grained grey rock displaying hypidiomorphic granular texture found on Spes Bona Farm. B) Microscopic image of the plagioclase showing the wavy extinction and the twinning in cpx.

Saffier dolerite

Field descriptions:

This unitis found on NamibRand Nature Reserve at 25°20.145'S/ 015°53.432' E. This dyke cross cuts a felsic unit (Fig. 4-10a). The dyke is only found on the eastern side of the hill about 15m wide and 2 km long. The dyke strikes in a north-northeast direction. In hand sample this unit is intermediate; medium to coarse grained and contains plagioclase, clinopyroxene, pyrite, biotite and olivine.

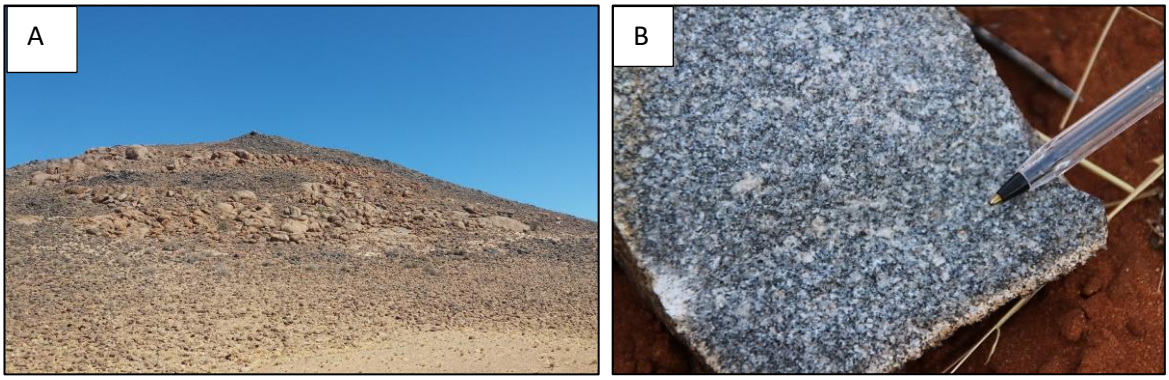

Figure 4-10: The dyke is only found on the eastern side of the hill about 15m wide and 2 km long.

Petrography:

The groundmass contains mostly of altered plagioclase and zoned clinopyroxene. The opaque minerals are surrounded by biotite rims. The same minerals in the groundmass are found as phenocrysts, only that the groundmass consists of mostly plagioclase whereas the clinopyroxene is the dominant phenocryst mineral. The plagioclase is altered to sericite though there are some grains that are preserved showing the twinning.

4.2.2 Northern Region

Basal pyroclastic volcanics

Field description:

This unit was found on Betta farm. This unit is found on a prominent hill and at the base there is the Kunja's sediments. The Kunjas unit which is found just at the base of the Barby units is a grey quartzite with cross-bedding. There is a visible fault that

cross-cuts the Kunjas Formation and Barby Formation. The outcrop contains quartz veins that came in after the rock formation. The pale red-brown rhyolitic ash-flow consists of the main minerals quartz, K-feldspar and plagioclase. The rock unit contains mafic clasts (Fig. 4-11). The clasts are angular and others are rounded. The clasts decrease in number as we go higher up the hill. At this hill one gets a good stratigrahic profile of the Barby Formation, starting from the bottom flow although to the top flow. There is a slight flow texture observed at outcrop and hand specimen scale. The groundmass is homogeneous lava.

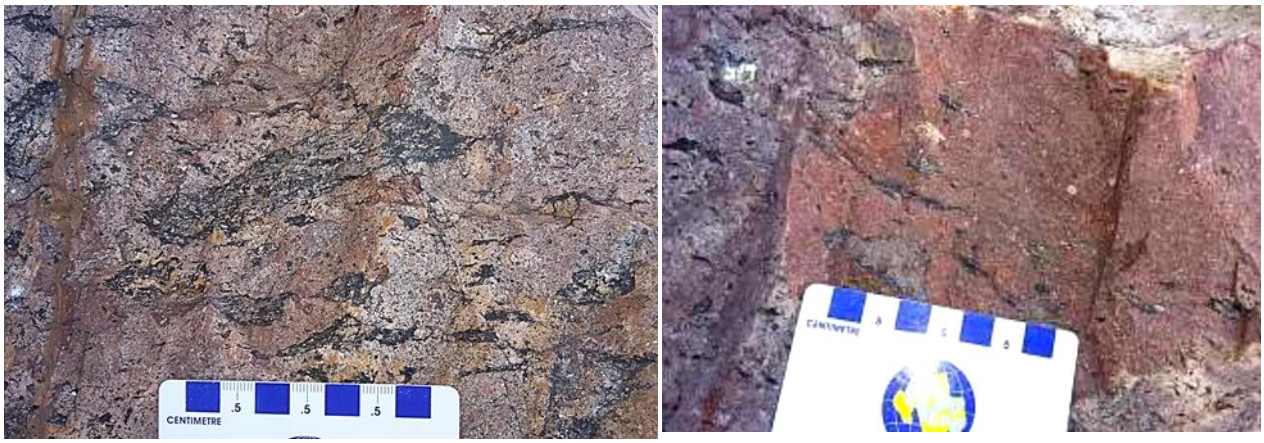

Figure 4-11: Photograph of the northern basal pyroclastic unit. The pale red-brown rhyolitic ash-flow consists of the main minerals quartz, K-feldspar and plagioclase. The rock unit contains mafic clasts.

Petrography:

In thin section, the northern basal pyroclastic unit contains phenocrysts of quartz (8 %), orthoclase (3%) and plagioclase (<1%). The orthoclase is finely perthitic with Carlsbad twinning. The rock unit contains accessory minerals such ilmenite and apatite. The plagioclase phenocrysts have embayment textures. No glomeroporphyritic clustering is present. The rock unit is strongly altered to saussurite.

Large feldspar trachyandesite

Field description:

The sample was taken on Nubib Farm and forms the middle section of the flow cycle. At this outcrop two facies were seen: plagioclase rich facies and a clinopyroxene rich facies. The porphyritic basalt which is plagioclase rich has plagioclase phenocrysts measuring up to ±5 mm in length. The phenocrysts make up 60-70% of the rock volume and have no preferred orientation. There are k-feldspar veins that are ±1 mm wide and cross-cut the rock. This rock sample contains minerals such as: plagioclase, clinopyroxene, olivine, k-feldspar, biotite, chlorite, epidote and pyrite. The rock is massive and jointed. This rock unit is a xenolith in a granitic body, the Nubib granite (Fig 4-12).

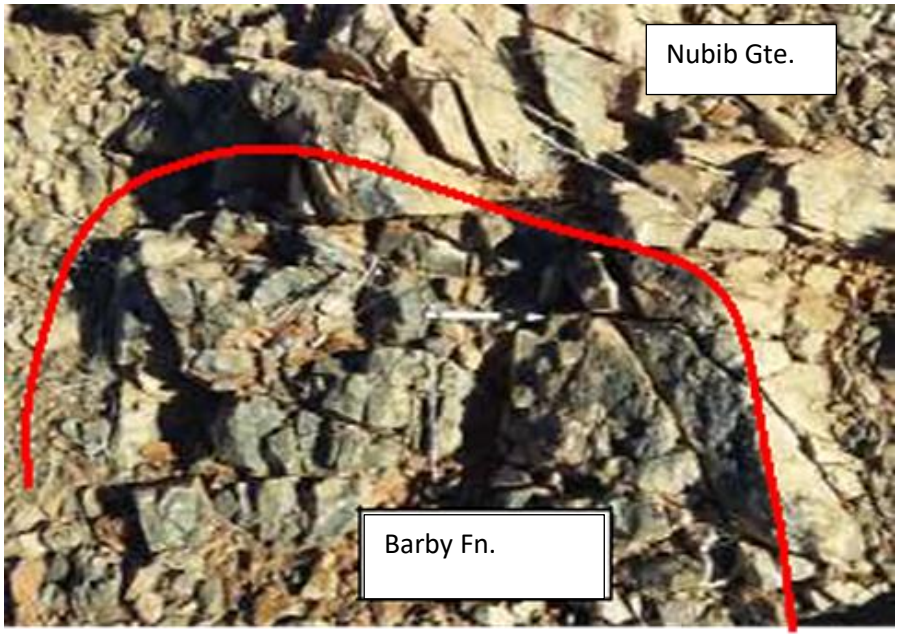

Figure 4-12: Photograph of the large feldspar trachyandesite showing the rock is massive and jointed. This rock unit is a xenolith in a granitic body, the Nubib granite.

Petrography:

Most of the clinopyroxene has been replaced by chlorite but its shape is still retained. The fine-grained groundmass contains minerals similar to that of the phenocrysts. The plagioclase and the k-feldspar in the groundmass are both altered, though sometimes twinning is present and the shape is preserved (Fig. 4-13). The texture observed is glomeroporphyritic. Amygdales are present and they are composed of quartz, acicular amphibole and occasionally epidote.

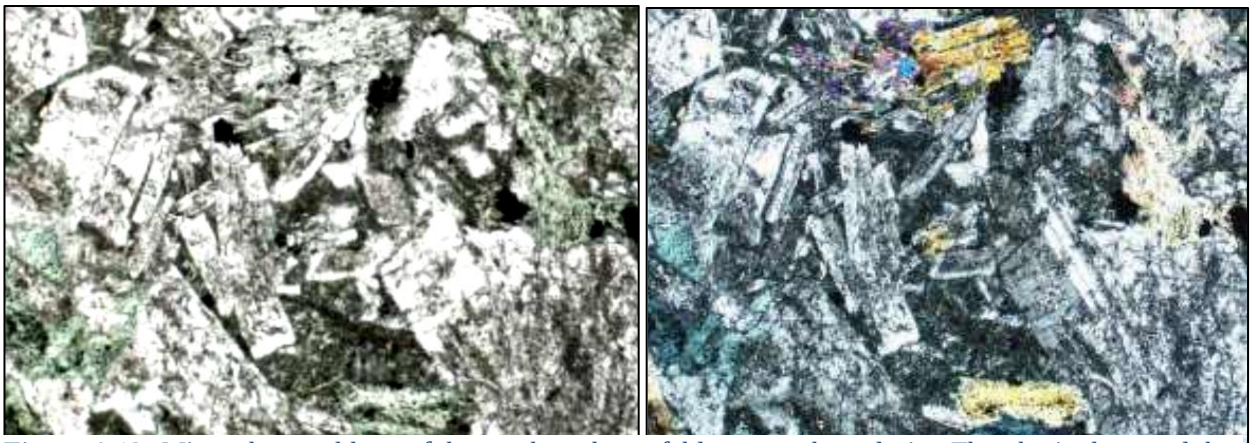

Figure 4-13: Mineral assemblage of the northern large feldspar trachyandesite. The plagioclase and the k-feldspar in the groundmass are both altered, though sometimes twinning is present and the shape is preserved. The images show PPL and XPL images.

Table 1: List of the rock samples collected from outcrops during field work

Sample ID	Lat deg	lat min S	Lon deg	Lon Min E	Unit	Lithology
Northern Samples						
DC 1677	25	2.729	16	5.617	Barby Fn.	Large-feldspar trachyandesite
DC 1678	25	2.841	16	5.619	Barby Fn.	Large-feldspar trachyandesite
DC1698	25	50.969	16	31.887	Barby Fn.	Large-feldspar trachyandesite
DC1709	25	18.212	16	23.371	Barby Fn.	Large-feldspar trachyandesite
DC1710	25	19.864	16	20.599	Barby Fn.	Basal pyroclastic volcanic
Southern Samples						
DC1533	25	35.869	16	14.336	Barby Fn.	Agglomerate
DC1535	25	36.474	16	12.926	Barby Fn.	Basal pyroclastic volcanic
DC1538	25	39.145	16	20.523	Barby Fn.	Phyric andesite lava
DC1540	25	32.473	16	16.164	Barby Fn.	Large-feldspar trachyandesite
DC1541	25	32.34	16	16.081	Spes Bona	Saffier syenite
DC1655	25	53.843	16	36.614	Barby Fn.	Phyric andesite lava
DC1656	25	52.521	16	34.588	Barby Fn.	Large-feldspar trachyandesite
DC1657	25	52.371	16	34.337	Barby Fn.	Large-feldspar trachyandesite
DC1658	25	50.993	16	31.931	Barby Fn.	Large-feldspar trachyandesite
DC1659	25	38.464	16	19.797	Barby Fn.	Phyric andesite lava
DC1664	25	17.742	16	0.781	Barby Fn.	Basalt
DC1695	25	49.566	16	29.199	Barby Fn.	Basal pyroclastic volcanic
DC1695					Barby Fn.	Basal pyroclastic volcanic
DC1696	25	50.275	16	29.685	Barby Fn.	Clinopyroxene basaltic andesite
DC1697	25	50.657	16	30.018	Barby Fn.	Clinopyroxene basaltic andesite
DC1699	25	19.389	15	58.568	Saffier	Saffier syenite
DC16-100	25	19.317	15	23.549	Barby Fn.	Basalt
DC16-101	25	20.145	15	0.786	Barby Fn.	Saffier dolerite
DC16-102	25	17.739	16	0.786	Barby Fn	Basalt
DC16-112	25	27.062	16	3.328	Saffier	Saffier syenite
DC16-113	25	22.015	16	5.442	Saffier	Saffier syenite
DC1714	25	38.948	16	34.321	Barby Fn.	Basal pyroclastic volcanic
DC1715	25	53.499	16	34.895	Barby Fn.	Phyric andesite lava
DC1716	25	53.724	16	34.935	Barby Fn.	Large-feldspar trachyandesite
DC1717	25	53.868	16	34.914	Barby Fn.	Large-feldspar trachyandesite

4.3 Geochemistry

Thirty-eight samples were prepared for geochemical analysis. Samples were prepared at the Geological survey of Namibia and analysed at ALS Sweden and at the University of Stellenboch. The whole rock major, trace and REE geochemistry data set includes analyses of 38 samples of the magmatic rocks of the Barby Formation Suite (Appendix B).

TAS Diagram

The rock samples collected from the study area were analysed for alkalis and plotted on a Total Alkali Silica (TAS) diagram. The TAS diagram is given in figure 4-14. The TAS diagram shows that most of the samples fall in the basaltic area i.e. basalts, basaltic andesite, basaltic trachyandesite and trachybasalts.

The northern samples are more alkaline, evolving from basalt to trachybasalt then to basaltic trachyandesite which then developes into trachyandesite and tephriphonolite, finally into trachyte suggesting tectonism was much more continental to rift type. The southern samples are evolving more towards the continental felsic type. These show a general trend from baslt into trachy basalts; then to basltic andesites, then andesites and dacites and finally rhyolites; following a true fractional crystallisation path. The southern samples are samples from the bottom flow cycle all the way to the middle flow cycle, and the northern samples are from the middle flow cycle to the top of the flow cycle.

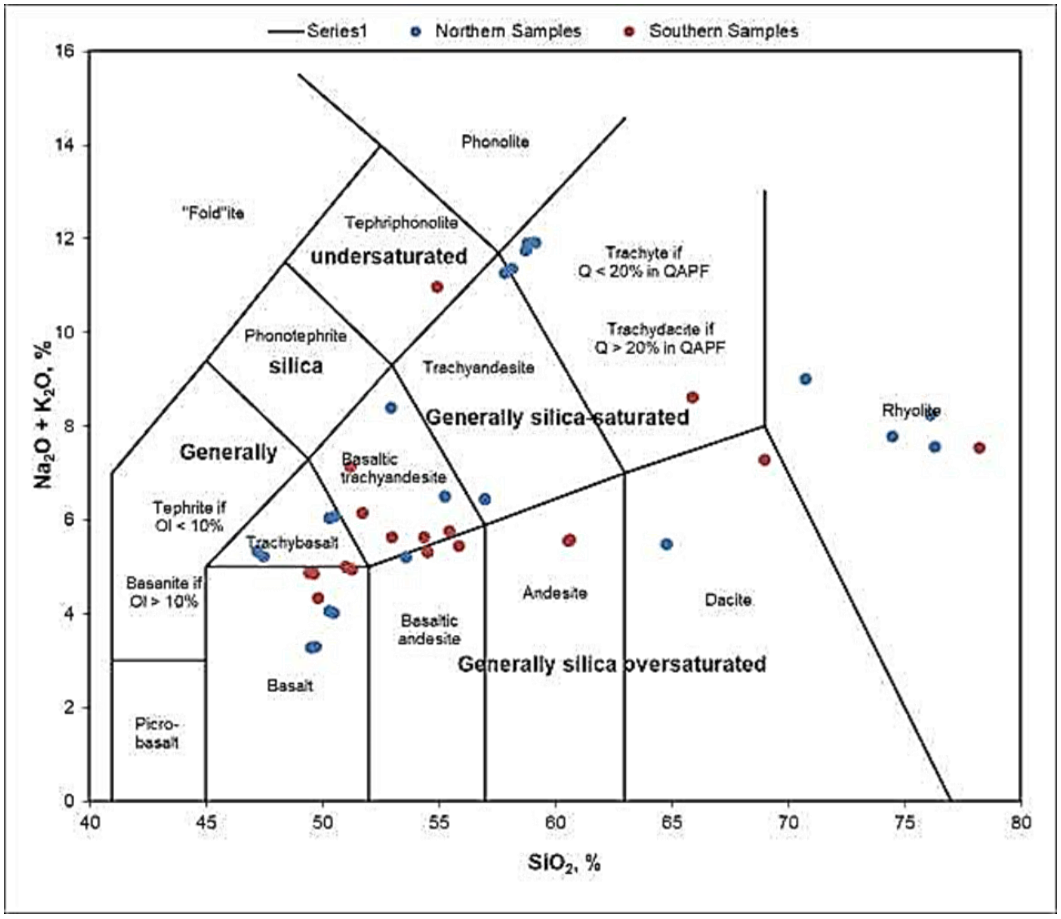

Figure 4-14: Total Alkali Silica diagram showing the southern samples represented by the blue dots and the northern samples represented by the red dots.

Ti-V plots

Plots of Ti vs. V for many modern volcanic rock associations are diagnostic of tectonic setting and can be used to determine possible tectonic settings of ophiolites as well (Shervais, 1982). Titanium and vanadium are present in basaltic and intermediate rocks in abundances that greatly exceed their detection limit in routine XRF analysis, making accurate determination reasonably easy. Most of the samples collected fall in the region of mid-oceanic ridge basalts (MORB) (Fig. 4-20). There are two southern samples that fall in an undefined region and four samples (two northern samples, two southern samples) that fall in the ocean island basalts (OIB) region.

MORBs are formed from partial melts of the upper mantle and therefore only partially reflects its mantle source. It is characterized by very low concentrations of K2O and TiO2; low iron, P2O5, Ba, Rb, Sr, Pb, Th, U and Zr; and high CaO. OIBs are found on islands and volcanoes located on oceanic crust. The chemical composition of these basalts varies from alkaline basalts to tholeiites.

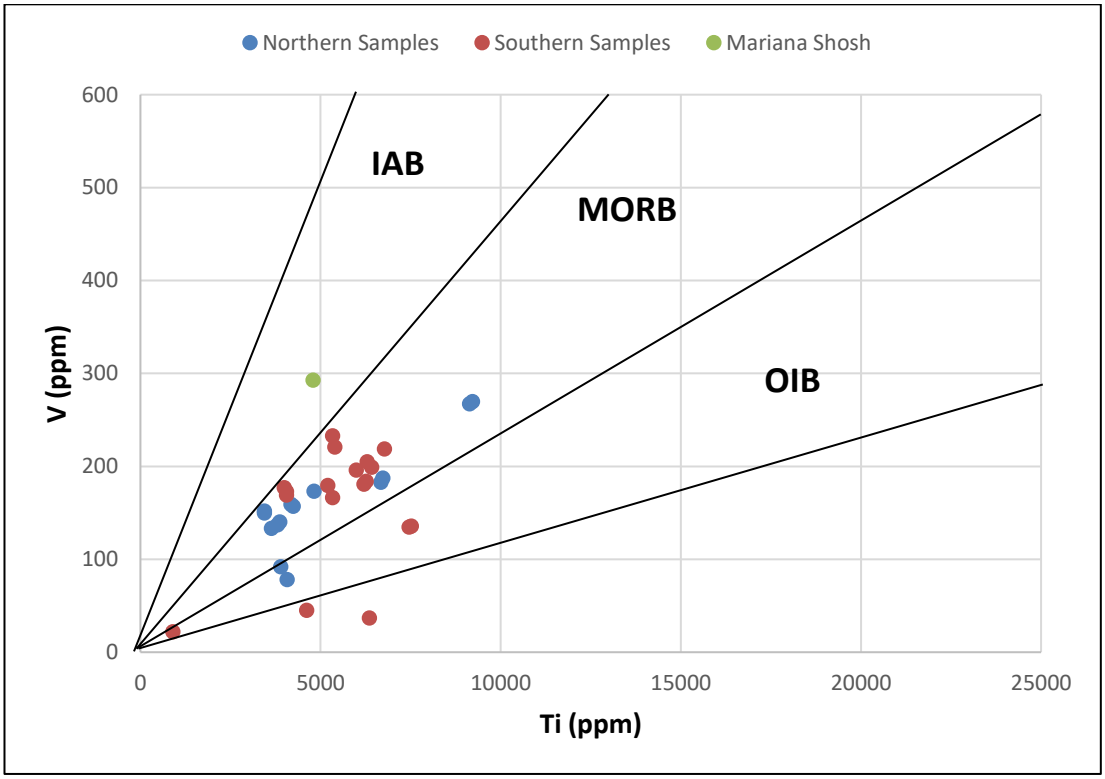

Figure 4-15: Plots of Ti vs. V. showing the southern samples represented by the red dots and the northern samples represented by the blue dots

AFM Diagram

The AFM plot showing tholeiitic and calc-alkali fields and the dividing line between them proposed by Irvine and Baragar 1971. The southern samples show an iron enrichment trend but within the calc-alkaline series (Fig. 4-16). The samples from the north show a subduction trend within the calc-alkaline series. There are some samples from both north and south that fall the tholeiitic series. A distinct bimodality is

observed for the northern samples, but a more continuous compositional range characterizes the southern samples. Both sample localities show a trend from basalt to rhyolite composition.

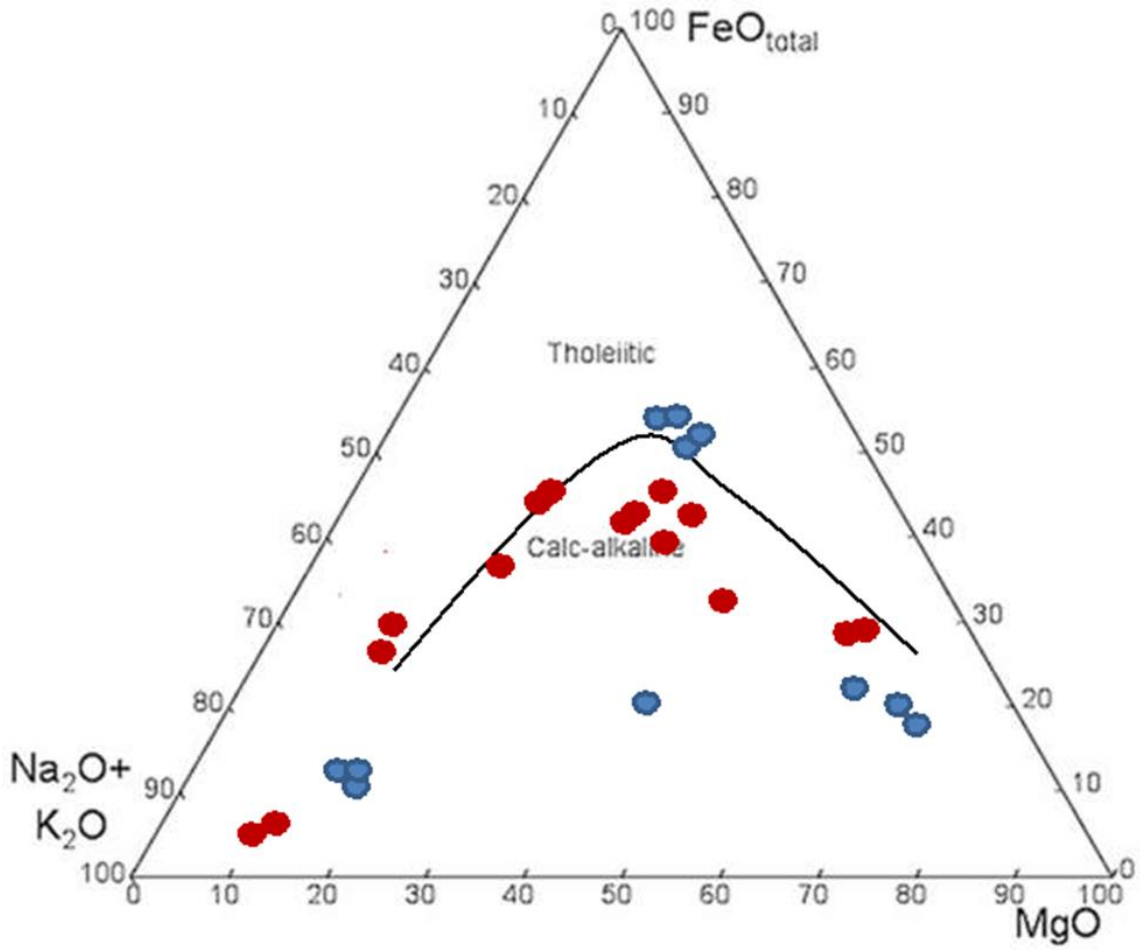

Figure 4-16: AFM diagram after Irvine and Baragar 1971 of the Barby samples collected. The northern samples in blue dot and southern samples in red dots.

K_2O vs. SiO_2 Diagram

The samples collected plot in regions of calc-alkaline trends and shoshonitic trends (Fig. 4-17). Most of the northern samples fall in the region of shoshonite series and the southern samples fall in the high-calc alkaline series (Fig. 4-17). The data define

calc-alkaline, high-K calc-alkaline and shoshonitic trends typical of mid-oceanic ridge basalts.

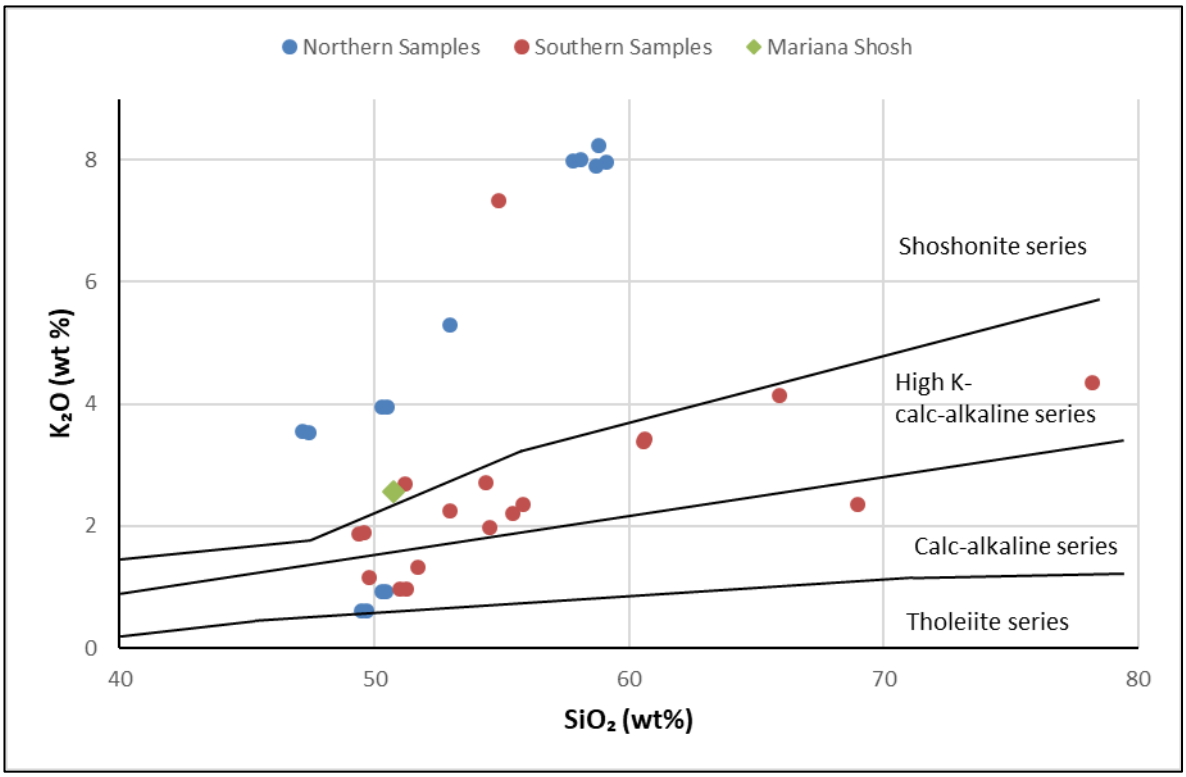

Figure 4-17: K_2O vs. SiO_2 diagram showing the southern samples represented by the red dots and the northern samples represented by the blue dots

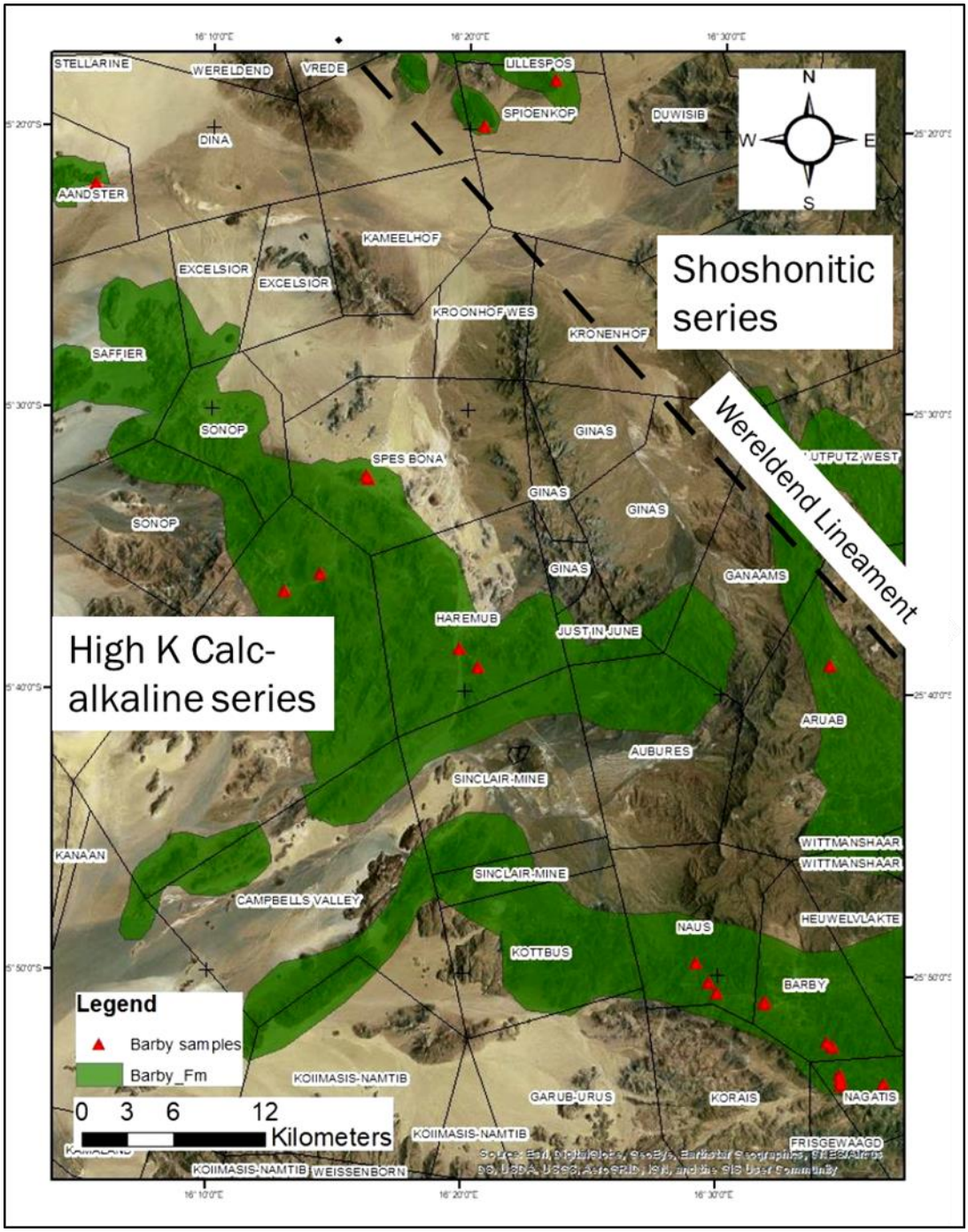

Figure 4-18: Geological map showing the Barby Formation outcrop and the sample localities. This image also shows the division between the shoshonitic series (northern samples) and the high K calc-alkaline series (southern samples).

Harker Diagram

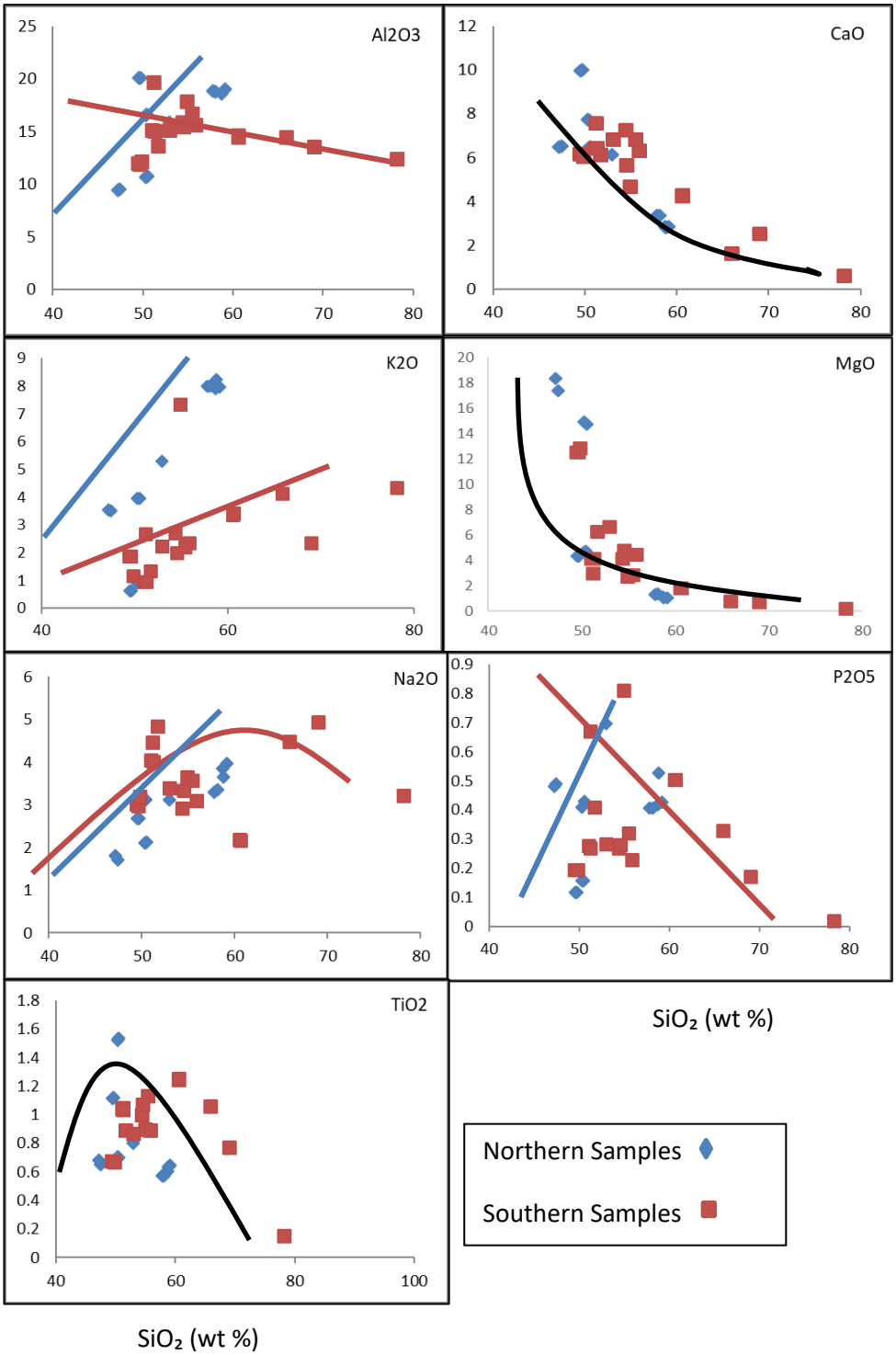

Figure 4-19: Harker diagrams showing major element variation with silica

The Barby Formation shows consistent trends and scatter on Harker diagrams, suggesting they have two different magma system. Al2O3 rises for northern samples

suggesting that an aluminous mineral has begun to crystallize alongside olivine and diopside which is observed in the rock samples with abundant plagioclase phenocrysts (Fig. 4-13). The olivine grains are about 10%, pyroxene grains about 30% and the rest are plagioclase grains in sample DC1677 and DC1678. All three phenocrysts are altered. The southern samples show a gradual decrease in aluminium. Diopside is rich in CaO and its crystallization alongside olivine therefore causes a steep decline in the CaO content of the melt (Fig. 4-19). Olivine and diopside are aluminous poor minerals, thus Al2O3 content is increasing in the melt as these two mafic minerals crystallize (Fig. 4-19). The samples from the northern area show an increase in sodium as silica increase. The rise is steep. The southern samples first show an increase as silica increase. The rise is steep, then at approximately 65 wt. % silica the sodium starts dropping but less steeply (Fig. 4-19). TiO2 content initial rise reflects the crystallization of Ti poor olivine and clinopyroxene, followed by a dramatic downturn where the Ti rich oxide minerals such as rutile and ilmenite.

The ‘elbow’ trend in every diagram observed caused by the crystallization of a new minerals, is a clear sign that fractional crystallization is the chief agent of magma differentiation in the rocks.

Spider and REE Diagrams

Mid-Ocean Ridge Basalt (MORB)-normalised spider diagrams are shown in figure 4-20. All samples show enrichment of the mobile elements Sr, K, Rb and Ba relative to MORB and decreasing immobile elements Th to Yb. The twofold nature of the Barby Formation is well illustrated, the shoshonitic samples (northern samples) in figure 4-20A having much lower Sr and large negative anomalies for Ba, P and Ti compared with the high calc-alkaline samples (southern samples) in figure 4-20B. All of the samples show the negative Nb-Ta, Ti and P anomalies typical of volcanic arc magmas.

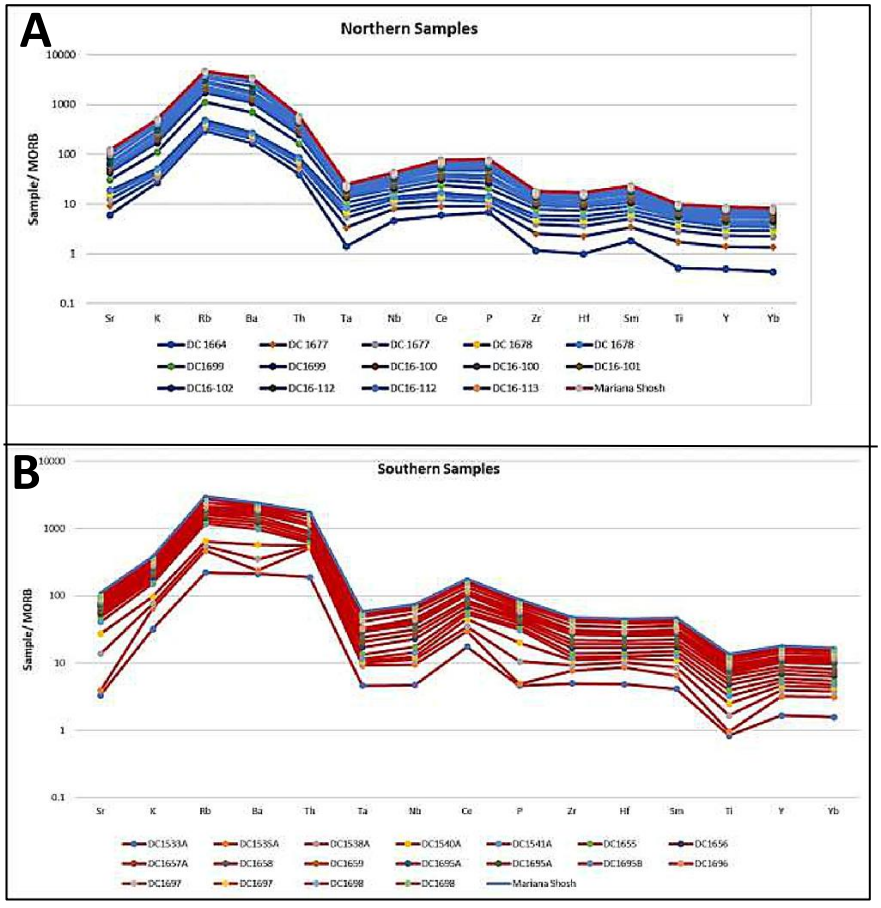

Figure 4-20: MORB-normalised spider diagrams of northern samples (top) and southern samples. The MORB normalization data follows Pearce (1983). The Mariana Central Hiyoshi data from a modern subduction zone is from Sun and Stern (2001).

The REE profiles of the alkaline samples including the Spes Bona Syenite shown in Figure 4-21B are very similar to each other and have more consistent slopes than the calc-alkaline samples, with heavy REE decreasing to ~10 times chondritic. They do not show Eu anomalies, suggesting magmatic processes at depths greater than about 40 km, where plagioclase is not stable (Figure 13 in Simon et al., 2008,). In the Rare Earth Element (REE) diagrams, the souhtern samples in figure 4-21B show moderate light-REE enrichment, small negative Eu anomalies suggesting plagioclase fractionation, and flat heavy REE profiles.

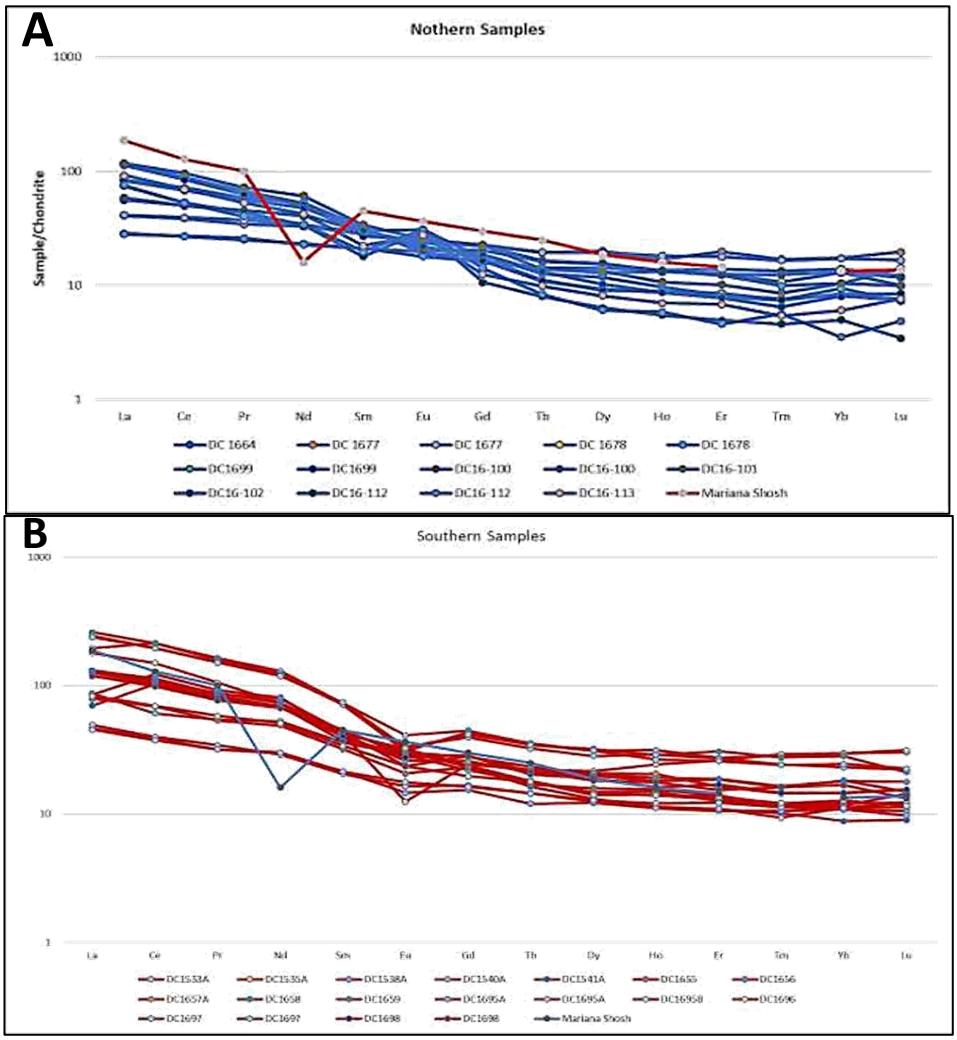

Figure 4-21: The Rare Earth Element (REE) diagram of northern samples (top) and southern samples. The chondrite normalization data follow McDonough and Sun, 1995.

4.4 Geochronology

U-Pb data

There is a considerable body of published geochronology data from the magmatic rocks of the Sinclair Supergroup and its lateral equivalence. Rb-Sr and conventional U-Pb zircon data, mostly from the 1970s and 1980s, provided a large range of mostly imprecise ‘‘crystallisation ages” of between 2.1 and 1.65 Ga. A total of 14 samples were collected and prepared for geochronological analysis but only four samples contained zircons or baddeleyite. LA-ICPMS U-Pb data of only 4 samples is presented on a sample-by-sample basis, with a brief interpretation of the data. The data is summarised in Tables 4 and Appendix C.

Table 2: Age calculations from U-Pb zircon data of samples with zircons or baddeleyite.

Probabilities > 0.15 are regarded as acceptable

Sample id	**Rock Type**	**Calculations**	**Age Ma**	**Error 2σ**
DC1533	Barby Felsic tuff	The weighted mean $^{207}Pb/^{206}Pb$ age	1214	5
DC1541	Spes Bona Syenite	The weighted mean $^{207}Pb/^{206}Pb$ age	1217	3
DC1540	Barby Rhomb porphyry	The weighted mean $^{207}Pb/^{206}Pb$ age	1218	2

DC1709	Barby quartz porphyritic lava	Concordia age	1337	9

Barby felsic tuff DC1535

This sample was taken from the basal pyroclastic unit. The rhyolitic ash-flow consists of main minerals quartz, K-feldspar, plagioclase, magnetite, ilmenite and accessory apatite and zircon. This unit belongs to the southern samples which are high K calc-alkaline series. The Barby Felsic Tuff consists of zircons which are seen in backscattered electron images to mainly comprise a main domain which has faint oscillatory zonation (Fig. 4-22) which is typical of magmatic zircon. The backscattered electron images show sector zonation; this is due to the different crystal faces taking in different amounts of Th and U from the magma as they grow. The Th/U ratio is higher than 0.5 which is typical of igneous rather than metamorphic zircon (Hoskin and Schaltegger, 2003). There are a few clearly discordant cores which are probably xenocrysts. Grain 17c (Fig. 4-22) has an unconformable core which seems to be a xenocryst. However, in this sample the two possible xenocrysts analysed have indistinguishable ages to the main domain and can thus be included in the age calculations. The discordia calculation (Fig. 4-23A) with all 19 points is not valid due to excess scatter. Omitting the four highest weighted residual points (2a; 5a2; 07a; 0; 28a) we get a valid upper intercept age of 1210 ± 5.9 Ma. The weighted mean $^{207}Pb/^{206}Pb$ age of points with less than 3% discordance is **1214 ± 5 Ma** with probability 0.78. The weighted mean $^{207}Pb/^{206}Pb$ age reflects the age of extrusion of the Barby felsic tuff.

Spes Bona Syenite DC1541

The syenite is a very distinctive, medium-grained grey rock displaying hypidiomorphic granular texture with minerals such as alkali feldspar, plagioclase and diopside. This unit belongs to the southern group of samples which are high K calc-alkaline series. This sample contained no zircon, which could be expected from its significant modal diopside, indicating silica deficiency. However, ≈500-micron long fragments of dark brown baddeleyite (Fig. 4-22), which was also observed in thin section, could be picked from the heavy mineral concentrate and mounted in the zircon puck. Wingate and Compston (2000) showed that the ion probe U-Pb calibration for this mineral change significantly with crystal orientation, that is all baddeleyite grains must be in the same orientation to receive the best results, but that the $^{207}Pb/^{206}Pb$ ages are reliable as it is not affected by the crystal orientation. Using the U-Pb calibration based on the zircon 91500 standard (Wiedenbeck et al., 1995), an analysis of ten grains was conducted and the apparent discordance was insignificant to 8% reverse discordant, probably reflecting the orientation effect, but suggesting that the baddeleyite is actually concordant. The weighted mean $^{207}Pb/^{206}Pb$ age of the data excluding two outliers is **1217 ±3 Ma** with probability 0.51, alternatively increasing the errors by 10% to allow the inclusion of all data gives an indistinguishable weighted mean age of 1216 ±4 Ma with probability 0.16. The 1217 ±3 Ma age is adopted as reflecting the age of intrusion of the Spes Bona Syenite (Fig. 4-23B).

Barby rhomb porphyry DC1540

The sample was taken at 25°32.5'S/ 016°16'E on Spes Bona farm. The rock texture is porphyritic with phenocrysts of plagioclase, feldspar, diopside, olivine, magnetite and

ilmenite. This unit belongs to the southern group of samples which are high K calc-alkaline series. In this sample baddeleyite was common and two zircon grains were found. The baddeleyite grains are about 500-micron long fragments of dark brown baddeleyite and the backscattered electron images to mainly comprise a main domain which has faint oscillatory zonation which is typical of magmatic baddeleyite. As described earlier from the findings of Wingate and Compston (2000); this sample was found to possess well oriented concordant crystals and therefore the ages obtained are reliable. An analysis of 16 baddeleyite grains was conducted using the U-Pb calibration based on the zircon 91500 standard (Wiedenbeck et al., 1995). The weighted mean $^{207}Pb/^{206}Pb$ age of the baddeleyite data is **1218 ±2 Ma** with probability 0.61 which is interpreted as crystallization age of the rock (Fig. 4-23C). The two zircon grains found in this sample are probably xenocrysts. The zircons are seen in backscattered electron images mainly comprise a main domain which has faint oscillatory zonation (Fig. 4-22) which is typical of magmatic zircon. The zircons give a discordia upper intercept of 1211 ±14 Ma which is the same age within error as that of the baddeleyite (Fig. 4-23D).

Barby quartz porphyritic lava DC1709

This sample was collected at 25° 19.864'S/ 016°20.599'E on Betta Farm. This sample belongs to the basal pyroclastic unit. The pale red-brown rhyolitic ash-flow consists of main minerals quartz, K-feldspar and plagioclase. This unit belongs to the northern samples which are a shoshonitic series. The zircons found in this unit have a CL-bright main domain (Fig. 4-22). Some grains have darker cores. The Barby quartz porphyritic lava consists of zircons which are seen in backscattered electron images to mainly

comprise a main domain with oscillatory zonation and is prismatic in shape (Fig. 4-22), typical for magmatic zircons. The data is all nearly concordant and the cores are not significantly older than the mains. However, combining the data does not yield statistically valid concordia ages. The 5 cores show excess scatter but yield an age of 1331.6 ±9.2 Ma. Eight main points give a concordia age of **1336.9 ±8.9 Ma** which agrees with the weighted mean Pb-Pb age of **1335 ± 16 Ma** (Fig. 4-23E). The 1336.9 ±8.9 Ma age is regarded as the age of extrusion of this sample.

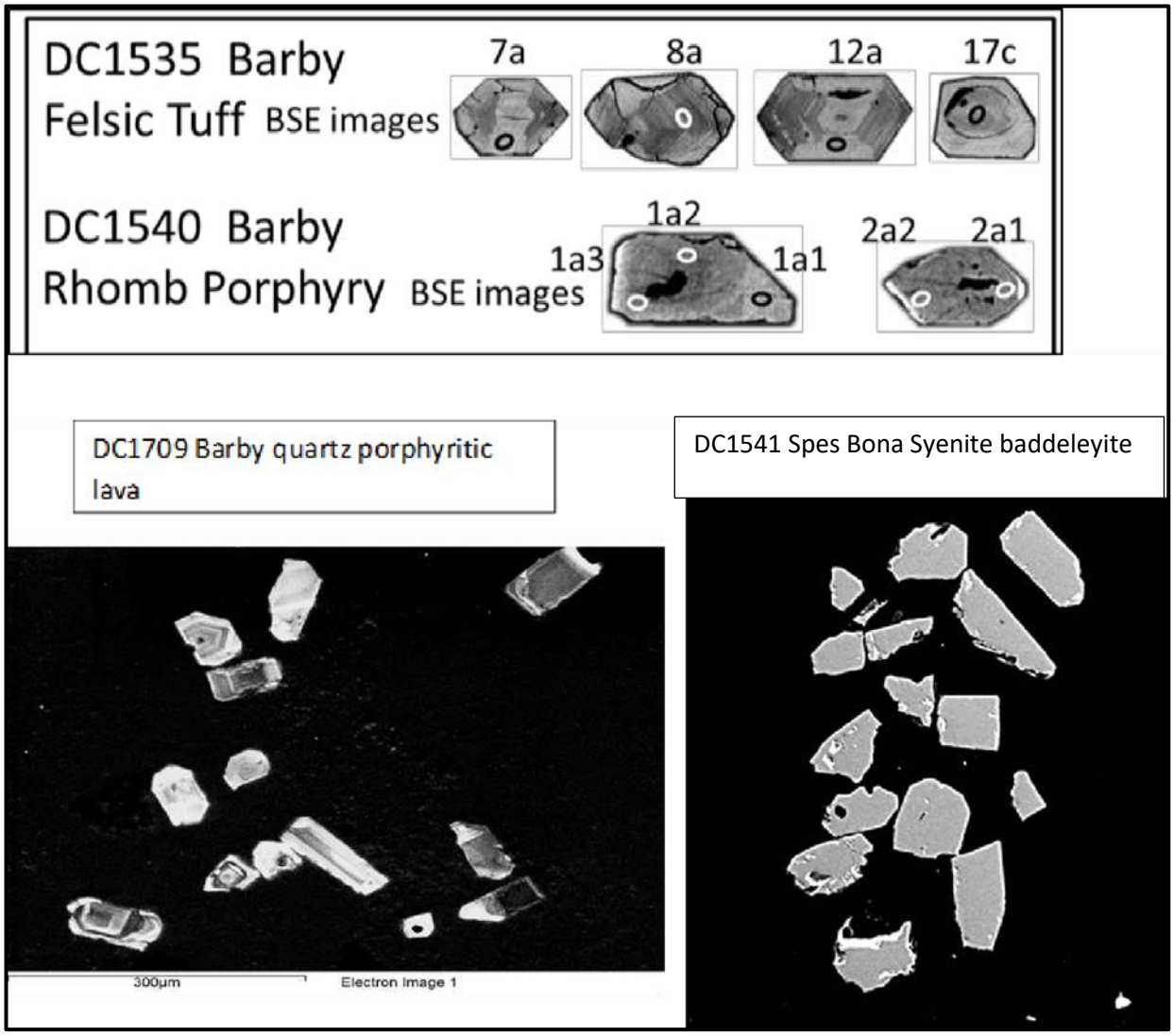

Figure 4-22: Cathodoluminescent images of representative zircons and baddeleyite grains analysed in this work

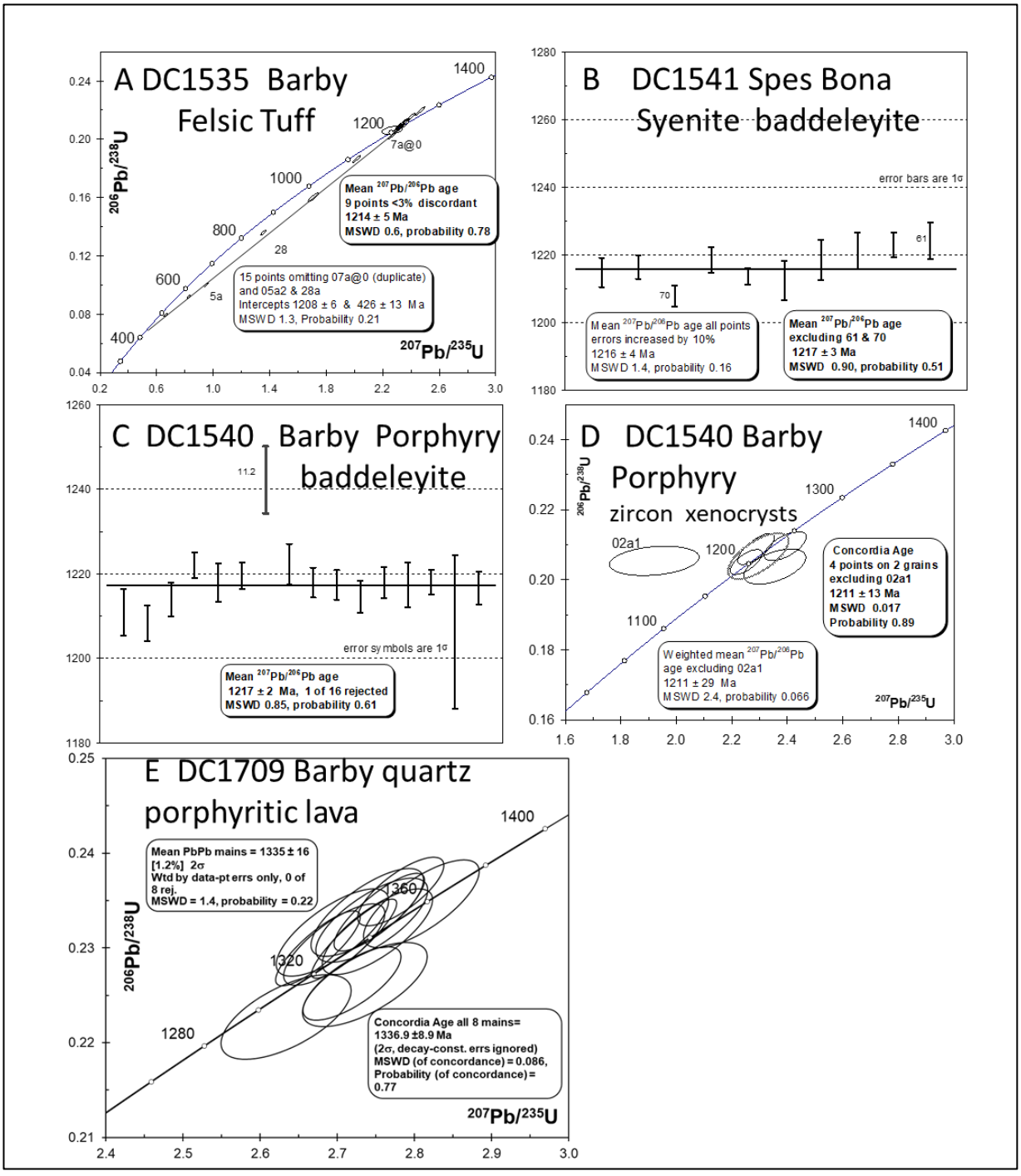

Figure 4-23: Concordia diagrams showing U–Pb data and age calculations for samples from Sinclaire- Helmeringhausen area

Lu-Hf Data

The Hf isotope data for zircons can be used to calculate the crustal residence ages for igneous rock samples. The Lu-Hf data for zircons and baddeleyites of four samples is shown in figure 4-26. The Spes Bona syenite and the Barby units have Lu-Hf crustal residence ages of 2.14 and 1.88 Ga respectively, assuming that they originated from a basaltic protolith emerging from the Depleted Mantle. The Lu/Hf ratio used for these samples was 0.022.

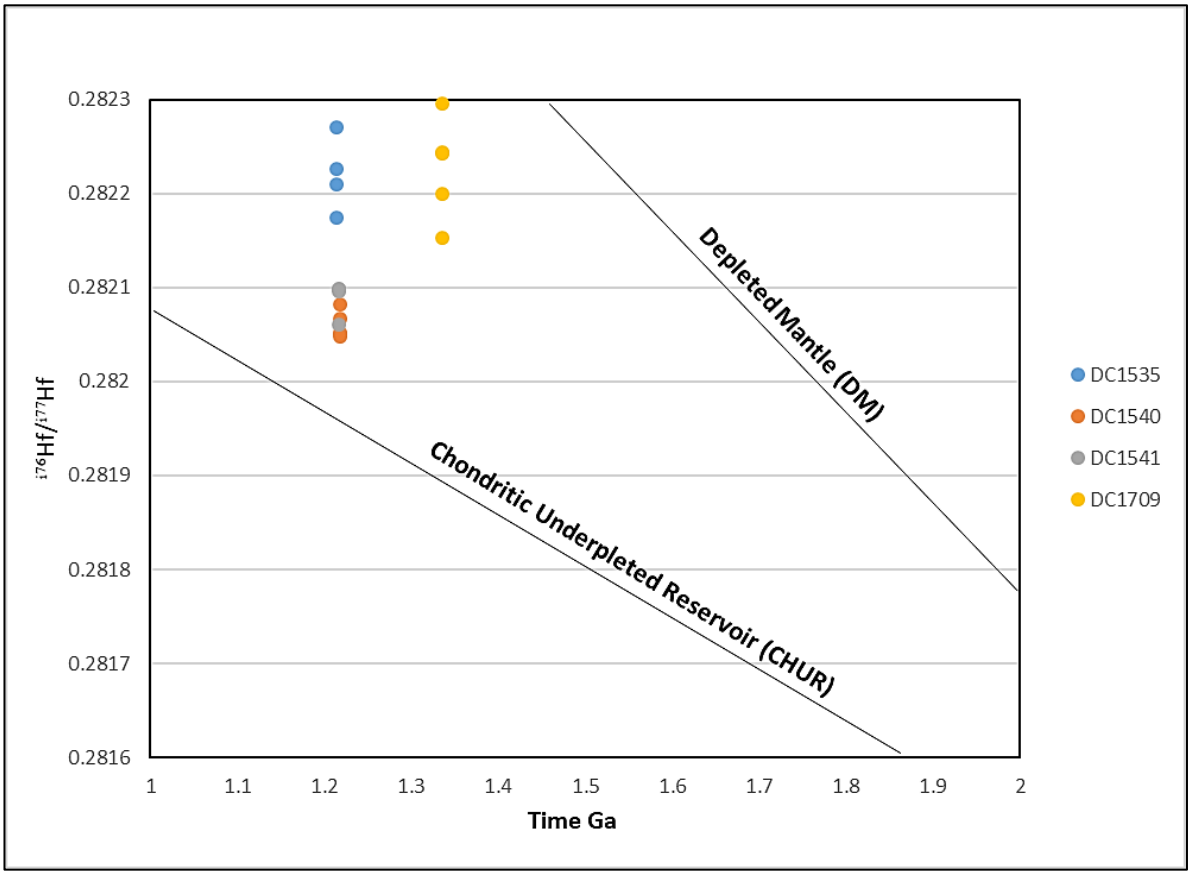

Figure 4-24: Lu-Hf data on zircons and baddelyites from three samples on a Hf isotope evolution

Rb-Sr Data

The Spes Bona syenite sample contains large igneous biotites which is suitable to apply the microbeam Rb-Sr method recently developed for laser ablation collision cell

ICPMS by Zack and Hogmalm (2016). The large spread of Rb/Sr ratios shown in Table 3 by the 50-micron spots in biotite, together with the low ratios of apatite and feldspars, enabled a precise mineral isochron to be calculated, with 2σ errors of 11 Ma based on the analytical errors, however the overall errors in ages of the method based on comparisons with well-dated rocks are estimated at 1.5% by Zack and Hogmalm (2016). Thus, the isochron age is shown with expanded errors as 1238 ±20 Ma in figure 4-25, which should represent the age of cooling below about 300°C following emplacement. This age is older than, but overlaps within the 20 Ma error the $^{207}Pb/^{206}Pb$ baddeleyite age of 1217 ± 3 Ma for the same sample, suggesting that the 'expanded' errors are realistic. Interestingly if the 'old' 1.42 $x10^{-11}$ decay constant is used the age decreases to 1218 Ma.

Spot#	mineral	87Rb/86Sr	1σ abs.	87Sr/86Sr	1σ abs.
75	biotite	175.154	2.557	3.7546	0.0240
76	biotite	177.325	2.589	3.7832	0.0242
77	biotite	155.673	2.273	3.4171	0.0219
78	biotite	101.669	1.484	2.4887	0.0159
79	biotite	124.099	1.812	2.9048	0.0186
80	biotite	181.634	2.652	3.9114	0.0250
81	biotite	162.231	2.369	3.5283	0.0226
82	biotite	173.202	2.529	3.6868	0.0236
83	apatite	0.16	0.00	0.704	0.005
84	apatite	0.00	0.00	0.701	0.004
85	K-feldspar	0.66	0.01	0.714	0.005
86	K-feldspar	0.60	0.01	0.714	0.005
95	biotite	104.741	1.529	2.5310	0.0162
96	biotite	94.47	1.38	2.387	0.015
97	biotite	116.51	1.70	2.711	0.017
98	biotite	117.73	1.72	2.750	0.018
99	apatite	0.07	0.00	0.704	0.005
100	apatite	0.11	0.00	0.707	0.005
101	K-feldspar	0.57	0.01	0.707	0.005
102	K-feldspar	0.61	0.01	0.709	0.005

103	biotite	82.87	1.21	2.120	0.014
104	biotite	64.26	0.94	1.809	0.012
107	plagioclase	0.14	0.00	0.704	0.005

Table 3: Rb-Sr data by Laser Ablation collision cell ICPMS for 50 micron spots in minerals of the Spes Bona Syenite sample DC1541

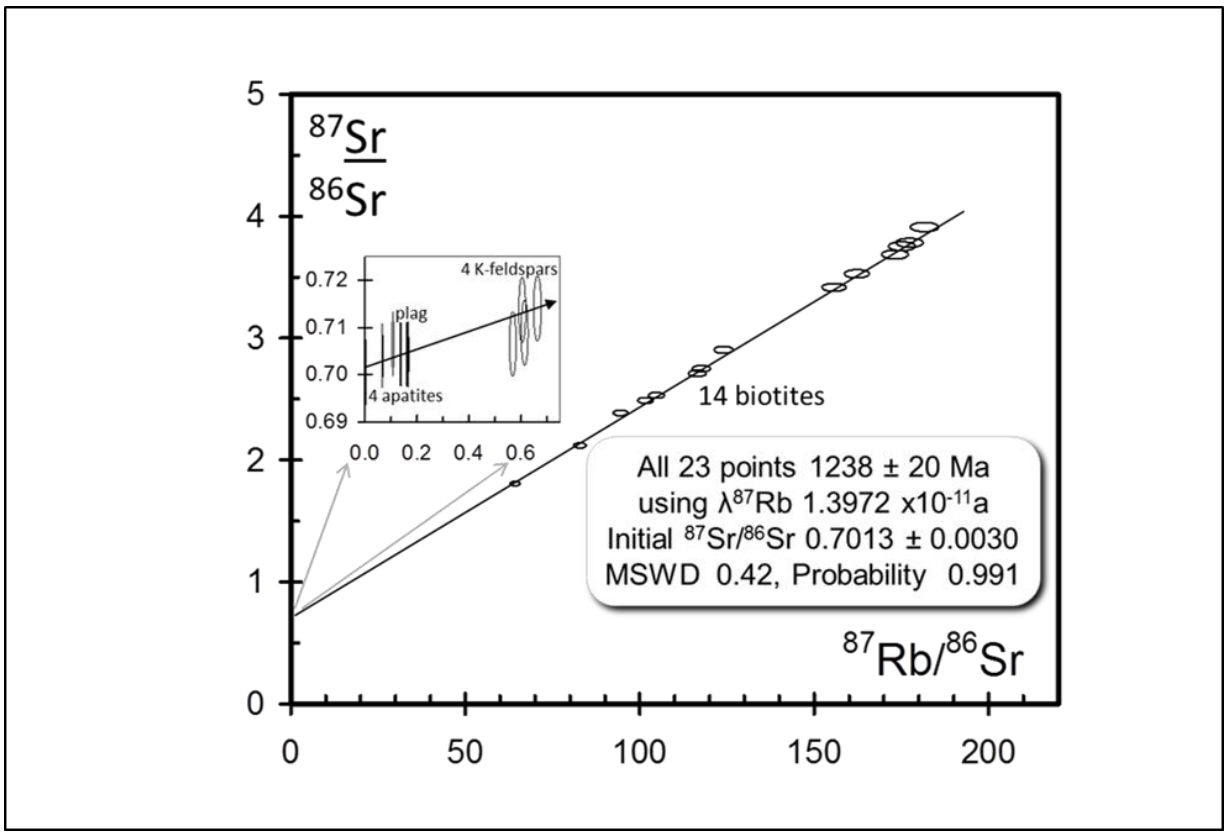

Figure 4-25: Rb-Sr mineral isochron by Laser Ablation ICP-MS/MS for the Spes Bona Syenite sample DC1541

5. DISCUSSION AND INTERPRETATION

The Barby Formation overlies the Kunjas Formation conformably, this was observed at both Klein Haremub Farm and Betta Farm (Fig. 4-1) at both farms there is a sharp contact between the two formations. The Kunjas Formation consists of conglomerate or grit, feldspathic quartzites, shales and sandstones. The Guperas Formation rests unconformably on the Barby Formation on the Aruab Farm (Miller, 2008). A considerable variety of plutonic and hypabyssal rocks intrude the Barby. The Spes Bona syenite is one of these plutonic rocks that intrude the Barby Formation. The contact between the Barby Formation and the Spes Bona syenite is a sharp contact. The Spes Bona syenite stratigraphically is overlaying the Barby

The Barby Formation shows the three flow cycles (Fig.4-2) (Becker, 2006). The flow cycles start with a basal unit of a porphyritic coarse to medium grained calc-alkaline basalt with large plagioclase grain (Fig. 4-7 & 4-12). This bottom flow cycle is found in both northern and southern group.

Porphyritic texture originates from when cooling went through two stages. The initial stage is at great depth and the cooling rate is slow where the phenocrysts are formed. After this partial crystallization, the magma experiences and episode of relatively rapid heat loss in a small intrusion at shallow depth thus forming the aphanitic groundmass (Gill, 2010). This is also observed in the Lu-Hf data where we have a large range of 176Hf/177Hf ratio.

The unit overlying the basal porphyritic rocks observed at figure 4-3 and 4-11 is a medium to coarse grained basalt with disseminated plagioclase phenocrysts. This middle flow is found close to the border between the northern and southern samples.

There are olivine and diopside phenocrysts in some of the samples collected i.e. DC1538, DC1656, DC1695 and DC16-102 (Fig. 4-7, 4-11). Olivine's crystallization depletes the evolving melt in MgO because olivine has a much more MgO content than that in the melt (Fig. 4-19).

The trend seen in the northern samples, as you head north on Betta farm, the samples move from the bottom flow to the top flow and the hand specimens show this from fine grained basaltic rocks (Fig. 4-9). The top flow is only observed in the northern group samples.

The Barby Formation Suite displays a complete spectrum of alkaline magmatic rock types, which are dominantly basaltic in composition (Fig. 4-17) (Brown & Wilson, 1986). One magma system is characterised as shoshonitic and the other magma series is calc-alkaline (Fig. 4-17). The northern samples contain alkaline elements and are depleted in silica whereas the southern samples are rich in silica and depleted in alkaline elements (Fig. 4-19). This suggests that the alkaline rich rocks (northern samples) are more evolved than the alkaline poor rocks (southern samples).

The 'elbow' trend in every Harker diagram observed caused by the crystallization of a new minerals (Fig. 4-19), is a clear sign that fractional crystallization is the chief agent of magma differentiation in the rocks.

Rocks of the medium-K and calc-alkaline association are the most characteristic products of mature island arc volcanism (Gill, 2010). Basaltic members of this association, sometimes referred to as high-alumina basalts are often notable porphyritic, containing phenocrysts of plagioclase, olivine and diopside as seen in the

samples collected (Fig. 4-7, 4-8, 4-11). High-alumina basalts with these features are common to many supra subduction zone magmas in mature island arcs and convergent margins such as Izu-Bonin-Mariana arc (Gill, 2010; Sun and Stern (2001). These chemical characteristics allow us to suggest the tectonic environment of the Barby Formation.

The spidergrams show an enrichment in LREE and alkalis (Rb, Sr. Cs, Ba) typical for island arcs which is what is observed in the figure 4-20 and 4-21 with a relative middle rare earth depletion, probably a result of amphibole fractionation. There are clear similarities between the continental crust and the island arc lavas: both exhibit incompatible element enrichment, negative Nb-Ta anomalies, and positive Pb anomalies. It is also true that at present, most new additions to crust occur in subduction zones. There is a small negative Eu and Ce anomalies seen in both REE diagrams (Fig. 4-21) suggesting plagioclase fractionation and no sedimentary component inherited. However, the results do not show any Nd depletion.

Geochemical, petrological and geochronological data, suggests that the Barby Formation comes from a mantle source similar to depleted mantle (Fig.4-24). The Hf isotope data for the calc-alkaline and shoshonitic rocks probably reflects magma mixing between 1.217 Ga mantle–derived magmas and crustal material older than the 2.1 to 1.9 Ga as calculated crustal residence ages (Appendix C). Evidence for such a mixing process is provided by the Hf isotope data of Cornell et al. (2015) for Hauchabfontein hybrid rocks of the same age, which extends below the CHUR evolution line.

The two felsic calc-alkaline samples investigated were surprisingly low in zircon, felsic agglomerate DC1533 yielding no zircons, DC1535 only 40 grains and DC1709 with 25 grains. The shoshonitic samples were rich in baddeleyite due to their silica-undersaturated character, which gave the most precise $^{207}Pb/^{206}Pb$ ages of 1217 Ma. The weighted mean of three Barby Formation ages is 1217 ±2 Ma which reflects the time of volcanic extrusion. From the geochronological data and geochemistry data it seems that it took approximately 14 Ma for the Barby volcanic extrusion to take place (Table 2), i.e., from the bottom flow cycle to the middle flow. The samples taken to represent the top flow contained no zircons or baddeleyites.

The agreement within error between the 1238 ±20 Ma Rb-Sr mineral isochron age and the 207Pb/206Pb baddeleyite age of 1217 ± 3 for the Spes Bona Syenite shows that the area had not been heated above the ~300°C biotite closure temperature after the syenite emplacement at 1217 Ma. This, together with the petrographic evidence of minor deuteric alteration rather than penetrative metamorphism in all samples, shows that the 1200 Ma-1150 Ma collision-related Namaqua metamorphism did not affect the area covered by the Barby Formation.

The plate tectonic setting envisaged for the Rehoboth Magmatic Arc of Watters (1976) is exemplified in the Barby Formation. The calc-alkaline geochemical trends derive from tholeiites associated with mid-oceanic ridge basalts (Fig. 4-16) whereas high K calc-alkaline basalts must be a mixture of alkaline and calc-alkaline rocks (Fig. 4-17).

The spidergram Ta-Nb anomalies (Fig. 4-20) are in both northern and southern samples similar to those of the Mariana arc, and are believed to be good evidence of

a subduction setting. The present data suggest that the southern area contains typical Barby volcanics. Hoal, 1990 (as cited in Miller, 2008, p.8-65) noted that the rocks from the Barby Formation have similar geochemical trends to that of the Cascades in northern Chile which are representative of mature active continental margins. From the geological distribution on maps and the geochemical data it is evident there is more than one magma system.

The Barby Formation has both the calc-alkali and tholeiitic series (Fig. 4-16). Von Brunn (1969) and Watters (1974) proposed the bimodal compositional resulted from the unrelated magmas. From the geochemical and petrographic data, we see that there is a clear separation from the northern samples and the southern samples. The northern samples have a shoshonitic trend which are rock types mostly formed at subduction zones. The southern samples are calc-alkaline, which are subduction related rock types. The Ti-V plot shows us that there is a MORB signature in these rocks that are commonly found in a subduction zones. Gill (2010) explains that in a back-arc extension as subduction progresses we can get a rift setting caused by decompression melting. This is most likely to explain the MORB signature which we see in both northern and southern samples. The tectonic setting of this formation is in an island arc. The over-ridding slab with the back-arc extension took approximately 40 Ma for arc rifting to occur, but as subduction continued the arc rifting signature was overprinted by subduction and only remnants of the rift setting is now visible (Fig. 5-1).

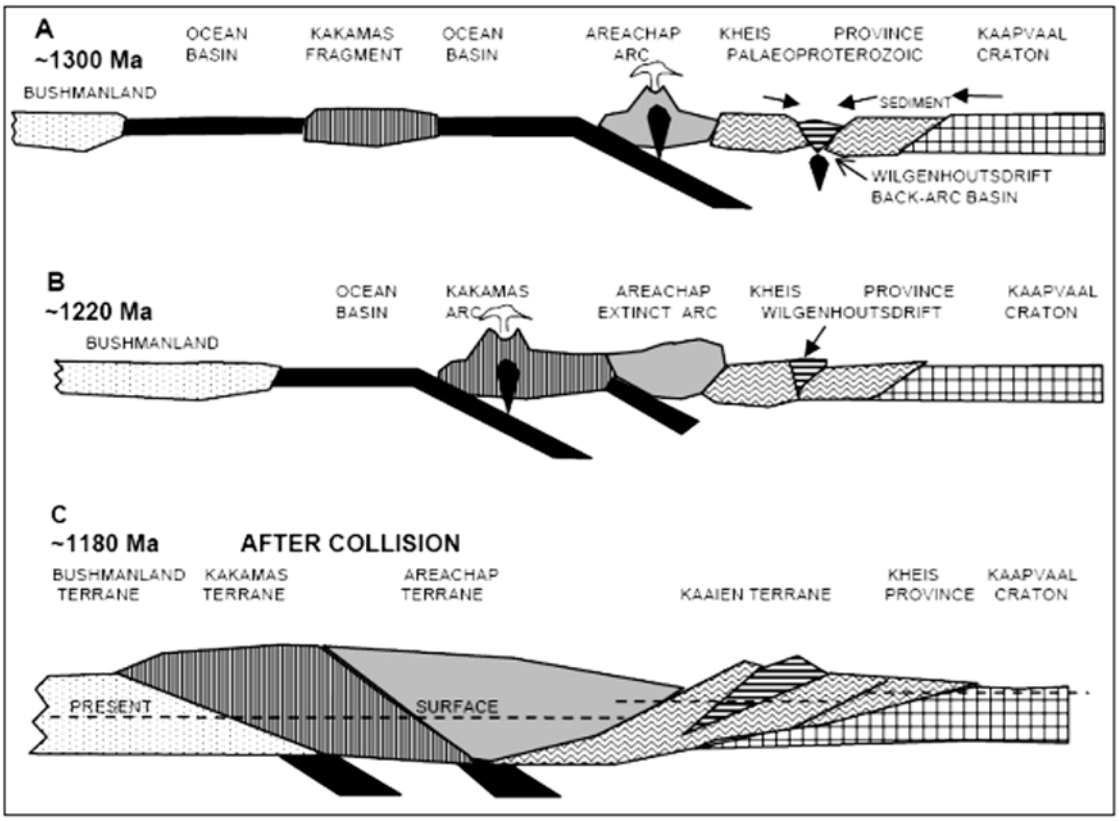

Figure 5-1 Sketch showing the possible plate tectonic evolution of the Namaque-Natal Province of southern Africa, after Cornell and Pettersson (2007). The sketch focuses on the Koras Group which is an equivalent of the Konkiep Group.

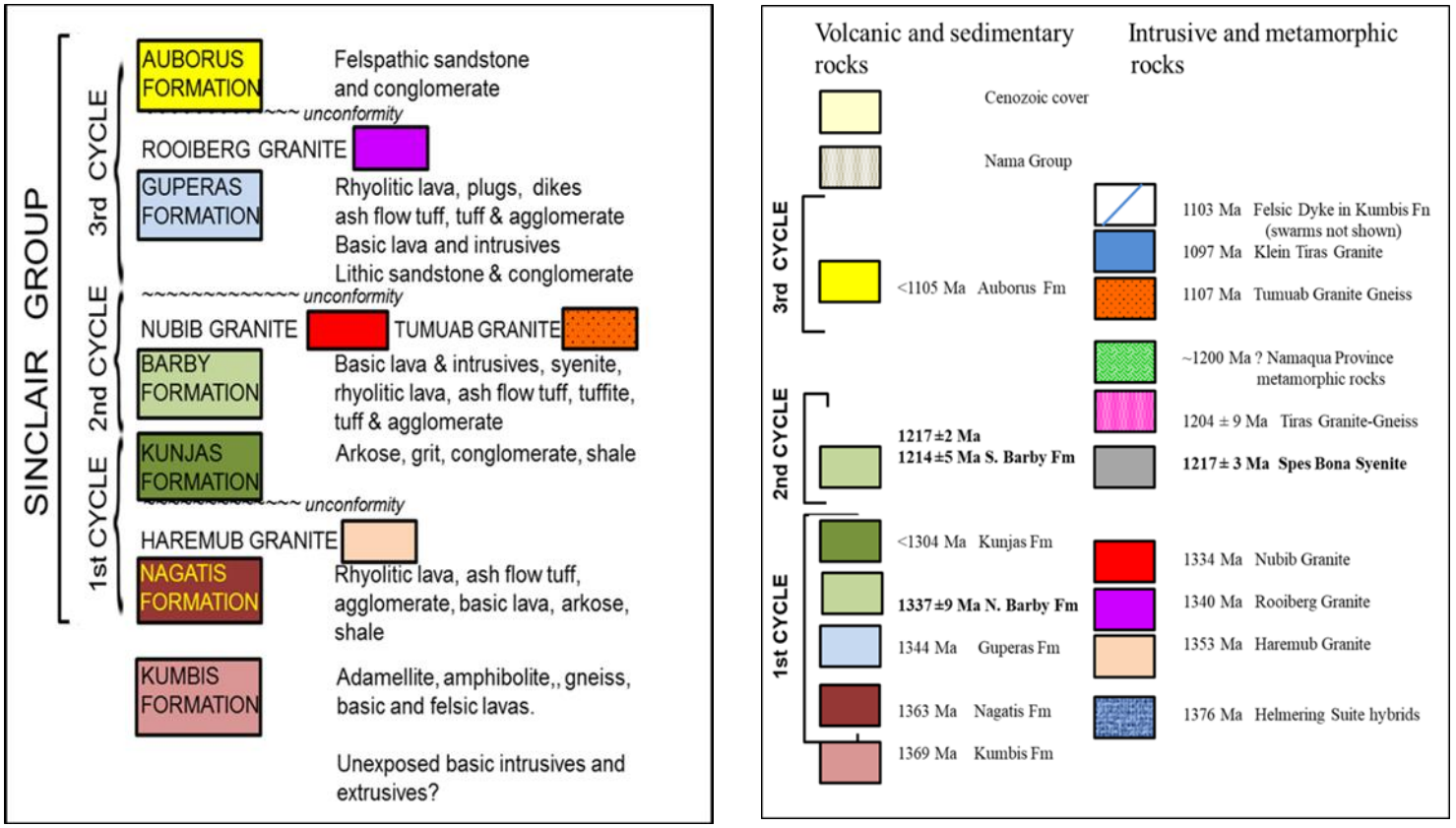

Figure 5-2: The precise U-Pb zircon dates obtained by our group are shown, for which 2σ errors are generally less than 10 Ma. This thesis only focused on the Barby Formation and Spes Bona Syenite.

6.CONCLUSION

1. From the geochronological data and geochemistry data it seems that it took approximately 14 Ma for the Barby volcanic extrusion to take place (Table 2), from the bottom flow cycle to the middle flow in the southern area.
2. The geochemical data define calc-alkaline and high-K calc-alkaline trends typical of arc rocks. The calc-alkaline and the shoshonitic rocks of the Barby Formation in the western Konkiep Terrane reflect the subduction-related magmatism of the Rehoboth Magmatic Arc which took place around 1217 Ma. The subduction-related magmatism continued until ~1210 Ma when juvenile arc and older terranes to the west began colliding with the Kaapvaal Craton and Rehoboth Province (Pettersson et al. 2007).
3. The weighted mean of the Barby Formation age is 1217 ±2 Ma which reflects the time of volcanic extrusion. From the geochronological data it shows that magmatism started at 1336.9 ±8.9 Ma. During this period the Konkiep Terrane was an active continental margin like the Andes.

Recommendation

1. A sedimentology study on the Sinclair Supergroup
2. A systematic study to identify the volcanic centers of various magma pulses.

REFERENCES

Becker, T., Schreiber, U., Kampunzu, A.B. and Armstrong, R., 2006., Mesoproterozoic rocks of Namibia and their plate tectonic setting. *Journal of African Earth Sciences* 46, pp.112-140.

Becker, T., 2008. In: Miller, R. Mc G. (Ed.), *The Geology of Namibia: Archaean to Mesoproterozoic, vol. 1.* Ministry of Mines and Energy, Geological Survey of Namibia,Windhoek, pp. 8–10, 8–67.

Brown G.C., Wilson A.H., 1986. The petrology and geochemistry of the Barby Formation, Sinclair Supergroup. *Communication of the Geological Survey Of Namibia*, 2, pp. 93-108.

Corner, B., 2008. The crustal framework of Namibia derived from an integrated interpretation of geophysical and geological data. In: Miller, R.M. (Ed.), *The Geology of Namibia: Archaean to Mesoproterozoic, vol. 1.* Ministry of Mines and Energy, Geological Survey of Namibia, Windhoek, pp. 1–19.

Cornell, D.H., van Schijndel, V., Simonsen, S.L. and Frei, D., 2015. Geochronology of the Mesoproterozoic hybrid intrusion in the Konkiep Terrane, Namibia, from passive to active continental margin in the Namaqua-Natal Wilson cycle. *Precambrian Research* 265, pp. 166-188.

Dalziel, I.W.D., Mosher, S., Gahagan, L.M., 2000. Laurentia–Kalahari collision and the assembly of Rodinia. *Journal of Geology*, 108, pp. 499– 513.

Elburg, M., Vroon, P., van der Wagt, B., & Tchalikian, A. (2005). Sr and Pb isotopic composition of five USGS glasses (BHVO-2G, BIR-1G, BCR-2G, TB-1G, NKT-1G). *Chemical Geology*, 223(4), pp. 196-207.

Gill, R., (2010). *Igneous Rocks and Processes: A Practical Guide*. West Sussex, United Kingdom

Hartnady, C.J., Joubert, P. and Stowe, C.W., 1985: Proterozoic crustal evolution in south western Africa. *Episodes* vol. 8, pp. 236-244.

Hoal, B.G., 1987. Terrane significance of the boundary between the Rehoboth and Gordonia subprovinces in southern Namibia, 42-45. In: Hartnady, C.J.H. (Ed.) Proceedings and Abstracts of the Alex L. du Toit Golden Jubilee Conference on Tectono-stratigraphic Terrane Analysis. *Precambrian Research Unit*., Univ. Cape Town, 69.

Hoal B.G., 1989. The geological history of the Awasib Mountain Terrain and its relationship to the Sinclair Supergroup and the Namaqua Metamorphic Complex. *Communication of the Geological Survey of Namibia* 5, pp. 43-53.

Hoal, B.G. 1993. The Proterozoic Sinclair Sequence in southern Namibia: intracratonic rift or active continental margin setting?, *Precambrian Research*, v. 63, p. 143-162.

Hoal, B., & Heaman, L. 1995. The Sinclair Supergroup: U-Pb age constraints from the Awasib Mountain are. *Communications Geological Survey Namibia*, pp. 83-92.

Hogmalm, K. J., Zack, T., Karlsson, A. K. O., Sjöqvist, A. S., & Garbe-Schönberg, D. (2017). In situ Rb–Sr and K–Ca dating by LA-ICP-MS/MS: an evaluation of N2O and SF6 as reaction gases. *Journal of Analytical Atomic Spectrometry*, 32(2), 305-313.

Hoskin, P.W.O., Schaltegger, U., 2003. The composition of zircon and igneous and metamorphic petrogenesis. *Reviews in Mineralogy and Geochemistry* 53.

Irvine, T.N. and Baragar, W.A.A. 1971. *A guide to chemical classification of the common volcanic rocks*. Can. J. Earth Sci., 8, pp. 528-548.

Kinny, P.D. and Maas, R., 2003. Lu-Hf and Sm-Nd isotope systems in zircon. Reviews in Mineralogy andGeochemistry, *Mineralogical Society of America*, 53, 1, pp 327-341

McDonough, W.F. and Sun, S.S., 1995, The Composition of the Earth; *Chemical Geology*, v. 120, p. 223-253.

Miller R., (2008). *The Geology of Namibia: Archaean to Mesoproterozoic, vol. 1*. Ministry of Mines and Energy, Geological Survey of Namibia, Windhoek, pp. 8–1 to 8-104.

Pettersson, Å., Cornell, D.H., Moen, H.F.G., Reddy, S., and Evans, D., 2007. Ion-probe dating of 1.2 Ga collision and crustal architecture in the Namaqua-Natal Province of southern Africa. *Precambrian Research*, 158, pp. 79-92.

Pearce, J.A. and Parkinson, I.J., 1993, Trace element models for mantle melting: application to volcanic arc patrogenesis; in Prichard, H.M., Alabaster, T., Harris, N.B.W., and Neary, C.R., eds., Magmatic Processes and Plate Tectonics, *Geological Society Special Publications*, no. 76, pp. 373-403.

Rollinson, H., 1993: *Using geochemical data: evaluation, presentation, interpretation*. 1st edition, Pearson Education Ltd, pp. 352.

Scherer, E.E., Cameron, K.L., Johnson, C.M., Beard, B.L., Barovich, K.M., and Collerson K.D., 1997. Lu-Hf geochronology applied to dating Cenozoic events affecting lower crustal xenoliths from Kilbourne Hole, New Mexico. *Chemical Geology*, 142, pp 63-78.

Seyfried, W.E, Ding, K., Bendt, M.E., Chem, X., (1999). Experimental and theoratical controls on the composition of mid-oceanic ridge hydrothermal fluids. In Bzone, C.T., Hannington, M.D. editors: Volcanic associated massive sulphide deposits. Processes and examples in modern and ancient rifts. Review in *Economic Geology*, 8, pp. 151-120

Shervais J. W. (1982) Ti-V plots and the petrogenesis of modern ophiolitic lavas. *Earth and Planetary Science Letters*, 59, pp. 101-118.

Simon, N.S., Neumann, E-R., Bonadiman, C., Coltorti, M., Delpech, G., Gregoire, M., Widom, E., 2008. Ultra-refractory Domains in the Oceanic Mantle Lithosphere Sampled as Mantle Xenoliths at Ocean Islands. *Journal of Petrology*, 49, pp. 1223-1251.

Sun, C-H, Stern, R. (2001). Genesis of Mariana shoshonites: contribution of the subduction component. *Journal of Geophysical Research*, 106, pp. 589-608.

Van Schijndel, V., Cornell, D.H., HofFormationann, K.L., Frei, D., 2011. Three episodes of crustal development in the Rehoboth Province, Namibia. *Special Publication of the Geological Society London* 357, pp. 27-47.

Van Schijndel, V., Cornell, D.H., Frei, D., Simonsen, S.L., Whitehouse, M., 2014. Crustal evolution of the Rehoboth Province from Archean to Mesoproterozoic times: Insights from the Rehoboth Basement Inlier. *Precambrian Research* 240, pp. 22-36.

Villa, I.M., De Bievre, P., Holden, N.E., Renne, P.R., 2015. IUPAC-IUGS recommendation on the half-life of 87Rb. *Geochimica Cosmochimica Acta*, 164, pp. 382–385.

Von Brunn, V., 1969. Igneous rocks of the Nagatis and Sinclair Formations north-east of Lüderitz, South West Africa. *Bulletin of the Precambrian Research Unit*, University of Cape Town 7, pp.54.

Yang, K. & Scott, S.D., (2006). Magmatic fluids as a source of metal in sea floor hydrothermal systems. In Christie, D.E. editor: Back-arc spreading systems-Geological, biological, chemical and physical interactions: American geophysical Union, Geophysical Morphology Series, 116, pp.163-184

Watters, B. R., 1974. Stratigraphy, igneous petrology and evolution of the Sinclair Group in South West Africa. *Bulletin of the Precambrian Research Unit*, Univ. Cape Town, 16, pp.235.

Watters, B. R., 1977, The Sinclair Group: Definition and regional correlations: *Geological Society of South Africa Transactions*, v. 80, p. 9-16.

Wiedenbeck, M., Alle, P., Corfu, F., Griffin, W.L., Meier, M., Oberli, F., von Quadt, A., Roddick, J.C., Spiegel, W., 1995. Three natural zircon standards for U–Th–Pb, Lu–Hf, trace element and REE analyses. *Geostandards Newsletter* 19, 1-23.

Wise, S.A., Watters, R.L., 2012. Certificate of Analysis: Standard Reference Material 610. National Institute of Standards and Technology (Gaithersburg, USA).

Woodhead, J. D., & Hergt, J. M. (2001). Strontium, neodymium and lead isotope analyses of NIST glass certified reference materials: SRM 610, 612, 614. *Geostandards and Geoanalytical Research*, 25(2-3), pp.261-266.

Zack, T., & Hogmalm, K. J. (2016). Laser ablation Rb/Sr dating by online chemical separation of Rb and Sr in an oxygen-filled reaction cell. *Chemical Geology*, 437, 120-133.

APPENDIX

APPENDIX A: Samples collected

Sample ID	Lat deg	lat min S	Lon deg	Lon Min E	Unit	Lithology
Northern Samples						
DC 1677	25	2.729	16	5.617	Barby Fn.	Large-feldspar trachyandesite
DC 1678	25	2.841	16	5.619	Barby Fn.	Large-feldspar trachyandesite
DC1698	25	50.969	16	31.887	Barby Fn.	Large-feldspar trachyandesite
DC1709	25	18.212	16	23.371	Barby Fn.	Large-feldspar trachyandesite
DC1710	25	19.864	16	20.599	Barby Fn.	Basal pyroclastic volcanic
Southern Samples						
DC1533	25	35.869	16	14.336	Barby Fn.	Agglomerate
DC1535	25	36.474	16	12.926	Barby Fn.	Basal pyroclastic volcanic
DC1538	25	39.145	16	20.523	Barby Fn.	Phyric andesite lava
DC1540	25	32.473	16	16.164	Barby Fn.	Large-feldspar trachyandesite
DC1541	25	32.34	16	16.081	Spes Bona	Saffier syenite
DC1655	25	53.843	16	36.614	Barby Fn.	Phyric andesite lava
DC1656	25	52.521	16	34.588	Barby Fn.	Large-feldspar trachyandesite
DC1657	25	52.371	16	34.337	Barby Fn.	Large-feldspar trachyandesite
DC1658	25	50.993	16	31.931	Barby Fn.	Large-feldspar trachyandesite
DC1659	25	38.464	16	19.797	Barby Fn.	Phyric andesite lava
DC1664	25	17.742	16	0.781	Barby Fn.	Basalt
DC1695	25	49.566	16	29.199	Barby Fn.	Basal pyroclastic volcanic
DC1695					Barby Fn.	Basal pyroclastic volcanic
DC1696	25	50.275	16	29.685	Barby Fn.	Clinopyroxene basaltic andesite
DC1697	25	50.657	16	30.018	Barby Fn.	Clinopyroxene basaltic andesite
DC1699	25	19.389	15	58.568	Saffier	Saffier syenite
DC16-100	25	19.317	15	23.549	Barby Fn.	Basalt
DC16-101	25	20.145	15	0.786	Barby Fn.	Saffier dolerite
DC16-102	25	17.739	16	0.786	Barby Fn	Basalt
DC16-112	25	27.062	16	3.328	Saffier	Saffier syenite
DC16-113	25	22.015	16	5.442	Saffier	Saffier syenite
DC1714	25	38.948	16	34.321	Barby Fn.	Basal pyroclastic volcanic
DC1715	25	53.499	16	34.895	Barby Fn.	Phyric andesite lava
DC1716	25	53.724	16	34.935	Barby Fn.	Large-feldspar trachyandesite
DC1717	25	53.868	16	34.914	Barby Fn.	Large-feldspar trachyandesite

APPENDIX B: MAJOR ELEMENTS

SAMPLE		SiO2	Al2O3	Fe2O3	CaO	MgO	Na2O	K2O	Cr2O3	TiO2	MnO	P2O5
DC1533A	Barby Fn.	65.9	14.5	5.34	1.66	0.78	4.49	4.14	0.01	1.06	0.09	0.33
DC1535A	Barby Fn.	78.2	12.45	1.48	0.63	0.24	3.22	4.34	0.04	0.15	0.07	0.02
DC1538A	Barby Fn.	51.7	13.65	10.8	6.13	6.29	4.84	1.33	0.04	0.89	0.12	0.41
DC1540A	Barby Fn.	51.2	19.7	6.72	7.58	2.97	4.46	2.68	0.02	1.05	0.05	0.67
DC1541A	Spes Bona	54.9	17.85	5.7	4.68	2.73	3.65	7.33	0.01	0.9	0.08	0.81
DC16-100	Barby Fn.	50.29	10.68	9.33	6.41	14.92	2.11	3.95	0.18	0.71	0.14	0.41
DC16-100	Barby Fn.	50.53	10.79	9.26	6.48	14.75	2.13	3.95	0.18	0.70	0.15	0.43
DC16-101	Barby Fn.	52.95	15.92	6.81	6.12	6.68	3.12	5.29	0.06	0.80	0.10	0.70
DC16-102	Barby Fn.	47.20	9.45	9.34	6.50	18.38	1.81	3.54	0.21	0.68	0.15	0.48
DC16-112	Spes Bona	57.82	18.84	3.57	3.35	1.33	3.29	7.99	0.01	0.57	0.05	0.41
DC16-112	Spes Bona	58.11	18.79	3.55	3.37	1.35	3.36	8.01	bdl	0.57	0.05	0.41
DC16-113	Spes Bona	58.80	18.65	3.25	2.82	1.08	3.66	8.25	0.01	0.64	0.05	0.53
DC1655	Barby Fn.	55.86	15.67	8.04	6.33	4.5	3.1	2.36	0.02	0.89	0.12	0.23
DC1656	Barby Fn.	55.44	16.71	7.97	6.82	2.85	3.58	2.2	0.01	1.13	0.11	0.32
DC1657A	Barby Fn.	54.36	15.9	7.82	7.26	4.16	2.92	2.72	0.03	1	0.11	0.27
DC1658	Barby Fn.	54.52	15.49	8.35	5.67	4.79	3.34	1.98	0.03	1.07	0.12	0.28
DC1659	Barby Fn.	68.98	13.59	4.06	2.53	0.72	4.94	2.35	0.01	0.77	0.05	0.17
DC1664	Barby Fn.	47.45	9.56	9.17	6.52	17.41	1.71	3.52	0.21	0.65	0.14	0.49
DC1677	Barby Fn.	50.30	16.52	12.78	7.74	4.69	3.15	0.92	0.01	1.52	0.18	0.16
DC1677	Barby Fn.	50.47	16.60	12.80	7.72	4.70	3.11	0.92	0.01	1.54	0.18	0.16
DC1678	Barby Fn.	49.52	20.10	9.67	9.95	4.33	2.68	0.61	0.01	1.11	0.14	0.12
DC1678	Barby Fn.	49.70	20.09	9.70	10.00	4.35	2.69	0.61	0.01	1.12	0.13	0.12
DC1695A	Barby Fn.	49.42	11.98	10.13	6.17	12.56	3.01	1.87	0.15	0.68	0.14	0.19
DC1695A	Barby Fn.	49.61	11.95	10.14	6.18	12.57	2.98	1.88	0.15	0.68	0.14	0.19
DC1695B	Barby Fn.	49.82	12.18	10.09	6.07	12.89	3.19	1.15	0.14	0.67	0.14	0.19
DC1696	Barby Fn.	52.98	15.17	8.74	6.82	6.64	3.40	2.24	0.03	0.87	0.14	0.28
DC1697	Barby Fn.	60.55	14.46	6.42	4.29	1.82	2.19	3.37	bdl	1.24	0.10	0.50
DC1697	Barby Fn.	60.61	14.65	6.45	4.25	1.83	2.17	3.42	bdl	1.26	0.10	0.50
DC1698	Barby Fn.	51.02	15.11	8.29	6.46	4.14	4.05	0.96	0.02	1.04	0.11	0.28
DC1698	Barby Fn.	51.25	15.03	8.29	6.45	4.15	4.00	0.96	0.02	1.04	0.11	0.27
DC1699	Spes Bona	58.72	18.61	3.51	2.87	1.10	3.86	7.90	0.01	0.61	0.06	0.42
DC1699	Spes Bona	59.13	19.06	3.59	2.84	1.04	3.97	7.96	bdl	0.65	0.06	0.43
DC1709	Barby Fn.	64.75	11.93	9.41	3.93	1.13	3.97	1.52	0.01	1.15	0.23	0.37
DC1710	Barby Fn.	76.28	12.15	1.3	0.16	0.33	2.72	4.85	0.01	0.17	0.04	0.02
DC1714	Barby Fn.	70.75	13.69	3.58	0.64	0.29	5.01	4.01	0.02	0.53	0.02	0.08
DC1715	Barby Fn.	53.58	16.72	8.64	7.09	4.7	3.74	1.47	0.01	1.04	0.14	0.23
DC1716	Barby Fn.	55.25	17.13	7.31	6	3.4	2.8	3.72	0.01	1.26	0.12	0.33
DC1717	Barby Fn.	56.98	15.86	7.28	5.47	3.25	3.74	2.72	0.01	1.33	0.11	0.37

APPENDIX B: Trace Elements

SAMPLE		Ba	Ce	Cr	Cs	Dy	Er	Eu	Gd	Hf	Ho	La	Lu	Nb	Nd	Pr	Rb	Sm	Sr	Ta	Tb	Th	Tm	U	V	Y	Yb	Zr
DC1533A	Barby Fn.	1325	131	10	2.32	7.63	4.36	2.31	8.85	9.9	1.71	46.2	0.74	10.9	59.4	15.2	123	10.8	295	0.6	1.28	22.5	0.7	5.03	37	46.2	4.77	367
DC1535A	Barby Fn.	160	91.9	310	1.43	5.3	4.16	0.7	4.82	7.8	1.33	42.4	0.77	11.1	33.3	9.75	140.5	6.27	54.7	0.6	0.8	38.5	0.72	8.45	22	42.4	4.75	203
DC1538A	Barby Fn.	709	37.1	300	0.42	3.64	2.02	1.62	4.39	3.1	0.81	20.5	0.3	3.9	24.1	5.05	43.6	5.33	872	0.1	0.64	4.8	0.3	1.73	233	20.5	1.94	111
DC1540A	Barby Fn.	1425	75.1	90	1.79	3.6	2.09	1.81	4.75	3.1	0.76	20	0.26	3.1	37	8.52	52.1	6.27	1210	<0.1	0.65	1.85	0.28	0.46	205	20	1.74	128
DC1541A	Spes Bona	2530	62.6	60	6.49	3.23	1.73	1.72	4.64	2.1	0.62	16.5	0.22	4.2	31.4	7.69	297	5.5	1195	0.1	0.59	6.49	0.25	1.73	221	16.5	1.41	83
DC16-100	Barby Fn.	932.81	30.74	1169	5.84	3.83	1.99	1.337	4.47	2.35	0.734	13.22	0.288	5.89	19.23	4.14	167.44	4.39	421.92	0.17	0.596	4.41	0.306	1.623	157.17	19.97	2.09	73.84
DC16-100	Barby Fn.	947.84	30.74	1159	5.35	3.8	2.22	1.142	4.02	2.08	0.739	13.87	0.298	9.01	18.48	4.22	168.6	4.55	423.82	0.139	0.583	4.54	0.33	1.568	159.19	19.78	2.25	73.36
DC16-101	Barby Fn.	1433.3	58.86	410.4	9.42	3.27	1.62	1.423	4.5	2.79	0.587	27.63	0.246	7.71	28.05	6.73	241.66	5.03	784.97	0.228	0.495	7.19	0.212	2.006	173.26	16.19	1.68	105.13
DC16-102	Barby Fn.	1009.7	41.74	1374	6.64	2.51	1.246	1.231	3.69	2.43	0.474	19.51	0.183	4.5	21.97	5.17	151.58	4.47	500.09	0.153	0.477	4.05	0.161	0.724	78.19	13.27	1.295	79.91
DC16-112	Spes Bona	3470.9	32.65	41.55	3.03	1.57	0.794	1.686	2.12	1.127	0.3	17.6	0.085	5.61	15.58	4.07	265.56	2.66	1476.1	0.101	0.289	3.24	0.113	0.862	151.86	7.65	0.801	43.69
DC16-112	Spes Bona	3500	32.57	43.97	2.99	1.49	0.736	1.726	2.83	1.04	0.32	17.82	0.12	7.62	15.68	3.75	265.58	2.95	1494.97	0.162	0.302	3.06	0.139	0.754	149.8	7.85	0.566	38.27
DC16-113	Spes Bona	2822.7	42.91	44.95	6.54	2	1.095	1.555	2.49	2.03	0.383	21.86	0.188	7.35	19.29	4.92	322.62	3.3	1154.82	0.179	0.356	5.72	0.134	1.464	137.18	10.07	0.973	88.83
DC1655	Barby Fn.	723	41.98	149.3	3.23	3.91	2.22	1.16	4.59	3.04	0.85	18.7	0.351	7.01	22.3	4.94	66.2	4.73	663.2	0.244	0.614	4.77	0.289	1.87	166.4	19.33	1.88	129.9
DC1656	Barby Fn.	811	69.3	95.3	1.9	4.98	2.99	1.7	5.53	5.22	1.04	31	0.437	13	36.2	7.98	78	6.53	561	0.483	0.84	9.08	0.406	2.48	218.8	26.88	2.9	204.5
DC1657A	Barby Fn.	852	63.7	165	2.7	5.1	2.62	1.47	5.12	4.56	1.12	29.91	0.38	9.55	31.8	7.23	87.3	6.05	532.4	0.432	0.76	9.41	0.356	2.13	196	26.22	2.33	184.5
DC1658	Barby Fn.	921	66.3	174	3.44	4.88	2.97	1.62	5.63	4.71	0.98	30.84	0.365	10.93	33.5	8.12	65.8	6.67	577.1	0.445	0.74	9.26	0.398	2.57	199.1	26.34	2.93	193.2
DC1659	Barby Fn.	978	130.7	161.6	0.46	7.88	4.9	1.73	8.6	8.82	1.56	61.7	0.521	12.75	56.4	14.76	52.1	10.5	434	0.71	1.24	24.92	0.68	6.22	45.3	42.5	4.55	366
DC1664	Barby Fn.	1058	44.1	1419	6.66	2.9	1.32	1.06	3.65	2.03	0.532	20.03	0.187	10.73	24.3	5.42	165.6	4.79	540.5	0.183	0.457	4.71	0.188	0.78	92	13.73	1.32	85.1
DC1677	Barby Fn.	215.84	24.19	74.39	2.41	4.78	2.86	1.328	4.43	2.81	0.993	9.81	0.408	5.08	15.46	3.47	30.54	4.32	287.79	0.269	0.703	1.73	0.408	0.521	267.43	25.42	2.77	103.36
DC1677	Barby Fn.	221.09	23.64	75.13	2.141	4.95	3.16	1.356	4.54	2.54	0.92	9.67	0.485	7.98	15.04	3.19	30.64	4.21	291.51	0.252	0.699	1.614	0.42	0.481	269.79	25.06	2.79	102.19
DC1678	Barby Fn.	107.75	16.64	60.24	2.51	3.13	1.97	1.01	3.23	1.99	0.733	6.66	0.348	3.93	10.37	2.409	23.82	3.14	287.1	0.217	0.518	1.093	0.246	0.339	183.15	17.99	1.67	72.56
DC1678	Barby Fn.	106.86	16.47	65.92	2.61	3.53	2.04	1.11	3.14	2.24	0.717	6.8	0.244	5.18	10.61	2.333	22.71	3.12	292.78	0.18	0.512	1.006	0.265	0.34	187.38	18.05	2.09	73.16
DC1695A	Barby Fn.	462.4	23.64	992.2	0.476	3	1.69	0.821	3.06	1.61	0.606	11	0.24	3.44	13.48	2.95	44.62	3.18	262.18	0.101	0.434	1.688	0.26	0.454	169.31	16.22	1.74	63.71
DC1695A	Barby Fn.	454.12	24.41	1017	0.478	3.06	1.759	0.922	3.32	1.651	0.608	11.64	0.278	5.94	13.25	3.18	44.42	3.04	266.05	0.099	0.524	1.735	0.23	0.433	172.85	15.85	1.8	63.82
DC1695B	Barby Fn.	313.81	23	996.2	0.63	3.14	1.945	0.998	3.24	1.748	0.663	10.7	0.301	5.96	13.72	2.95	38.39	3.16	355.91	0.113	0.52	1.744	0.28	0.494	177.11	16.65	1.79	66.34
DC1696	Barby Fn.	718.99	42.5	259.6	1.65	3.47	2.18	1.327	3.91	2.68	0.763	19.66	0.285	4.06	23.34	5.38	60.02	5.02	616.06	0.15	0.645	4.24	0.3	1.027	179.44	18.65	2.05	103.82
DC1697	Barby Fn.	668.36	120.2	51.99	3.79	6.95	4.31	1.868	7.89	9.14	1.576	57.62	0.545	20.67	54.79	14.13	175.6	10.55	205.89	1.061	1.167	21.31	0.596	5.01	134.93	39.9	3.71	368.68
DC1697	Barby Fn.	684.87	119.7	51.28	3.84	7.68	4.13	1.838	8.26	9.66	1.446	56.3	0.555	19.81	54.31	13.97	186	10.97	205.89	1.02	1.247	21.21	0.593	5.06	135.92	39.91	3.94	375.54
DC1698	Barby Fn.	260.36	60.89	159.4	1.04	4.63	2.71	1.549	5.64	4.69	0.879	28.07	0.38	8.78	30.71	7.38	30.19	5.98	299.98	0.397	0.733	8.86	0.362	2.167	183.93	24.92	2.35	178.58
DC1698	Barby Fn.	257.03	60.05	158.9	1.21	4.46	2.46	1.32	5.59	4.92	0.962	28.09	0.324	9.91	30.38	7.09	27.82	6.46	303.57	0.395	0.775	8.99	0.399	2.147	180.88	24.97	2.69	179.43
DC1699	Spes Bona	2539.7	52.03	47.66	10.66	2.3	1.266	1.408	3.28	2.98	0.476	26.7	0.208	6.92	23.24	5.8	341.52	4.01	1055.55	0.325	0.394	9.6	0.184	2.448	133.37	12.64	1.357	118.91
DC1699	Spes Bona	2673.5	54.74	39.43	11.14	2.22	1.37	1.739	3.41	3.37	0.487	28	0.179	6.96	24.05	6.26	356.93	4.41	1075.76	0.317	0.4	9.83	0.184	2.46	140.28	13.58	1.51	135.82
DC1709	Barby Fn.	352.2	71.78	158.6	0.229	13.85	8.37	3.58	14.23	13.73	2.99	29.9	1.229	10.38	48	9.91	15.03	12.3	171.2	0.758	2.25	3.59	1.209	1.343	47.22	77.78	7.73	575.2
DC1710	Barby Fn.	221	81.2	186.4	1.65	4.87	3.47	0.51	4.12	6.32	1.22	41.37	0.666	9.07	28.7	8.07	146.6	5.58	73.2	0.534	0.832	29.64	0.453	6.61	22.48	37.3	4.19	176.6
DC1714	Barby Fn.	853	86.34	161.2	0.835	5.33	3.79	1.35	5.96	9.88	1.14	43.81	0.638	8.96	39.1	9.78	113.4	7.97	100.3	0.638	0.883	18.53	0.519	4.66	22.63	33.65	3.82	378.9
DC1715	Barby Fn.	677.2	33.48	85.9	2.09	3.82	2.08	1.32	3.87	3.25	0.767	15.91	0.306	2.58	19.26	4.32	43.8	4.34	521.2	0.197	0.628	2.72	0.32	1.085	181.8	20.92	2.09	106.6
DC1716	Barby Fn.	1146	70.09	51.5	2.62	4.85	2.61	1.99	6.33	5.18	1.041	34.54	0.415	6.15	34.67	8.62	135.4	6.86	504.1	0.436	0.925	9.44	0.396	2.62	214.4	27.55	2.92	212.4
DC1717	Barby Fn.	768	83.03	85.4	1.617	5.83	3.33	2.1	7.45	6.64	1.241	40.73	0.44	7.65	41.9	9.88	100.3	8.18	494.2	0.504	1.05	12.18	0.466	3.1	204.6	32.21	3.04	252.1

APPEDIX C: U-Pb data

Point		Error Correction	Discordan %	$^{207}Pb/^{206}Pb$	±σ	$^{207}Pb/^{235}U$	±σ	$^{206}Pb/^{238}U$	±σ	$^{208}Pb/^{232}Th$	±σ
DC1535 Barby Felsic Tuff											
02a		0.95	-5.2	1157.7	5.6	1121.0	6.3	1102.1	8.9	1142.8	49.3
03a		0.88	-16.5	1130.8	12.9	1011.9	9.0	957.8	11.0	939.0	41.7
04a		0.35	-38.3	1252.3	256.5	931.2	97.5	801.5	40.6	989.3	102.8
05a1		0.85	-21.6	621.8	12.9	515.9	4.6	492.3	4.6	464.1	20.5
05a2		0.84	-32.4	890.8	11.6	677.7	5.1	615.4	5.1	577.8	25.4
07a		0.96	4.1	1232.9	5.0	1261.6	6.5	1278.5	10.0	1333.7	57.2
06a1		0.94	3.5	1217.0	6.0	1241.7	6.5	1255.9	9.7	1315.8	56.4
06a2		0.92	0.1	1213.4	8.2	1213.9	7.7	1214.3	11.0	1242.3	53.8
07a@0		0.97	-3.0	1224.7	4.9	1203.3	7.4	1191.4	11.0	1218.4	52.9
08a		0.87	-28.6	781.1	10.8	612.1	4.8	567.4	4.9	537.4	23.7
09a		0.41	1.7	1190.0	38.2	1201.8	15.2	1208.4	9.6	1190.0	51.7
12a		0.96	0.4	1215.1	5.5	1217.8	6.8	1219.2	10.1	1246.5	54.7
13a1		0.95	1.9	1206.3	6.1	1219.9	6.8	1227.6	10.1	1254.7	54.0
13a2		0.94	-0.4	1223.0	6.0	1220.5	6.5	1219.0	9.6	1247.8	53.7
17c		0.77	0.8	1219.8	14.0	1225.7	8.1	1229.0	9.8	1239.0	54.2
22a		0.92	2.0	1211.4	7.1	1225.3	6.8	1233.2	9.9	1236.6	53.4
23a		0.93	2.3	1211.8	6.7	1227.9	6.8	1237.0	10.0	1271.7	54.8
28a		0.88	-18.5	994.9	9.5	870.1	5.8	821.8	6.7	752.8	33.3
32c		0.91	2.3	1211.7	8.0	1228.1	7.1	1237.5	10.2	1260.3	54.3

Point		Error Correction	Discordan %	$^{207}Pb/^{206}Pb$	±σ	$^{207}Pb/^{235}U$	±σ	$^{206}Pb/^{238}U$	±σ	$^{208}Pb/^{232}Th$	±σ
DC1541 Spes Bona Syenite											
60		0.97	6.3	1214.8	4.3	1258.3	6.7	1283.9	10.5	866.0	30.2
66		0.98	6.2	1216.4	3.5	1259.3	6.4	1284.6	10.2	849.8	26.2
71		0.98	9.0	1218.4	3.8	1280.5	6.7	1317.8	10.6	916.5	28.9
59		0.99	7.5	1213.6	2.4	1265.5	6.4	1296.3	10.3	855.2	25.3
62		0.94	2.9	1212.4	5.8	1232.7	6.3	1244.3	9.4	801.9	26.8
64		0.94	10.5	1218.5	6.1	1290.1	6.8	1333.6	10.5	995.5	50.2
69		0.95	1.9	1221.2	5.5	1234.8	6.7	1242.6	10.0	796.8	24.8
67		0.98	5.3	1222.9	3.6	1260.0	6.6	1281.8	10.3	840.3	27.9

Point		Error Correction	Discordan %	$^{207}Pb/^{206}Pb$	±σ	$^{207}Pb/^{235}U$	±σ	$^{206}Pb/^{238}U$	±σ	$^{208}Pb/^{232}Th$	±σ
DC1540 Barby Rhomb Porphyry											
1		0.99	2.7	1210.9	5.5	1230.1	13.4	1241.1	20.8	894.7	36.8
2		0.99	17.1	1208.3	4.2	1322.1	12.0	1393.5	20.1	1011.0	39.2
3		0.99	6.1	1213.9	4.1	1256.5	11.8	1281.5	18.7	900.7	36.3
9		1.00	7.6	1222.0	3.0	1274.8	11.7	1306.3	18.8	872.3	34.7
9.2*		0.99	11.6	1217.9	4.6	1297.3	12.1	1345.8	19.7	907.4	44.5
11		1.00	19.0	1219.6	3.1	1346.1	12.2	1427.1	20.7	1057.9	51.0
11.2*		1.00	12.4	1242.2	7.9	1327.3	41.1	1380.7	67.7	1005.3	67.6
12		0.99	6.5	1222.3	4.8	1267.6	12.3	1294.4	19.6	961.6	44.0
13		0.99	17.6	1217.9	3.5	1335.7	12.7	1410.3	21.5	1061.6	41.1
13.2*		0.99	13.9	1217.3	3.5	1311.1	12.2	1369.2	20.2	998.3	38.5
14		0.99	5.3	1214.5	3.8	1251.5	11.5	1273.2	18.2	885.7	34.9
14.2*		0.99	5.3	1218.0	3.7	1254.7	11.3	1276.3	17.9	882.2	34.6
15		0.99	16.4	1217.4	5.4	1327.7	17.5	1397.1	29.3	1016.0	51.3
17		1.00	13.2	1218.0	2.9	1307.7	11.7	1363.0	19.4	967.3	36.3
18		0.87	27.9	1206.2	18.2	1386.0	14.6	1505.7	22.6	1010.7	395.6
18.2*		0.99	19.8	1216.7	3.9	1348.4	13.0	1432.9	22.1	1121.5	59.8
*Second point take on the same grain											

Point		Error Correction	Discordan %	$^{207}Pb/^{206}Pb$	±σ	$^{207}Pb/^{235}U$	±σ	$^{206}Pb/^{238}U$	±σ	$^{208}Pb/^{232}Th$	±σ
DC1709 Barby quartz porphyritic lava											
1		0.72	2.0	1325.9	23.7	1340.7	13.1	1349.9	15.3	1397.1	34.6
3		0.73	3.7	1300.3	23.7	1326.7	13.4	1343.1	15.9	1338.4	34.0
5		0.74	0.2	1356.7	23.0	1358.0	13.3	1358.8	16.0	1377.8	32.5
9		0.66	-5.0	1376.7	28.1	1338.2	14.6	1314.3	15.4	1335.9	35.8
11a		0.77	2.0	1312.7	20.1	1327.3	12.0	1336.4	14.9	1334.0	30.8
11b		0.74	3.3	1314.9	22.7	1339.1	13.2	1354.3	16.0	1378.5	36.0
16a		0.89	1.2	1326.0	11.7	1334.5	10.0	1339.8	14.5	1327.7	25.5
16b		0.75	0.2	1341.1	22.0	1342.6	12.8	1343.5	15.6	1388.5	36.2
17		0.62	-3.0	1332.9	32.0	1310.0	15.7	1296.1	15.6	1265.3	64.0
2		0.84	2.8	1301.0	14.3	1321.6	10.1	1334.3	13.7	1322.7	26.2
20		0.83	2.4	1325.9	15.4	1343.3	10.5	1354.3	14.2	1391.9	28.1
21_x		0.73	-4.0	1363.9	20.4	1333.6	11.5	1314.8	13.4	1202.1	29.5
25a_x		0.76	3.2	1327.3	16.6	1350.8	10.0	1365.7	12.5	1267.6	23.1

Appendix C. The localities of the geochronological samples and showing the ages.

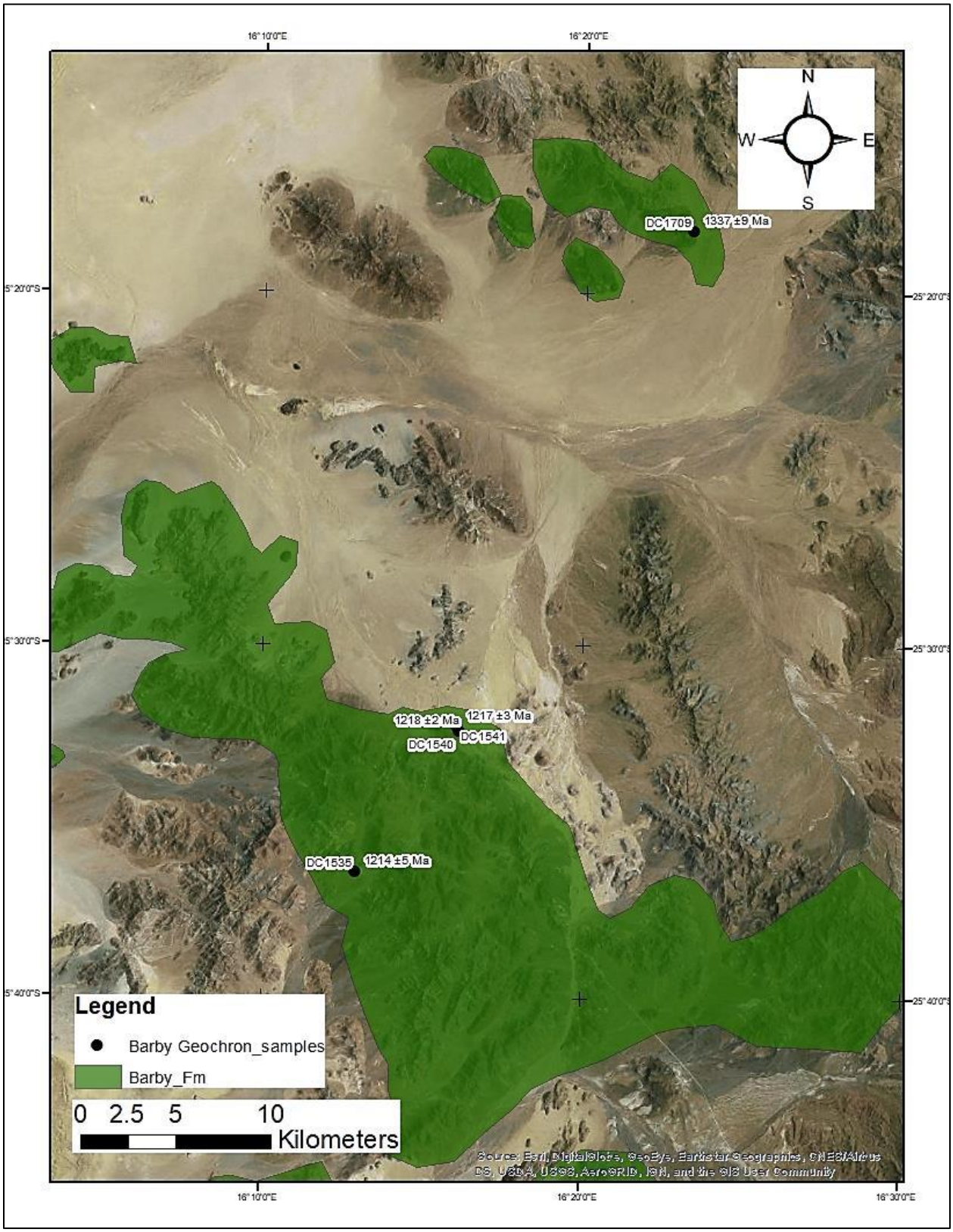

APPENDIX C: Lu-Hf data

Point	$^{176}Lu/^{177}Hf$	1σ	$^{176}Hf/^{177}Hf$	1σ	tDM Myr	2s	Protolith age Myr
DC1535 Barby Felsic Tuff							
DC1535-3	0.003302	0.00013	0.28217	1.8E-05	1.60	0.020505	1.79
DC1535-5	0.005328	0.00013	0.28227	2.3E-05	1.55	0.029709	1.68
DC1535-8	0.005417	0.00031	0.28221	1.7E-05	1.64	0.011304	1.82
DC1535-12	0.004263	0.00011	0.28223	1.3E-05	1.57	0.014615	1.72
DC1541 Spes Bona Syenite							
DC1541-59	8.22E-05	0.0000024	0.2821	1.7E-05	1.57	0.022736	1.79
DC1541-60	7.38E-05	4.5E-07	0.2821	1.1E-05	1.57	0.014753	1.80
DC1541-71	0.000135	0.0000015	0.2821	9.9E-06	1.57	0.013255	1.79
DC1541-70	8.1E-05	0.0000012	0.28206	1.5E-05	1.62	0.020078	1.87
DC1540 Barby Rhomb Porphyry							
DC1540b1	7.33E-05	3.8E-07	0.28205	1.8E-05	1.63	0.024126	1.89
DC1540-b9	0.000104	8.9E-07	0.28205	1.2E-05	1.64	0.01607	1.90
DC1540-b11	0.000157	3.3E-07	0.28207	1.5E-05	1.62	0.020155	1.86
DC1540b-12	5.67E-05	4.6E-07	0.28208	0.00001	1.59	0.013399	1.83
DC1540b-14	9.8E-05	0.000001	0.28205	1.4E-05	1.64	0.018746	1.90
DC1709 Barby quartz porphyritic lava							
DC1709-01	0.282153	0.00002	0.00258	2.5E-05	1.60	0.027589	1.74
DC1709-03	0.282243	0.000034	0.00286	7.2E-05	1.48	0.046253	1.56
DC1709-11	0.282199	0.000018	0.00192	1.4E-05	1.51	0.024837	1.60
DC1709-25	0.282244	0.000014	0.00316	4.3E-05	1.49	0.018661	1.57
DC1709-17	0.282296	0.000023	0.0069	0.0002	1.58	0.027555	1.66

APPENDIX A: Samples collected

Sample ID	Lat deg	lat min S	Lon deg	Lon Min E	Unit	Lithology
Northern Samples						
DC 1677	25	2.729	16	5.617	Barby Fn.	Large-feldspar trachyandesite
DC 1678	25	2.841	16	5.619	Barby Fn.	Large-feldspar trachyandesite
DC1698	25	50.969	16	31.887	Barby Fn.	Large-feldspar trachyandesite
DC1709	25	18.212	16	23.371	Barby Fn.	Large-feldspar trachyandesite
DC1710	25	19.864	16	20.599	Barby Fn.	Basal pyroclastic volcanic
Southern Samples						
DC1533	25	35.869	16	14.336	Barby Fn.	Agglomerate
DC1535	25	36.474	16	12.926	Barby Fn.	Basal pyroclastic volcanic
DC1538	25	39.145	16	20.523	Barby Fn.	Phyric andesite lava
DC1540	25	32.473	16	16.164	Barby Fn.	Large-feldspar trachyandesite
DC1541	25	32.34	16	16.081	Spes Bona	Saffier syenite
DC1655	25	53.843	16	36.614	Barby Fn.	Phyric andesite lava
DC1656	25	52.521	16	34.588	Barby Fn.	Large-feldspar trachyandesite
DC1657	25	52.371	16	34.337	Barby Fn.	Large-feldspar trachyandesite
DC1658	25	50.993	16	31.931	Barby Fn.	Large-feldspar trachyandesite
DC1659	25	38.464	16	19.797	Barby Fn.	Phyric andesite lava
DC1664	25	17.742	16	0.781	Barby Fn.	Basalt
DC1695	25	49.566	16	29.199	Barby Fn.	Basal pyroclastic volcanic
DC1695					Barby Fn.	Basal pyroclastic volcanic
DC1696	25	50.275	16	29.685	Barby Fn.	Clinopyroxene basaltic andesite
DC1697	25	50.657	16	30.018	Barby Fn.	Clinopyroxene basaltic andesite
DC1699	25	19.389	15	58.568	Saffier	Saffier syenite
DC16-100	25	19.317	15	23.549	Barby Fn.	Basalt
DC16-101	25	20.145	15	0.786	Barby Fn.	Saffier dolerite
DC16-102	25	17.739	16	0.786	Barby Fn	Basalt
DC16-112	25	27.062	16	3.328	Saffier	Saffier syenite
DC16-113	25	22.015	16	5.442	Saffier	Saffier syenite
DC1714	25	38.948	16	34.321	Barby Fn.	Basal pyroclastic volcanic
DC1715	25	53.499	16	34.895	Barby Fn.	Phyric andesite lava
DC1716	25	53.724	16	34.935	Barby Fn.	Large-feldspar trachyandesite
DC1717	25	53.868	16	34.914	Barby Fn.	Large-feldspar trachyandesite

APPENDIX B: MAJOR ELEMENTS

SAMPLE		SiO2	Al2O3	Fe2O3	CaO	MgO	Na2O	K2O	Cr2O3	TiO2	MnO	P2O5
DC1533A	Barby Fn.	65.9	14.5	5.34	1.66	0.78	4.49	4.14	0.01	1.06	0.09	0.33
DC1535A	Barby Fn.	78.2	12.45	1.48	0.63	0.24	3.22	4.34	0.04	0.15	0.07	0.02
DC1538A	Barby Fn.	51.7	13.65	10.8	6.13	6.29	4.84	1.33	0.04	0.89	0.12	0.41
DC1540A	Barby Fn.	51.2	19.7	6.72	7.58	2.97	4.46	2.68	0.02	1.05	0.05	0.67
DC1541A	Spes Bona	54.9	17.85	5.7	4.68	2.73	3.65	7.33	0.01	0.9	0.08	0.81
DC16-100	Barby Fn.	50.29	10.68	9.33	6.41	14.92	2.11	3.95	0.18	0.71	0.14	0.41
DC16-100	Barby Fn.	50.53	10.79	9.26	6.48	14.75	2.13	3.95	0.18	0.70	0.15	0.43
DC16-101	Barby Fn.	52.95	15.92	6.81	6.12	6.68	3.12	5.29	0.06	0.80	0.10	0.70
DC16-102	Barby Fn.	47.20	9.45	9.34	6.50	18.38	1.81	3.54	0.21	0.68	0.15	0.48
DC16-112	Spes Bona	57.82	18.84	3.57	3.35	1.33	3.29	7.99	0.01	0.57	0.05	0.41
DC16-112	Spes Bona	58.11	18.79	3.55	3.37	1.35	3.36	8.01	bdl	0.57	0.05	0.41
DC16-113	Spes Bona	58.80	18.65	3.25	2.82	1.08	3.66	8.25	0.01	0.64	0.05	0.53
DC1655	Barby Fn.	55.86	15.67	8.04	6.33	4.5	3.1	2.36	0.02	0.89	0.12	0.23
DC1656	Barby Fn.	55.44	16.71	7.97	6.82	2.85	3.58	2.2	0.01	1.13	0.11	0.32
DC1657A	Barby Fn.	54.36	15.9	7.82	7.26	4.16	2.92	2.72	0.03	1	0.11	0.27
DC1658	Barby Fn.	54.52	15.49	8.35	5.67	4.79	3.34	1.98	0.03	1.07	0.12	0.28
DC1659	Barby Fn.	68.98	13.59	4.06	2.53	0.72	4.94	2.35	0.01	0.77	0.05	0.17
DC1664	Barby Fn.	47.45	9.56	9.17	6.52	17.41	1.71	3.52	0.21	0.65	0.14	0.49
DC1677	Barby Fn.	50.30	16.52	12.78	7.74	4.69	3.15	0.92	0.01	1.52	0.18	0.16
DC1677	Barby Fn.	50.47	16.60	12.80	7.72	4.70	3.11	0.92	0.01	1.54	0.18	0.16
DC1678	Barby Fn.	49.52	20.10	9.67	9.95	4.33	2.68	0.61	0.01	1.11	0.14	0.12
DC1678	Barby Fn.	49.70	20.09	9.70	10.00	4.35	2.69	0.61	0.01	1.12	0.13	0.12
DC1695A	Barby Fn.	49.42	11.98	10.13	6.17	12.56	3.01	1.87	0.15	0.68	0.14	0.19
DC1695A	Barby Fn.	49.61	11.95	10.14	6.18	12.57	2.98	1.88	0.15	0.68	0.14	0.19
DC1695B	Barby Fn.	49.82	12.18	10.09	6.07	12.89	3.19	1.15	0.14	0.67	0.14	0.19
DC1696	Barby Fn.	52.98	15.17	8.74	6.82	6.64	3.40	2.24	0.03	0.87	0.14	0.28
DC1697	Barby Fn.	60.55	14.46	6.42	4.29	1.82	2.19	3.37	bdl	1.24	0.10	0.50
DC1697	Barby Fn.	60.61	14.65	6.45	4.25	1.83	2.17	3.42	bdl	1.26	0.10	0.50
DC1698	Barby Fn.	51.02	15.11	8.29	6.46	4.14	4.05	0.96	0.02	1.04	0.11	0.28
DC1698	Barby Fn.	51.25	15.03	8.29	6.45	4.15	4.00	0.96	0.02	1.04	0.11	0.27
DC1699	Spes Bona	58.72	18.61	3.51	2.87	1.10	3.86	7.90	0.01	0.61	0.06	0.42
DC1699	Spes Bona	59.13	19.06	3.59	2.84	1.04	3.97	7.96	bdl	0.65	0.06	0.43
DC1709	Barby Fn.	64.75	11.93	9.41	3.93	1.13	3.97	1.52	0.01	1.15	0.23	0.37
DC1710	Barby Fn.	76.28	12.15	1.3	0.16	0.33	2.72	4.85	0.01	0.17	0.04	0.02
DC1714	Barby Fn.	70.75	13.69	3.58	0.64	0.29	5.01	4.01	0.02	0.53	0.02	0.08
DC1715	Barby Fn.	53.58	16.72	8.64	7.09	4.7	3.74	1.47	0.01	1.04	0.14	0.23
DC1716	Barby Fn.	55.25	17.13	7.31	6	3.4	2.8	3.72	0.01	1.26	0.12	0.33
DC1717	Barby Fn.	56.98	15.86	7.28	5.47	3.25	3.74	2.72	0.01	1.33	0.11	0.37

APPENDIX B: Trace Elements

SAMPLE		Ba	Ce	Cr	Cs	Dy	Er	Eu	Gd	Hf	Ho	La	Lu	Nb	Nd	Pr	Rb	Sm	Sr	Ta	Tb	Th	Tm	U	V	Y	Yb	Zr
DC1533A	Barby Fn.	1325	131	10	2.32	7.63	4.36	2.31	8.85	9.9	1.71	46.2	0.74	10.9	59.4	15.2	123	10.8	295	0.6	1.28	22.5	0.7	5.03	37	46.2	4.77	367
DC1535A	Barby Fn.	160	91.9	310	1.43	5.3	4.16	0.7	4.82	7.8	1.33	42.4	0.77	11.1	33.3	9.75	140.5	6.27	54.7	0.6	0.8	38.5	0.72	8.45	22	42.4	4.75	203
DC1538A	Barby Fn.	709	37.1	300	0.42	3.64	2.02	1.62	4.39	3.1	0.81	20.5	0.3	3.9	24.1	5.05	43.6	5.33	872	0.1	0.64	4.8	0.3	1.73	233	20.5	1.94	111
DC1540A	Barby Fn.	1425	75.1	90	1.79	3.6	2.09	1.81	4.75	3.1	0.76	20	0.26	3.1	37	8.52	52.1	6.27	1210	<0.1	0.65	1.85	0.28	0.46	205	20	1.74	128
DC1541A	Spes Bona	2530	62.6	60	6.49	3.23	1.73	1.72	4.64	2.1	0.62	16.5	0.22	4.2	31.4	7.69	297	5.5	1195	0.1	0.59	6.49	0.25	1.73	221	16.5	1.41	83
DC16-100	Barby Fn.	932.81	30.74	1169	5.84	3.83	1.99	1.337	4.47	2.35	0.734	13.22	0.288	5.89	19.23	4.14	167.44	4.39	421.92	0.17	0.596	4.41	0.306	1.623	157.17	19.97	2.09	73.84
DC16-100	Barby Fn.	947.84	30.74	1159	5.35	3.8	2.22	1.142	4.02	2.08	0.739	13.87	0.298	9.01	18.48	4.22	168.6	4.55	423.82	0.139	0.583	4.54	0.33	1.568	159.19	19.78	2.25	73.36
DC16-101	Barby Fn.	1433.3	58.86	410.4	9.42	3.27	1.62	1.423	4.5	2.79	0.587	27.63	0.246	7.71	28.05	6.73	241.66	5.03	784.97	0.228	0.495	7.19	0.212	2.006	173.26	16.19	1.68	105.13
DC16-102	Barby Fn.	1009.7	41.74	1374	6.64	2.51	1.246	1.231	3.69	2.43	0.474	19.51	0.183	4.5	21.97	5.17	151.58	4.47	500.09	0.153	0.477	4.05	0.161	0.724	78.19	13.27	1.295	79.91
DC16-112	Spes Bona	3470.9	32.65	41.55	3.03	1.57	0.794	1.686	2.12	1.127	0.3	17.6	0.085	5.61	15.58	4.07	265.56	2.66	1476.1	0.101	0.289	3.24	0.113	0.862	151.86	7.65	0.801	43.69
DC16-112	Spes Bona	3500	32.57	43.97	2.99	1.49	0.736	1.726	2.83	1.04	0.32	17.82	0.12	7.62	15.68	3.75	265.58	2.95	1494.97	0.162	0.302	3.06	0.139	0.754	149.8	7.85	0.566	38.27
DC16-113	Spes Bona	2822.7	42.91	44.95	6.54	2	1.095	1.555	2.49	2.03	0.383	21.86	0.188	7.35	19.29	4.92	322.62	3.3	1154.82	0.179	0.356	5.72	0.134	1.464	137.18	10.07	0.973	88.83
DC1655	Barby Fn.	723	41.98	149.3	3.23	3.91	2.22	1.16	4.59	3.04	0.85	18.7	0.351	7.01	22.3	4.94	66.2	4.73	663.2	0.244	0.614	4.77	0.289	1.87	166.4	19.33	1.88	129.9
DC1656	Barby Fn.	811	69.3	95.3	1.9	4.98	2.99	1.7	5.53	5.22	1.04	31	0.437	13	36.2	7.98	78	6.53	561	0.483	0.84	9.08	0.406	2.48	218.8	26.88	2.9	204.5
DC1657A	Barby Fn.	852	63.7	165	2.7	5.1	2.62	1.47	5.12	4.56	1.12	29.91	0.38	9.55	31.8	7.23	87.3	6.05	532.4	0.432	0.76	9.41	0.356	2.13	196	26.22	2.33	184.5
DC1658	Barby Fn.	921	66.3	174	3.44	4.88	2.97	1.62	5.63	4.71	0.98	30.84	0.365	10.93	33.5	8.12	65.8	6.67	577.1	0.445	0.74	9.26	0.398	2.57	199.1	26.34	2.93	193.2
DC1659	Barby Fn.	978	130.7	161.6	0.46	7.88	4.9	1.73	8.6	8.82	1.56	61.7	0.521	12.75	56.4	14.76	52.1	10.5	434	0.71	1.24	24.92	0.68	6.22	45.3	42.5	4.55	366
DC1664	Barby Fn.	1058	44.1	1419	6.66	2.9	1.32	1.06	3.65	2.03	0.532	20.03	0.187	10.73	24.3	5.42	165.6	4.79	540.5	0.183	0.457	4.71	0.188	0.78	92	13.73	1.32	85.1
DC1677	Barby Fn.	215.84	24.19	74.39	2.41	4.78	2.86	1.328	4.43	2.81	0.993	9.81	0.408	5.08	15.46	3.47	30.54	4.32	287.79	0.269	0.703	1.73	0.408	0.521	267.43	25.42	2.77	103.36
DC1677	Barby Fn.	221.09	23.64	75.13	2.141	4.95	3.16	1.356	4.54	2.54	0.92	9.67	0.485	7.98	15.04	3.19	30.64	4.21	291.51	0.252	0.699	1.614	0.42	0.481	269.79	25.06	2.79	102.19
DC1678	Barby Fn.	107.75	16.64	60.24	2.51	3.13	1.97	1.01	3.23	1.99	0.733	6.66	0.348	3.93	10.37	2.409	23.82	3.14	287.1	0.217	0.518	1.093	0.246	0.339	183.15	17.99	1.67	72.56
DC1678	Barby Fn.	106.86	16.47	65.92	2.61	3.53	2.04	1.11	3.14	2.24	0.717	6.8	0.244	5.18	10.61	2.333	22.71	3.12	292.78	0.18	0.512	1.006	0.265	0.34	187.38	18.05	2.09	73.16
DC1695A	Barby Fn.	462.4	23.64	992.2	0.476	3	1.69	0.821	3.06	1.61	0.606	11	0.24	3.44	13.48	2.95	44.62	3.18	262.18	0.101	0.434	1.688	0.26	0.454	169.31	16.22	1.74	63.71
DC1695A	Barby Fn.	454.12	24.41	1017	0.478	3.06	1.759	0.922	3.32	1.651	0.608	11.64	0.278	5.94	13.25	3.18	44.42	3.04	266.05	0.099	0.524	1.735	0.23	0.433	172.85	15.85	1.8	63.82
DC1695B	Barby Fn.	313.81	23	996.2	0.63	3.14	1.945	0.998	3.24	1.748	0.663	10.7	0.301	5.96	13.72	2.95	38.39	3.16	355.91	0.113	0.52	1.744	0.28	0.494	177.11	16.65	1.79	66.34
DC1696	Barby Fn.	718.99	42.5	259.6	1.65	3.47	2.18	1.327	3.91	2.68	0.763	19.66	0.285	4.06	23.34	5.38	60.02	5.02	616.06	0.15	0.645	4.24	0.3	1.027	179.44	18.65	2.05	103.82
DC1697	Barby Fn.	668.36	120.2	51.99	3.79	6.95	4.31	1.868	7.89	9.14	1.576	57.62	0.545	20.67	54.79	14.13	175.6	10.55	205.89	1.061	1.167	21.31	0.596	5.01	134.93	39.9	3.71	368.68
DC1697	Barby Fn.	684.87	119.7	51.28	3.84	7.68	4.13	1.838	8.26	9.66	1.446	56.3	0.555	19.81	54.31	13.97	186	10.97	205.89	1.02	1.247	21.21	0.593	5.06	135.92	39.91	3.94	375.54
DC1698	Barby Fn.	260.36	60.89	159.4	1.04	4.63	2.71	1.549	5.64	4.69	0.879	28.07	0.38	8.78	30.71	7.38	30.19	5.98	299.98	0.397	0.733	8.86	0.362	2.167	183.93	24.92	2.35	178.58
DC1698	Barby Fn.	257.03	60.05	158.9	1.21	4.46	2.46	1.32	5.59	4.92	0.962	28.09	0.324	9.91	30.38	7.09	27.82	6.46	303.57	0.395	0.775	8.99	0.399	2.147	180.88	24.97	2.69	179.43
DC1699	Spes Bona	2539.7	52.03	47.66	10.66	2.3	1.266	1.408	3.28	2.98	0.476	26.7	0.208	6.92	23.24	5.8	341.52	4.01	1055.55	0.325	0.394	9.6	0.184	2.448	133.37	12.64	1.357	118.91
DC1699	Spes Bona	2673.5	54.74	39.43	11.14	2.22	1.37	1.739	3.41	3.37	0.487	28	0.179	6.96	24.05	6.26	356.93	4.41	1075.76	0.317	0.4	9.83	0.184	2.46	140.28	13.58	1.51	135.82
DC1709	Barby Fn.	352.2	71.78	158.6	0.229	13.85	8.37	3.58	14.23	13.73	2.99	29.9	1.229	10.38	48	9.91	15.03	12.3	171.2	0.758	2.25	3.59	1.209	1.343	47.22	77.78	7.73	575.2
DC1710	Barby Fn.	221	81.2	186.4	1.65	4.87	3.47	0.51	4.12	6.32	1.22	41.37	0.666	9.07	28.7	8.07	146.6	5.58	73.2	0.534	0.832	29.64	0.453	6.61	22.48	37.3	4.19	176.6
DC1714	Barby Fn.	853	86.34	161.2	0.835	5.33	3.79	1.35	5.96	9.88	1.14	43.81	0.638	8.96	39.1	9.78	113.4	7.97	100.3	0.638	0.883	18.53	0.519	4.66	22.63	33.65	3.82	378.9
DC1715	Barby Fn.	677.2	33.48	85.9	2.09	3.82	2.08	1.32	3.87	3.25	0.767	15.91	0.306	2.58	19.26	4.32	43.8	4.34	521.2	0.197	0.628	2.72	0.32	1.085	181.8	20.92	2.09	106.6
DC1716	Barby Fn.	1146	70.09	51.5	2.62	4.85	2.61	1.99	6.33	5.18	1.041	34.54	0.415	6.15	34.67	8.62	135.4	6.86	504.1	0.436	0.925	9.44	0.396	2.62	214.4	27.55	2.92	212.4
DC1717	Barby Fn.	768	83.03	85.4	1.617	5.83	3.33	2.1	7.45	6.64	1.241	40.73	0.44	7.65	41.9	9.88	100.3	8.18	494.2	0.504	1.05	12.18	0.466	3.1	204.6	32.21	3.04	252.1

APPEDIX C: U-Pb data

Point		Error Correction	Discordan %	$^{207}Pb/^{206}Pb$	±σ	$^{207}Pb/^{235}U$	±σ	$^{206}Pb/^{238}U$	±σ	$^{208}Pb/^{232}Th$	±σ
DC1535 Barby Felsic Tuff											
02a		0.95	-5.2	1157.7	5.6	1121.0	6.3	1102.1	8.9	1142.8	49.3
03a		0.88	-16.5	1130.8	12.9	1011.9	9.0	957.8	11.0	939.0	41.7
04a		0.35	-38.3	1252.3	256.5	931.2	97.5	801.5	40.6	989.3	102.8
05a1		0.85	-21.6	621.8	12.9	515.9	4.6	492.3	4.6	464.1	20.5
05a2		0.84	-32.4	890.8	11.6	677.7	5.1	615.4	5.1	577.8	25.4
07a		0.96	4.1	1232.9	5.0	1261.6	6.5	1278.5	10.0	1333.7	57.2
06a1		0.94	3.5	1217.0	6.0	1241.7	6.5	1255.9	9.7	1315.8	56.4
06a2		0.92	0.1	1213.4	8.2	1213.9	7.7	1214.3	11.0	1242.3	53.8
07a@0		0.97	-3.0	1224.7	4.9	1203.3	7.4	1191.4	11.0	1218.4	52.9
08a		0.87	-28.6	781.1	10.8	612.1	4.8	567.4	4.9	537.4	23.7
09a		0.41	1.7	1190.0	38.2	1201.8	15.2	1208.4	9.6	1190.0	51.7
12a		0.96	0.4	1215.1	5.5	1217.8	6.8	1219.2	10.1	1246.5	54.7
13a1		0.95	1.9	1206.3	6.1	1219.9	6.8	1227.6	10.1	1254.7	54.0
13a2		0.94	-0.4	1223.0	6.0	1220.5	6.5	1219.0	9.6	1247.8	53.7
17c		0.77	0.8	1219.8	14.0	1225.7	8.1	1229.0	9.8	1239.0	54.2
22a		0.92	2.0	1211.4	7.1	1225.3	6.8	1233.2	9.9	1236.6	53.4
23a		0.93	2.3	1211.8	6.7	1227.9	6.8	1237.0	10.0	1271.7	54.8
28a		0.88	-18.5	994.9	9.5	870.1	5.8	821.8	6.7	752.8	33.3
32c		0.91	2.3	1211.7	8.0	1228.1	7.1	1237.5	10.2	1260.3	54.3

Point		Error Correction	Discordan %	$^{207}Pb/^{206}Pb$	±σ	$^{207}Pb/^{235}U$	±σ	$^{206}Pb/^{238}U$	±σ	$^{208}Pb/^{232}Th$	±σ
DC1541 Spes Bona Syenite											
60		0.97	6.3	1214.8	4.3	1258.3	6.7	1283.9	10.5	866.0	30.2
66		0.98	6.2	1216.4	3.5	1259.3	6.4	1284.6	10.2	849.8	26.2
71		0.98	9.0	1218.4	3.8	1280.5	6.7	1317.8	10.6	916.5	28.9
59		0.99	7.5	1213.6	2.4	1265.5	6.4	1296.3	10.3	855.2	25.3
62		0.94	2.9	1212.4	5.8	1232.7	6.3	1244.3	9.4	801.9	26.8
64		0.94	10.5	1218.5	6.1	1290.1	6.8	1333.6	10.5	995.5	50.2
69		0.95	1.9	1221.2	5.5	1234.8	6.7	1242.6	10.0	796.8	24.8
67		0.98	5.3	1222.9	3.6	1260.0	6.6	1281.8	10.3	840.3	27.9

Point		Error Correction	Discordan %	$^{207}Pb/^{206}Pb$	±σ	$^{207}Pb/^{235}U$	±σ	$^{206}Pb/^{238}U$	±σ	$^{208}Pb/^{232}Th$	±σ
DC1540 Barby Rhomb Porphyry											
1		0.99	2.7	1210.9	5.5	1230.1	13.4	1241.1	20.8	894.7	36.8
2		0.99	17.1	1208.3	4.2	1322.1	12.0	1393.5	20.1	1011.0	39.2
3		0.99	6.1	1213.9	4.1	1256.5	11.8	1281.5	18.7	900.7	36.3
9		1.00	7.6	1222.0	3.0	1274.8	11.7	1306.3	18.8	872.3	34.7
9.2*		0.99	11.6	1217.9	4.6	1297.3	12.1	1345.8	19.7	907.4	44.5
11		1.00	19.0	1219.6	3.1	1346.1	12.2	1427.1	20.7	1057.9	51.0
11.2*		1.00	12.4	1242.2	7.9	1327.3	41.1	1380.7	67.7	1005.3	67.6
12		0.99	6.5	1222.3	4.8	1267.6	12.3	1294.4	19.6	961.6	44.0
13		0.99	17.6	1217.9	3.5	1335.7	12.7	1410.3	21.5	1061.6	41.1
13.2*		0.99	13.9	1217.3	3.5	1311.1	12.2	1369.2	20.2	998.3	38.5
14		0.99	5.3	1214.5	3.8	1251.5	11.5	1273.2	18.2	885.7	34.9
14.2*		0.99	5.3	1218.0	3.7	1254.7	11.3	1276.3	17.9	882.2	34.6
15		0.99	16.4	1217.4	5.4	1327.7	17.5	1397.1	29.3	1016.0	51.3
17		1.00	13.2	1218.0	2.9	1307.7	11.7	1363.0	19.4	967.3	36.3
18		0.87	27.9	1206.2	18.2	1386.0	14.6	1505.7	22.6	1010.7	395.6
18.2*		0.99	19.8	1216.7	3.9	1348.4	13.0	1432.9	22.1	1121.5	59.8
*Second point take on the same grain											

Point		Error Correction	Discordan %	$^{207}Pb/^{206}Pb$	±σ	$^{207}Pb/^{235}U$	±σ	$^{206}Pb/^{238}U$	±σ	$^{208}Pb/^{232}Th$	±σ
DC1709 Barby quartz porphyritic lava											
1		0.72	2.0	1325.9	23.7	1340.7	13.1	1349.9	15.3	1397.1	34.6
3		0.73	3.7	1300.3	23.7	1326.7	13.4	1343.1	15.9	1338.4	34.0
5		0.74	0.2	1356.7	23.0	1358.0	13.3	1358.8	16.0	1377.8	32.5
9		0.66	-5.0	1376.7	28.1	1338.2	14.6	1314.3	15.4	1335.9	35.8
11a		0.77	2.0	1312.7	20.1	1327.3	12.0	1336.4	14.9	1334.0	30.8
11b		0.74	3.3	1314.9	22.7	1339.1	13.2	1354.3	16.0	1378.5	36.0
16a		0.89	1.2	1326.0	11.7	1334.5	10.0	1339.8	14.5	1327.7	25.5
16b		0.75	0.2	1341.1	22.0	1342.6	12.8	1343.5	15.6	1388.5	36.2
17		0.62	-3.0	1332.9	32.0	1310.0	15.7	1296.1	15.6	1265.3	64.0
2		0.84	2.8	1301.0	14.3	1321.6	10.1	1334.3	13.7	1322.7	26.2
20		0.83	2.4	1325.9	15.4	1343.3	10.5	1354.3	14.2	1391.9	28.1
21_x		0.73	-4.0	1363.9	20.4	1333.6	11.5	1314.8	13.4	1202.1	29.5
25a_x		0.76	3.2	1327.3	16.6	1350.8	10.0	1365.7	12.5	1267.6	23.1

Appendix C. The localities of the geochronological samples and showing the ages.

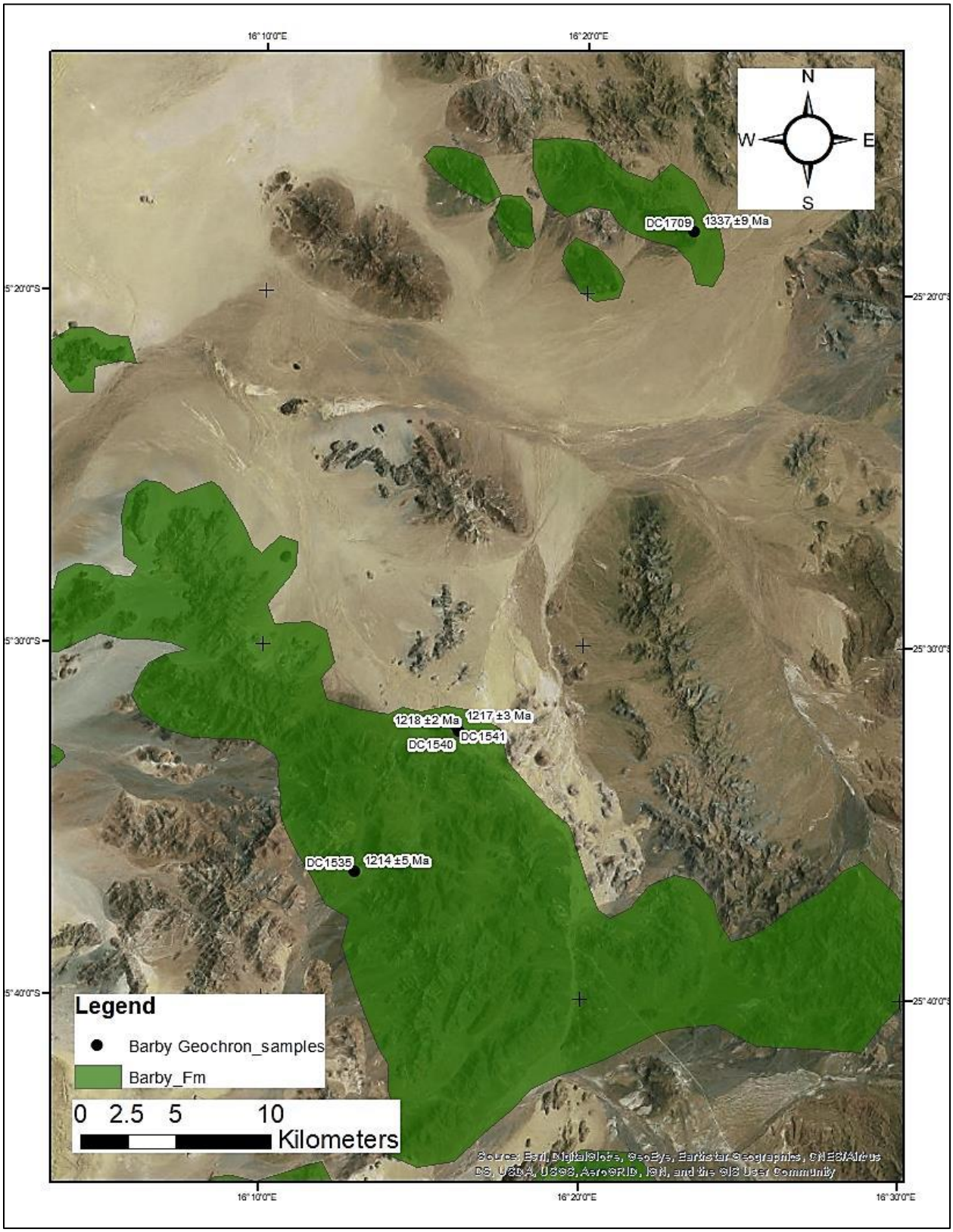

APPENDIX C: Lu-Hf data

Point	$^{176}Lu/^{177}Hf$	1σ	$^{176}Hf/^{177}Hf$	1σ	tDM Myr	2s	Protolith age Myr
DC1535 Barby Felsic Tuff							
DC1535-3	0.003302	0.00013	0.28217	1.8E-05	1.60	0.020505	1.79
DC1535-5	0.005328	0.00013	0.28227	2.3E-05	1.55	0.029709	1.68
DC1535-8	0.005417	0.00031	0.28221	1.7E-05	1.64	0.011304	1.82
DC1535-12	0.004263	0.00011	0.28223	1.3E-05	1.57	0.014615	1.72
DC1541 Spes Bona Syenite							
DC1541-59	8.22E-05	0.0000024	0.2821	1.7E-05	1.57	0.022736	1.79
DC1541-60	7.38E-05	4.5E-07	0.2821	1.1E-05	1.57	0.014753	1.80
DC1541-71	0.000135	0.0000015	0.2821	9.9E-06	1.57	0.013255	1.79
DC1541-70	8.1E-05	0.0000012	0.28206	1.5E-05	1.62	0.020078	1.87
DC1540 Barby Rhomb Porphyry							
DC1540b1	7.33E-05	3.8E-07	0.28205	1.8E-05	1.63	0.024126	1.89
DC1540-b9	0.000104	8.9E-07	0.28205	1.2E-05	1.64	0.01607	1.90
DC1540-b11	0.000157	3.3E-07	0.28207	1.5E-05	1.62	0.020155	1.86
DC1540b-12	5.67E-05	4.6E-07	0.28208	0.00001	1.59	0.013399	1.83
DC1540b-14	9.8E-05	0.000001	0.28205	1.4E-05	1.64	0.018746	1.90
DC1709 Barby quartz porphyritic lava							
DC1709-01	0.282153	0.00002	0.00258	2.5E-05	1.60	0.027589	1.74
DC1709-03	0.282243	0.000034	0.00286	7.2E-05	1.48	0.046253	1.56
DC1709-11	0.282199	0.000018	0.00192	1.4E-05	1.51	0.024837	1.60
DC1709-25	0.282244	0.000014	0.00316	4.3E-05	1.49	0.018661	1.57
DC1709-17	0.282296	0.000023	0.0069	0.0002	1.58	0.027555	1.66